CONTROLLING SO_2 POISONING, PORE SIZE AND OXIDATIVE DEGRADATION OF AMINE-CONTAINING ADSORBENTS TO ENHANCE CO_2 CAPTURE

Chanjot Kaur.

Thesis submitted to the University of Ottawa

in partial Fulfillment of the requirements for the degree of

Doctorate in Philosophy in Chemistry

Department of Chemistry and Biomolecular Sciences

Faculty of Science

University of Ottawa

© Chanjot Kaur., Ottawa, Canada, 2025

ABSTRACT

The increasing concentration of atmospheric CO_2 is a key contributor to global climate change. With global mitigation efforts already falling short of critical targets, the development of efficient and durable carbon capture technologies has become imperative to reduce CO_2 emissions on a global scale. Among the various strategies that have been explored, supported amine-based adsorbents have emerged as a highly promising solution due to their ability to capture CO_2 selectively and reversibly. However, the technical route is not wholesome yet, because the CO_2 uptake capacity and long-term stability of these adsorbents are significantly compromised by fundamental challenges, such as SO_2 poisoning and oxidative degradation. This thesis is therefore aimed at addressing these challenges while also focusing on the rational design of adsorbents to optimize CO_2 uptake. Overall, this work comprises three interconnected research projects. The first one focuses on mitigating SO_2 poisoning, the second one develops strategies for slowing down oxidative degradation, and the third one is dedicated to tailoring the pore structure to enhance adsorption performance.

SO_2 poisoning is a major challenge, as amines form stable salts even at trace concentrations of SO_2, resulting in a substantial decline in CO_2 adsorption capacity. To address this, silica-supported polyethylenimine (PEI) adsorbent, functionalized with glycidol (GD-PEI/S), was developed. This material contains only tertiary amines, which are selective for SO_2 over CO_2. The GD-PEI/S adsorbent was characterized using infrared (IR) spectroscopy, nuclear magnetic resonance (NMR) spectroscopy, and thermogravimetric analysis (TGA). Column breakthrough experiments demonstrated that the material is highly selective for SO_2 over CO_2, even in gas streams where CO_2 concentration was significantly higher. Moreover, the SO_2 uptake of the adsorbent nearly doubled under humid conditions, likely due to enhanced SO_2 diffusion facilitated by increased moisture content. Furthermore, the adsorbent showed good reversibility under dry and humid recycling conditions.

Oxidative degradation is another limitation for deploying amine adsorbents on an industrial scale, where adsorbents are inevitably exposed to air at elevated temperatures during cooling stage after CO_2 regeneration. This oxidative degradation leads to formation of less degradation products along with scission of amine chain, which significantly reduces CO_2 uptake and hence compromising adsorbent lifespan. To enhance oxidation stability, hydroxyethyl starch (HES) was co-impregnated with PEI on a support as an additive (HES-PEI/S). The performance of HES-PEI/S was evaluated under various oxidation conditions using CO_2 uptake measurements and mass spectrometry, with the findings supported by FTIR and NMR analyses. The enhancement in oxidation stability by HES was compared to other hydroxyl-containing additives, such as polyvinyl alcohol (PVA) and polyethylene glycol (PEG), as well as to 1,2-epoxy butane (EB). The results demonstrated that HES-PEI/S showed oxidation stability comparable to EB-PEI/S, while maintaining twice the CO_2 uptake based on PEI content. Additionally, HES-PEI/S showed significantly higher oxidation stability than PEI/S and other co-impregnated adsorbents, such as PVA-PEI/S and PEG-PEI/S.

While the previous projects addressed challenges such as SO_2 poisoning and oxidative degradation to enhance the stability of the adsorbent, consequently improving CO_2 uptake, third project presents a strategic innovation to optimize CO_2 uptake of the adsorbents. The project focused on maximizing CO_2 uptake of amine adsorbents by leveraging the relationship between relative humidity (RH) of the feed gas, pore size of the material, and CO_2 uptake. To study the relationship, periodic mesoporous silicas with 3 to 9 nm pore sizes and consistent morphology were synthesized, followed by grafting with comparable triamine loadings. H_2O and CO_2 adsorption isotherms as a function of RH were obtained for adsorbents with different pore sizes using Dynamic Vapor Sorption (DVS) analyzer. The adsorption isotherms showed pronounced maxima at the RH corresponding to water capillary condensation within the adsorbent, which was attributed to the formation of ammonium bicarbonate facilitated by the presence of liquid-like water. Furthermore, the results revealed that the RH of the water capillary condensation and hence the optimum CO_2 uptake of the adsorbent shifted to higher RH as the pore size of the adsorbent increased. This pore-size-dependent

behavior of maximum CO_2 uptake allows precise tailoring of adsorbents for feed gases with different RHs.

DEDICATION

To my Family

ACKNOWLEDGEMENTS

I would like to express my deepest gratitude to my supervisor, Prof. Abdelhamid Sayari, for his exceptional mentorship, unwavering support, and invaluable guidance throughout my Ph.D. journey. I am sincerely grateful to him for accepting me into his research group and providing me with the opportunity to work under his supervision. Prof. Sayari's passion for research is truly inspiring, and he consistently encourages his students to cultivate the same enthusiasm and curiosity. His willingness to offer support and readiness to help were invaluable during moments of challenge and uncertainty. His trust in my abilities allowed me to take full ownership of my projects and develop independent thinking—skills that will continue to guide me throughout my career. His patience, insightful feedback, and openness to discussing my ideas were instrumental in refining my research.

Beyond academic guidance, Prof. Sayari played a crucial role in supporting my professional development. Presenting my work at an international conference provided me with valuable exposure and the opportunity to engage with experts in the field, and I am grateful for the support that made this possible. I am particularly grateful for the research assistantship funding he provided, which enabled me to dedicate myself fully to my work. As I approached the final stages of my Ph.D., his flexibility and timely feedback on manuscript revisions and thesis submissions helped me meet critical deadlines with confidence. Prof. Sayari's leadership, integrity, and dedication to fostering an environment of academic excellence have left a lasting impact on me. I hope to carry forward the qualities I have learned under his mentorship and apply them in my future academic and professional endeavors.

I would also like to sincerely thank the members of my thesis advisory committee, Prof. Giorgi Javier, Prof. Darrin Richeson, and Prof. Edward Lai, for their insightful feedback and thoughtful guidance throughout my research. Their valuable discussions have helped refine my work and

challenged me to think critically. I also appreciate their prompt responses in coordinating meetings, ensuring that I could present my research at key milestones.

I am deeply grateful to Prof. Bahoueddine Tangour for his guidance and valuable insights during his visit to the University of Ottawa. Collaborating with him broadened my understanding of reaction kinetics and offered a valuable learning experience. I would also like to thank Peter Pallister, Volodymyr Semeniuchenko, and Patrick Szell for their valuable discussions and assistance in obtaining NMR data. Their expertise and support contributed significantly to the successful completion of this aspect of my research.

I would like to acknowledge the support of my colleagues in Prof. Sayari's research group. I am thankful to Joel, who, despite his busy schedule, took the time to train me in instrumental techniques and synthesis during my initial days in the lab. I am grateful to Sheila and Imen for their assistance whenever needed, as well as to Rahul, whose insights enriched my research. I am truly thankful to Chuanyu and Hadi for their patience, generosity, and constant support, which significantly contributed to my intellectual growth and deepened my understanding of various research problems throughout my Ph.D. journey. I am also appreciative of the support from senior colleagues, including Mohammadreza Fayaz, Ritesh Tailor, Govind Sethia, Avi Mathur, and Varinder Singh, who were always willing to provide guidance whenever needed.

I extend my deepest gratitude to my family, whose unwavering support has been fundamental to my achievements. I am deeply grateful to my father (Mr. Harminder Singh), whose aspirations for me to pursue a doctoral degree have been a constant source of motivation throughout my journey. While I may not have fully understood the significance of this path at the time, I now recognize the importance of his vision. His encouragement continues to inspire me, and I hope this accomplishment reflects the realization of his hopes. My mother (Mrs. Surinder Kaur), whose belief in me, positivity, and encouragement have been a constant source of strength. Her resilience, support, and sacrifices

motivated me to overcome challenges and stay focused on my goals. This accomplishment would not have been possible without her enduring dedication. My siblings, for their support and willingness to listen even during their own busy moments, especially when I needed it the most. Your presence and encouragement, especially when I needed it most, have been a source of strength throughout this journey. My grandmother, whose wisdom and reminders about the importance of education and perseverance have been a lasting source of inspiration for me. My nephew, whose fascination with my experiments and genuine excitement made me feel that I was doing something truly meaningful. His belief that I could create anything magical in this world has been a heartwarming reminder of the joy and wonder that science can inspire.

I am also incredibly grateful to my friends, whose presence and support have made this journey more meaningful. Ritu, your constant encouragement and positivity have been invaluable. Thank you for always checking in on me and lifting my spirits during difficult times. Despite the geographical distance, you have shown me that true friendship remains unaffected. Our shared experiences during our PhD journeys have strengthened our bond, and I truly appreciate the reassurance and support you have always provided. Adi and Rajdip, I am sincerely grateful for your unwavering support throughout this journey. I also appreciate the effort you both made to stay connected, never forgetting to check in and making special occasions even more meaningful. Your friendship has been invaluable.

Shubha di and Tamali di, I sincerely appreciate your kindness and support, particularly during the final stages of my PhD. Despite your own commitments, you always made time to offer guidance and respond to my questions. Shubha di, your empathy and ability to truly listen made me feel deeply understood at times when I needed it most. Your encouragement and thoughtful presence provided a sense of reassurance that I will always be grateful for. Thank you both for being an integral part of this journey—not only as seniors, but as individuals whose support helped me remain grounded and hopeful. Neha and Subah, I truly appreciate your support, insightful discussions, and thoughtfulness throughout this journey. Your willingness to share important information and offer guidance has been

invaluable. Whether discussing research challenges or simply taking a break to recharge when we were overwhelmed with work, your presence made a significant difference. I am also sincerely thankful to all the wonderful individuals I had the privilege of meeting along the way, whose support and kindness have enriched this experience.

Finally, I am profoundly grateful to God for His unwavering guidance, for illuminating the right path, and for granting me the strength to persevere before each challenge arose. His endless blessings and support have sustained me throughout this journey, and for that, I am truly thankful.

STATEMENT OF CONTRIBUTIONS

I hereby declare that this dissertation is my original work and has been entirely composed by me. The experimental design, execution of all experiments, and corresponding data analysis presented in this thesis were conceptualized, conducted, and completed by me.

I am deeply grateful to my Ph.D. supervisor, Professor Abdelhamid Sayari, for his invaluable guidance throughout this research. His expert insights, constructive feedback, and editorial support in refining manuscripts and thesis revisions were instrumental in shaping this work. I would also like to extend my sincere appreciation to Dr. Yun Liu for kindly providing the SEM images used in Chapter 4 of this thesis. Additionally, I acknowledge McMaster University for conducting the nitrogen adsorption analysis for the samples presented in Chapter 4.

This dissertation does not contain any material that infringes upon copyright. All sources of information have been duly cited, and permissions have been obtained from the respective publishers for the inclusion of my original work in this thesis. Chapters 2, 3, and 4 of this thesis are based on published and submitted research and have been published in peer-reviewed journals, as cited below.

Chapter 2: Kaur, C.; Sayari, A. Glycidol-Modified PEI: A Highly Selective Adsorbent for SO_2 in the Presence of CO_2. *J. Mater. Chem. A* 2024, *12*, 31526-31532.

Chapter 3: Kaur, C.; Sayari, A. Enhancing Oxidation Stability of Amine-Containing CO_2 Adsorbents Using Hydroxyethyl Starch. *Chem. Eng. J.* 2024, *496*, 153756.

Chapter 4: Kaur, C. and Sayari, A., 2025. CO_2 uptake - Relative humidity - Pore size relationship: A new tool for the design of amine-containing adsorbents. *Chem. Eng. J.* 2025, 162716.

TABLE OF CONTENTS

LIST OF FIGURES

LIST OF TABLES

LIST OF SCHEMES

LIST OF ABBREVIATIONS

^{1}H	Proton (Hydrogen-1)
^{13}C	Carbon-13
APTMS	Aminopropyltrimethoxysilane
BET	Brunauer-Emmett-Teller
BJH	Barret, Joyner, and Halenda
Cab-O-Sil	Fumed silica
$CDCl_3$	Chloroform-d
CO_2	Carbon dioxide
COFs	Covalent organic frameworks
CCS	Carbon capture and storage
CTAB	Cetyltrimethylammonium bromide
DETA	Diethylenetriamine
D_2O	Deuterium oxide
DMDA	N,N-dimethyldodecyl amine
DVS	Dynamic Vapor Sorption
EB	1,2-epoxy butane
EOR	Enhanced oil recovery
EDA	Ethylenediamine
FGD	Flue Gas Desulfurization
FTIR	Fourier transform infrared spectroscopy
GD	Glycidol
GHG	Greenhouse gas
HCl	Hydrochloric acid
HCP	Hydroxyl-containing polymers

HES	Hydroxyethyl starch
IPCC	Intergovernmental Panel on Climate Change
IR	Infrared Spectroscopy
IUPAC	International Union of Pure and Applied Chemistry
Lys	Lysine
MOFs	Metal organic frameworks
MCM-41	Mobil Composition of Matter
MF	Mesoporous silica foam
MS	Mass Spectrometry
$NaAlO_2$	Sodium aluminate
NH_4OH	Ammonium solution
NMR	Nuclear Magnetic Resonance
NOE	Nuclear Overhauser Effect
P123	$OH[CH_2CH_2O]_2O[CH_2CH(CH_3)O]_{70}[CH_2CH_2O]_2OH$
PAA	Polyallylamine
PEI	Polyethylenimine
PE-$AlSiO_2$	Pore-expanded alumino-silica
PEHA	Pentaethylenehexamine
PEG	Polyethylene glycol
PPI	Poly(propyleneimine)
ppm	parts per million
PVA	Polyvinyl alcohol
PSDs	Pore size distributions
RF	Radiofrequency
RH	Relative humidity

SBA-15	Santa Barbara Amorphous
SO_2	Sulfur dioxide
STP	Standard temperature and pressure
TAPA	tris(3-aminopropyl)amine
TEOS	Tetraethyl orthosilicate
TMPEDA	N-[3-(trimethoxysilyl)propyl]ethylenediamine
TRI	2-[2-(3-trimethoxysilylpropylamino)ethylamino]ethylamine/ Triamine
TEPA	Tetraethylenepentamine
TER-PE-MCM-41	N,N-dimethylpropyl amine pore expanded MCM-41
TETA	Triethylenetetramine
TPD	Temperature-programmed desorption
TMAOH	Tetramethylammonium hydroxide
TCD	Thermal conductivity detector
TGA	Thermogravimetric Analysis

LIST OF SYMBOLS

A	Integrated peak intensities
B_0	Magnetic field
C	Material-dependent constant
CO	Carbon monoxide
CO_2	Carbon dioxide
C_0	Inlet concentration
C_A	Downstream concentration
F	Flowrate
H_2	Hydrogen
I	Spin quantum number
m	Mass of the adsorbent
N	Adsorbate molecules
N_A	Avogadro's number
n_m	Molecules that form monolayer
P	Vapor pressure
P_0	Saturation pressure
P/P_0	Relative partial pressure
R	Radius of the pore
R	Universal gas constant
S	Surface area
SO_2	Sulphur dioxide
T	Temperature
t_q	Stoichiometric time
v_m	Molar volume

V_{total}	Total pore volume
θ	Angle of contact between the liquid and the pore surface
σ	Cross-sectional area
γ_s	Surface tension
γ_m	Gyromagnetic ratio
ν_0	Larmor frequency
1°	Primary
2°	Secondary
3°	Tertiary

CHAPTER 1 GENERAL INTRODUCTION

Part 1: Background, Challenges, and Research Gap

1.1. CO_2 Emissions and its Growing Concerns

Carbon dioxide (CO_2) is an integral component of Earth's carbon cycle, essential for maintaining ecological balance. However, anthropogenic activities, particularly the combustion of fossil fuels, have led to a significant and unprecedented increase in atmospheric CO_2 concentrations. Despite being less potent than other greenhouse gases, exceedingly large emissions of anthropogenic CO_2 have positioned CO_2 as the largest contributor to global warming.[1] In 2024, the global power sector CO_2 emissions reached *ca.* 13.8 billion metric tons, marking a 1% increase from the previous year, primarily due to increased fossil fuel-based generation.[2] This trend is further evident by the significant increase in atmospheric CO_2 concentrations, which reached 429 parts per million (ppm) in 2025, 150% of pre-industrial levels.[3,4] These levels are unprecedented in human history; the last time atmospheric CO_2 concentrations were this high was approximately 3 million years ago. This dramatic rise in CO_2 amplifies the atmospheric greenhouse effect, driving higher global temperatures. Warming at these levels, contributes to a range of environmental impacts, including melting of glaciers, ocean acidification and an increase in wildfires[5].[4] These effects threaten ecosystems, global weather patterns, and human livelihoods. To address this escalating crisis, the Intergovernmental Panel on Climate Change (IPCC) has emphasized the urgent need to limit global warming to 1.5 °C to prevent the severe consequences of climate change.[6] However, current policies and mitigation efforts are falling short. Projections from the Climate Action Tracker indicate that existing global policies could lead to a temperature rise of approximately 2.7 °C above pre-industrial levels, with significant gaps in both 2030 targets and implementation efforts (Figure 1.1).[7] These alarming trends highlight the necessity for immediate and comprehensive strategies to limit CO_2 emissions. Consequently, efforts to mitigate climate change have centred on reducing greenhouse gas (GHG) emissions through various strategies, including renewable energy adoption, energy efficiency

improvements, and carbon capture and storage (CCS) technologies.[8] Among these, CCS has emerged as a critical tool to reduce CO_2 emissions from point sources, such as power plants and industrial facilities. By capturing CO_2 at the source and preventing its release into the atmosphere, CCS has the potential to significantly contribute to achieving net-zero emissions targets.[8,9]

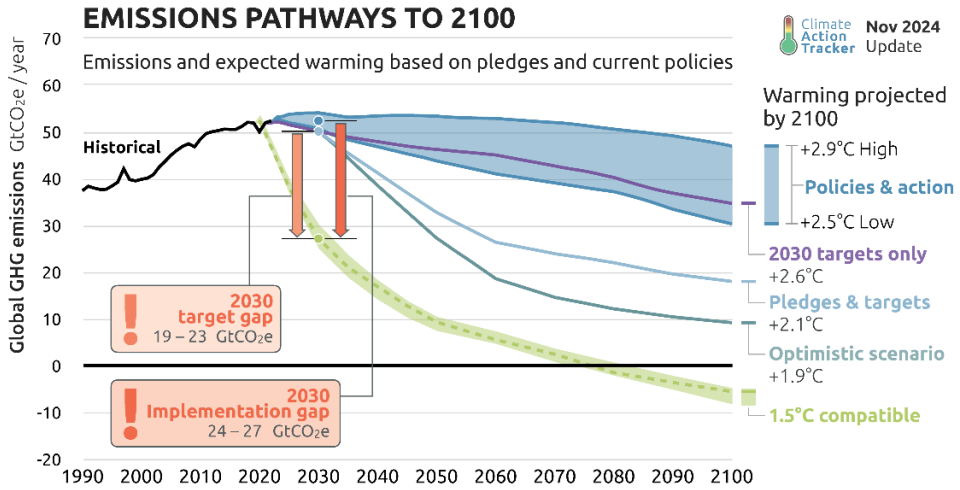

Figure 1.1. Projected global GHG emissions pathways, highlighting 2030 target and implementation gaps and warming projections.[7] Reproduced with the permission from © 2024 Climate Analytics and NewClimate Institute.

CCS involves capturing CO_2 from emission sources, transporting it to storage sites, and securely storing it to prevent its release into the atmosphere.[9] As shown in Figure 1.2, primary CCS approaches are[10]: 1) Pre-combustion capture, where fuel is converted into carbon monoxide (CO) and hydrogen (H_2), with CO further reacted with steam to produce CO_2 and H_2, enabling CO_2 separation prior to combustion; 2) Oxy-fuel combustion, which uses pure oxygen for combustion, resulting in exhaust gases with a high CO_2 concentration; and 3) Post-combustion, where CO_2 is extracted from flue gases after combustion, commonly implemented in existing facilities.[11] The captured CO_2 is compressed and used in enhanced oil recovery (EOR) or stored underground.[8]

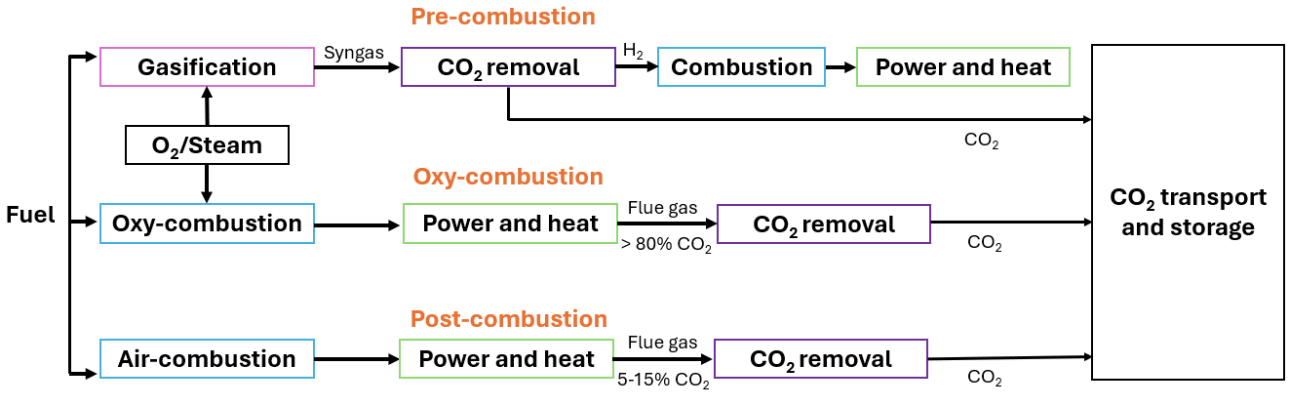

Figure 1.2. Different pathways for CO_2 capture.[12,13]

Among various carbon capture technologies, post-combustion carbon capture stands out as the most widely adopted globally, owing to its advanced maturity and seamless integration into existing power plants with minimal modifications. Nonetheless, the efficiency of any carbon capture system is significantly influenced by the composition of the flue gas and the properties of the capture medium, particularly its selectivity and stability.[14] Flue gas typically contains a mixture of components such as SO_x, NO_x, water vapor, and O_2 (Table 1.1), necessitating careful optimization of the CO_2 separation method and the materials used to ensure effective and stable performance.[15]

Table 1.1. Common composition of key components in different flue gases, expressed on a wet basis. Reprinted from ref.[15] with permission from © 2019 Royal Society of Chemistry.

Components	Pulverized coal	Waste incineration	Coal-fired IGCC	Natural gas-fires CC	Cement rotary kiln
O_2 (vol%)	6	7-14	12	14	7
N_2 (vol%)	76	Balance	66	76	59
CO_2 (vol%)	11	6-12	7	3	19
H_2O (vol%)	6	10-18	14	6	13
Ar (vol%)	1	1	1	1	1
SO_2 (ppm)	300-5000	200-1500	10-200	-	5-1200
NO_x (ppm)	500-800	200-500	10-100	10-300	100-1500

1.2. Technologies for CO_2 Capture

Many technologies are used for post-combustion carbon capture (Figure 1.3), including (i) absorption,[16,17] (ii) adsorption,[18] (iii) membranes,[19] and (iv) cryogenic separation[20]. As of 2024, a total of 628 large-scale CCS facilities have been established worldwide, including 50 operational, 44 under construction, and the rest in various phases of development.[21] Among these, amine scrubbing remains the most widely adopted method in commercial applications.[22] However, liquid amine absorbents suffer from high regeneration cost, low thermal stability and cause equipment corrosion.[23] Moreover, they form heat stable salts with O_2 and SO_2, which limits both their efficiency and lifetime.[15,24,25] To address these issues, a wide variety of materials, such as zeolites, carbons, clays, basic oxides, metal organic frameworks (MOFs) and supported amines have been developed[26–28] and successfully used in many industries (Table 1.2). While still in the developmental stage, solid amine adsorbents, particularly, show significant promise for low-temperature carbon capture due to their high selectivity, superior adsorption capacity, and ease of regeneration.[29–31]

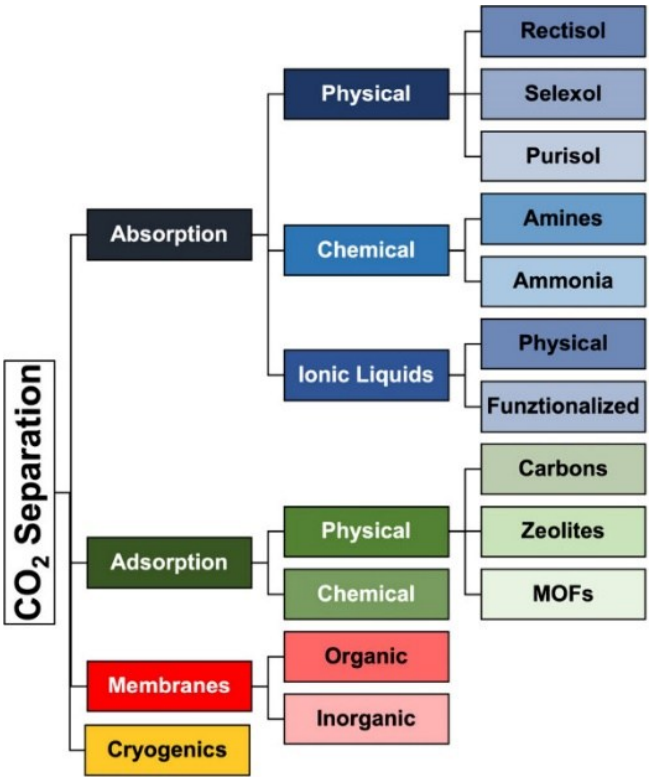

Figure 1.3. Classification of CO_2 capture techniques. Reprinted from ref.[14] with permission from © 2024 American Chemical Society.

Table 1.2. Adsorption technologies for post-combustion CO_2 capture used in industries globally. Reproduced from ref.[28] with permission from © 2020 Royal Society of Chemistry.

Project	Feed Flow Rate	Adsorbent(s)	Process	Reactor	CCR (%)	CP (%)	Energy	Sources	Country
Single-stage VPSA	46 N m^3 h^{-1} (dehydrated)	Zeolite 5A	VPSA	Fixed bed	79	85	2.37 MJ_e kg^{-1}	Power generation	China
Two-stage VPSA	35 N m^3 h^{-1} (dehydrated)	Zeolite 13X APG & activated carbon beads	VPSA	Fixed bed	90.2	95.6	2.44 MJ_e kg^{-1}	Power generation	China
DR-VPSA	100 N m^3 h^{-1} (dehydrated)	Activated carbon	VPSA	Fixed bed	44.6	87.5	3.52 MJ_e kg^{-1}	Power generation	Poland
ASCOA-3	330 N m^3 h^{-1}	Zeolite (zeolum F9)	VSA	Fixed bed	80	90	0.44 MJ_e kg^{-1}	Steel	Japan
TEPCO's two-stage VSA	1000 N m^3 h^{-1} (dehydrated)	Ca–X zeolite	PTSA/VSA	Fixed bed	90	99	2.02 MJ_e kg^{-1}	Power generation	Japan
KIERDARY	35,000 N m^3 h^{-1}	K_2CO_3-based sorbent	TSA	Fluidized bed	80	95	4.0–5.0 MJ_{th} kg^{-1}	Power generation	Korea
ADAsorb	0.38 kg s^{-1}	Amine-based ion exchange polymer	TSA	Three-staged fluidized bed	90	89.4	4.75 MJ_{th} kg^{-1}	Power generation	USA
RTI's TSA	—	PEI-based sorbent	TSA	Fluidized bed	90	—	2.4 MJ_{th} kg^{-1}	Cement	USA
KCC	1000 N m^3 h^{-1}	Amine-coated porous material	VTSA	Moving bed	75	95	1.3 MJ_e kg^{-1}	Power generation	Japan
SRI's ACS	120 m^3 h^{-1}	Carbon beads	TSA	Moving bed	67	93	—	Power generation	USA
TDA's SMB	0.63 kg s^{-1}	Alkalized alumina	TSA	Simulated moving bed	—	—	—	Power generation	USA
VeloxoTherm	—	Diamine-tethered silica gel	RTSA	Rotary wheel	—	90	1.5 MJ_e kg^{-1}	Power generation	Canada

1.3. Amine-Containing Solid Adsorbents

1.3.1 Nature of Support

Amine-containing solid adsorbents are promising material for CO_2 capture as they combine the structural stability and high porosity of solid support materials with the chemical specificity and reactivity of amine groups.[32] The selection of the appropriate support is crucial for optimizing the performance and to some extent the stability of these adsorbents.

Among silica supports, Santa Barbara Amorphous (SBA-15)[33–49] and Mobil Composition of Matter (MCM-41)[37–39,44,49–61] and other mesoporous silicas have attracted significant attention due to their large surface area, high pore volume, and the ability to tailor their pore sizes with a narrow distribution.[62] These attributes are crucial, as they facilitate high amine loadings within the adsorbent structure without compromising amine accessibility.[63] Advancing further, pore-expanded alumino-silica (PE-$AlSiO_2$)[64] support represents a significant enhancement in adsorbent materials by integrating the beneficial properties of alumina and silica. The incorporation of alumina enhances the hydrothermal and chemical stability of the material, while silica reinforces the structural integrity and mechanical strength.[64,65] Additionally, the pore expansion of supports not only increases the surface area available for amine loading but also promotes rapid diffusion of CO_2 molecules to the active sites, thereby optimizing the adsorption kinetics.[60,63,66] These attributes make PE-$AlSiO_2$ exceptionally effective for industrial CO_2 capture applications, where robustness and efficiency are paramount.

1.3.2 Synthesis

Silica supports are synthesized using surfactants as structure-directing agents.[67] Specifically, cationic surfactants are used for MCM-41 synthesis[68], while block copolymers are used for SBA-15[69] (Figure 1.4). These surfactants facilitate the orderly arrangement of mesopores by forming micelles around which the silica source, typically tetraethyl orthosilicate (TEOS), condenses to form the mesoporous

framework. The synthesis is performed under carefully controlled acidic or basic conditions, enabling the precise tailoring of pore characteristics. Following the initial mixing, the resultant mixtures are aged at controlled temperatures, allowing for the development of well-defined mesostructures. Post-aging, the particles are separated through filtration, dried and subsequently calcined at *ca.* 500 °C. This calcination step is crucial as it removes the organic templates, leaving behind a pure silica structure.[67] For the synthesis of pore-expanded PE-$AlSiO_2$, a similar methodology is used but is augmented by the inclusion of an alumina source, such as aluminum isopropoxide, alongside the silica source. An expanding agent, such as dimethylhexadecylamine (DMHA), is introduced prior to the aging process to increase the pore size, followed by a final calcination step.[64]

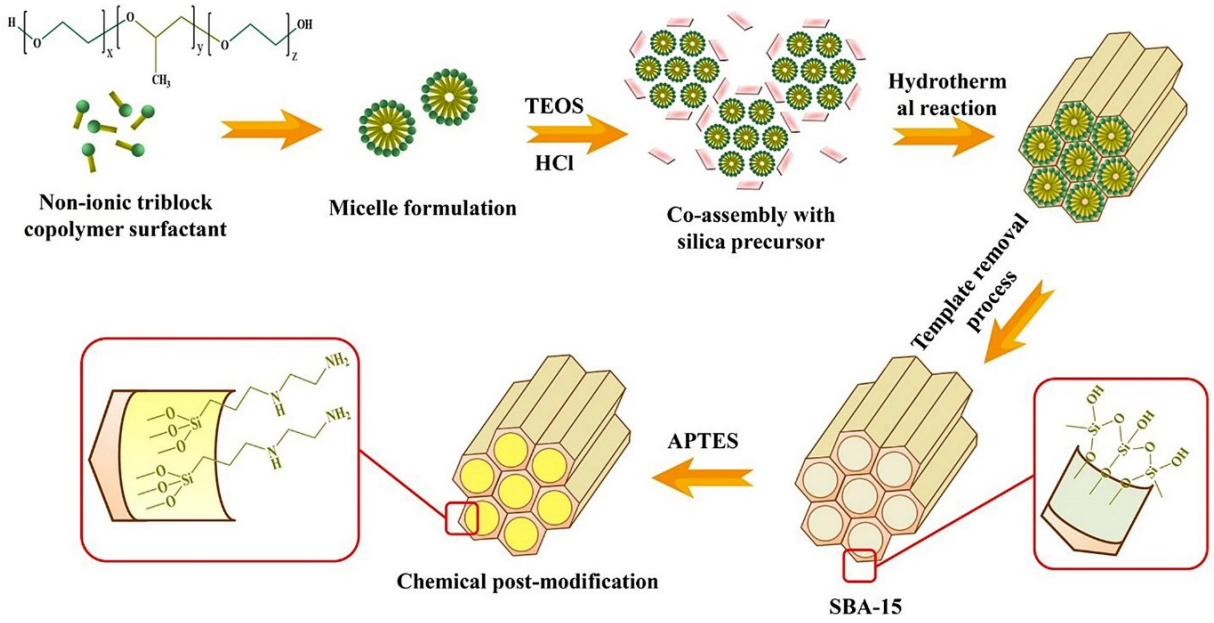

Figure 1.4. Schematic for synthesis of SBA-15 mesoporous silica using a Pluronic P123 surfactant, followed by amine grafting. Reprinted from ref.[70] with permission from © 2024 Springer Nature.

Following the synthesis and calcination of mesoporous supports, the subsequent step in developing amine-based adsorbents involves the immobilization of amine functional groups onto these structured supports. This is typically achieved through two principal methods: grafting[66] and impregnation[71,72] (Figure 1.5). Both techniques are designed to enhance the interaction between CO_2 and the adsorbent by securely anchoring amine groups to the robust silica framework. Grafting

involves the covalent bonding of amine-containing silanes to the surface of a porous support, creating strong chemical bonds that enhance both thermal stability and adsorption kinetics. A range of silanes, such as aminopropyltrimethoxysilane (APTMS),[40,47,61,73–77] N-[3-(trimethoxysilyl)propyl]ethylenediamine (TMPEDA),[78–80] and 2-[2-(3-trimethoxysilylpropylamino)ethylamino]ethylamine (TRI),[50,51,60,61] are used as grafting agents to functionalize solid supports. As illustrated by Hiyoshi *et al.*,[81] TRI, is particularly advantageous due to its high amine density, which significantly enhances CO_2 capture capacity. Furthermore, TRI-grafted SBA-15 demonstrates stable performance over multiple adsorption-desorption cycles, making them suitable for practical CO_2 capture applications.

In contrast, impregnation leverages non-covalent interactions, such as hydrogen bonding, to immobilize polyamines on the support. This approach is known for achieving high CO_2 adsorption capacities due to the substantial amine density of the polyamines. Polyethyleneimine (PEI),[34,37,44,46,79,82–95], is particularly favored due to its availability in wide range of molecular weights, high amine content, and cost-effectiveness, making it economically viable choice.[96] Additionally, PEI's highly branched molecular structure enhances its van der Waals interactions with the support, thereby improving its stability over multiple regeneration cycles. Conversely, smaller polyamines like tetraethylenepentamine (TEPA),[34,36,44,46,49,54,57,77,87,92,97–106] diethylenetriamine (DETA),[37,44,46,107] ethylenediamine (EDA),[44,45,47,54,57,58] pentaethylenehexamine (PEHA),[38,39,52,57,106,108–110] triethylenetetramine (TETA),[44,47,106,111] are used for their high amine loading and rapid kinetics, which enhance the overall CO_2 adsorption efficiency. However, these smaller polyamines tend to undergo higher leaching, primarily due to their weaker van der Waals interactions with the support.[112]

Both grafting and impregnation techniques have been rigorously explored to optimize CO_2 capture performance. While grafting ensures robust chemical stability and functional integrity under operational conditions, impregnation methods, offer the flexibility to achieve high amine content and superior adsorption capacities.[31,96,113]

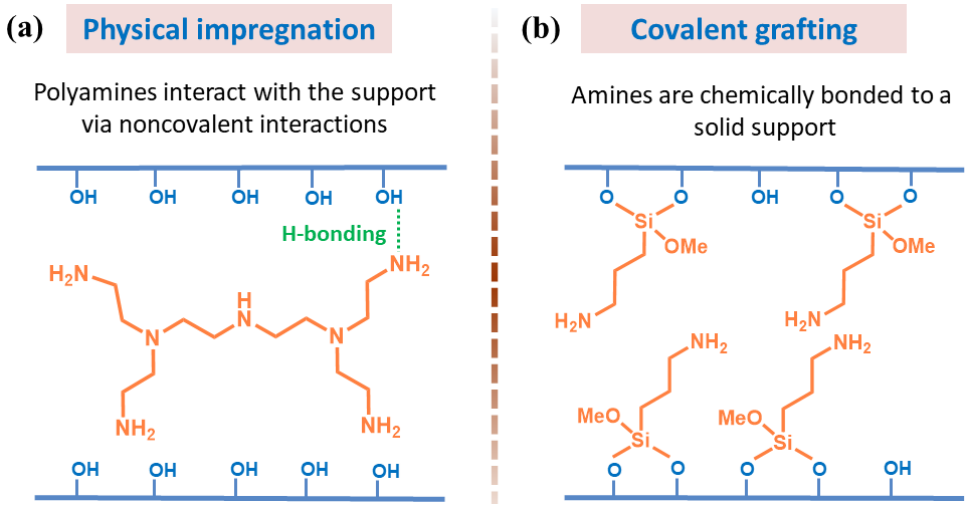

Figure 1.5. Schematic representation of amine-based adsorbents with (a) physical impregnation and (b) covalent grafting.

1.3.3 CO_2-Amine Chemistry

Once amine-functionalized silica adsorbents are synthesized, a thorough understanding of their CO_2 adsorption mechanisms is critical to further enhance their efficacy.[112,114] Specifically, these adsorbents show selective chemical bonding between the amine groups and CO_2 molecules, which interact differently under dry and wet conditions.[96] Under dry conditions, each CO_2 molecule can react with either two primary amines, two secondary amines, or one primary and one secondary amine to form ammonium carbamate. This interaction is illustrated by chemical Eq. 1.1. In contrast, wet conditions modify the reaction pathway, where a single amine group reacts with CO_2 and water to yield bicarbonate along with carbamate (Eq. 1.2).[115–117]

$$2\,RNH_2 + CO_2 \rightleftharpoons RNHCO_2^- RNH_3^+ \qquad \text{Eq. 1.1}$$

$$2\,RNH_2 + CO_2 + H_2O \rightleftharpoons RNH_3^+ + HCO_3^- \qquad \text{Eq. 1.2}$$

Tertiary amines show distinct CO_2 adsorption behavior compared to primary and secondary amines, due to their different amine structures. Unlike primary and secondary amines, tertiary amines lack a hydrogen atom next to nitrogen, which is essential for the direct formation of carbamates under

dry conditions. Consequently, they do not readily form carbamates under moisture-free conditions. Nonetheless, in the presence of water vapor, water molecules provide a proton that transforms the tertiary amine into an ammonium ion, thus facilitating the capture of CO_2 through bicarbonate formation (Eq. 1.3).[118] The reaction can be represented as follows:

$$R_3N + CO_2 + H_2O \rightleftharpoons R_3N^+ + HCO_3^- \quad \text{Eq. 1.3}$$

Such insights into the interaction dynamics of amine-functionalized silica adsorbents under different environmental conditions are pivotal for tailoring these materials to specific industrial applications, thereby optimizing their performance in CO_2 capture systems.

1.3.4 Advantages

Amine-functionalized adsorbents offer considerable advantages for CO_2 capture, primarily due to their high selectivity, which arises from specific chemical interactions between the amine groups and CO_2 molecules. This selectivity enables efficient CO_2 removal from various gas streams.[31] Additionally, these adsorbents exhibit a high adsorption capacity, significantly enhancing the overall efficacy of the CO_2 capture process.[63,119] Additionally, the regeneration process for amine-functionalized adsorbents generally requires less energy than traditional amine scrubbing technologies, thereby enhancing overall energy efficiency.[30,31] Notably, these adsorbents can be regenerated and reused multiple times without a significant loss of capacity.[120,121] Furthermore, the regeneration energy[122–124] and kinetics[125] of these adsorbents can be effectively modulated to optimize performance and economic viability. Moreover, these materials not only retain their performance in humid conditions, but their stability also increases in the presence of water vapor.[126,127] This characteristic is particularly beneficial for applications within flue gas environments, where water is a ubiquitous component,[128,129] and stability to moisture is essential. Collectively, these advantages (Figure 1.6) underscore the potential of amine-functionalized adsorbents as an efficient solution for overcoming challenges associated with CO_2 capture, thereby contributing to the reduction of CO_2 emissions.

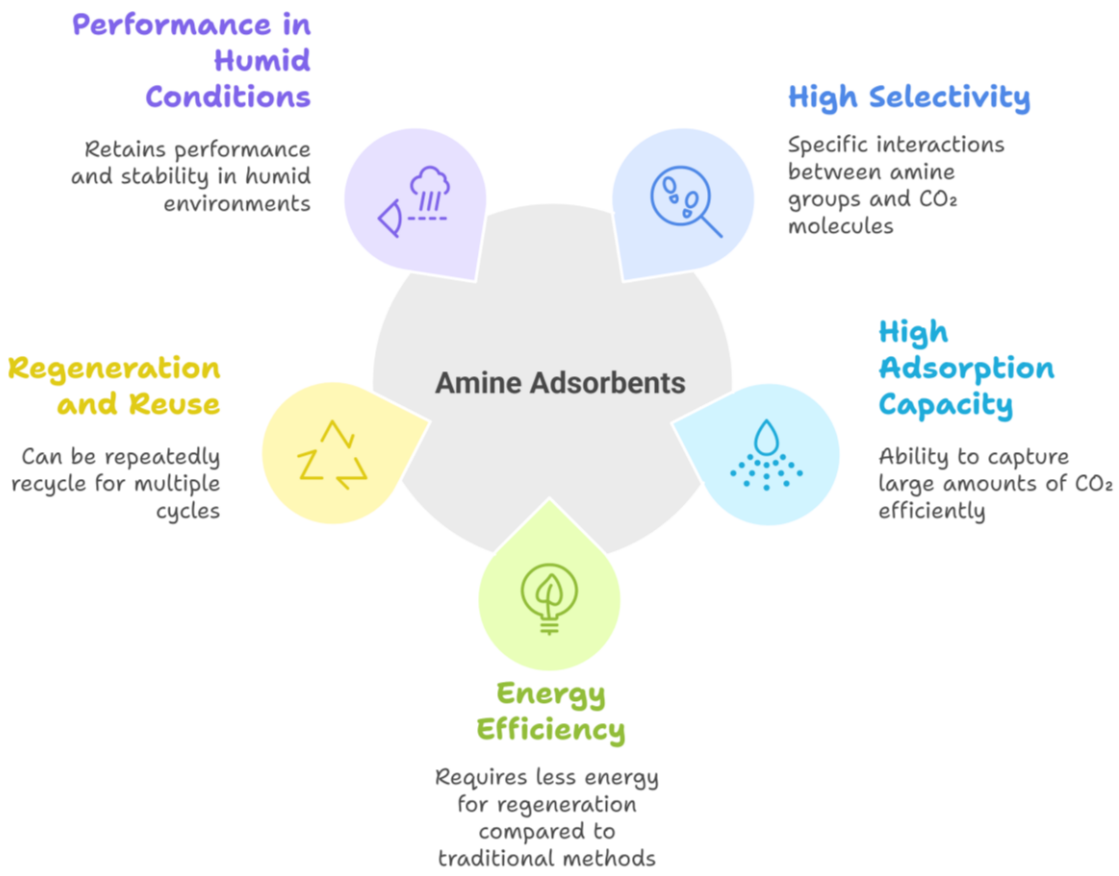

Figure 1.6. Advantages of amine-containing solid adsorbents.

1.3.5 Limitations and Research Gaps

While amine-functionalized adsorbents offer significant advantages for CO_2 capture, their performance is substantially influenced by the presence of sulfur dioxide (SO_2), oxygen, and water vapor in the feed gas. These components interact with the amines in complex ways that can either impede or promote the CO_2 uptake of the adsorbent, depending on the specific conditions.[15,114]

1.3.5.1 SO_2 Poisoning

A major limitation of amine-based adsorbents for CO_2 capture is their susceptibility to SO_2 poisoning[130–132], which is commonly present in industrial flue gases[129,133]. SO_2 reacts with primary (1°) and secondary (2°) amines to form zwitterion (Eq. 1.4)[15,134], which remain stable at the typical regeneration temperatures used for CO_2. Consequently, 1° and 2° amines get irreversibly poisoned by SO_2, hindering their ability to capture CO_2 effectively in subsequent cycles.[130,131,135] For example, when supported PEI and APTMS were exposed to SO_2 concentration as low as 20 ppm in a gas stream

containing 10% CO_2 balanced with N_2, there was a marked reduction in their CO_2 adsorption capacity (Figure 1.7). Notably, there was approximately 40% decrease in CO_2 uptake for both the adsorbents after just a single adsorption cycle. This degradation exacerbates overtime, with the adsorbents experiencing up to *ca.* 70% loss in CO_2 uptake after four regeneration cycles. Moreover, SO_2 uptake also decreased significantly during these cycles.[130] These observations highlight the high vulnerability of amine-functionalized adsorbents to even trace concentrations of SO_2 resulting in significant decrease in CO_2 uptake and durability of the adsorbent. This significantly hinders their use in industrial carbon capture applications.

$$R_1R_2NH + SO_2 \rightleftharpoons R_1R_2NH^+SO_2^- \qquad \text{Eq. 1.4}$$

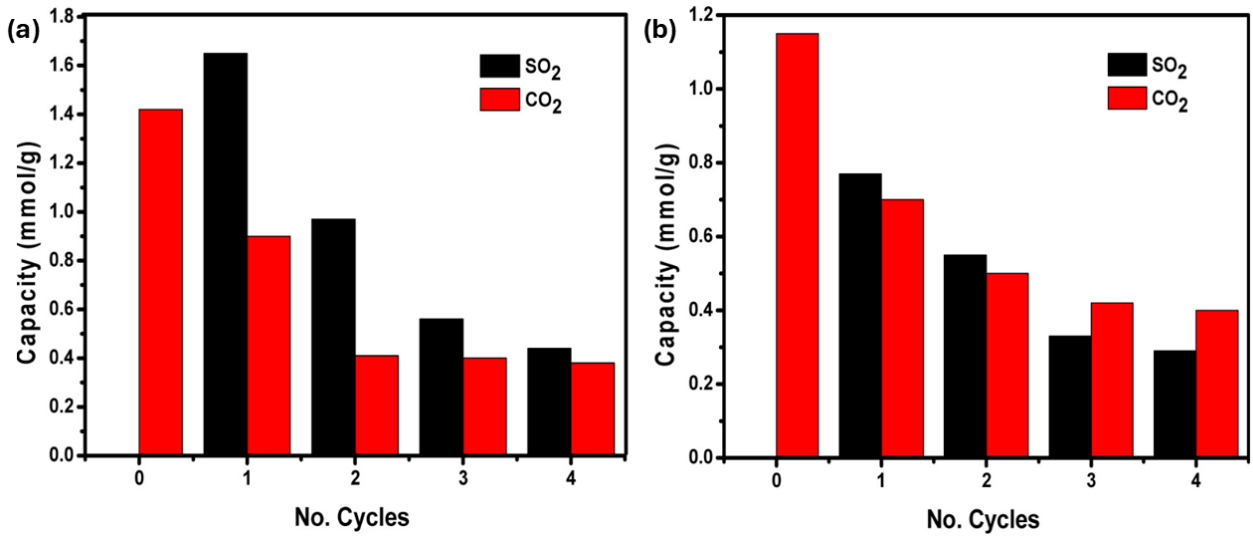

Figure 1.7. CO_2 and SO_2 uptake of supported (a) PEI and (b) APTMS over regeneration cycles. Reprinted from ref.[130] with permission from © 2024 American Chemical Society.

One strategy to prevent this deactivation involves the removal of SO_2 from exhaust gas prior to the CO_2 adsorption stage. Traditional methods like Wet Flue Gas Desulfurization (WFGD) using calcium carbonate, are widely used due to their cost-effectiveness and high efficiency at removing high levels of SO_2.[136,137] However, this method not only produce low-value by-products such as calcium sulfate but also faces challenges in reducing SO_2 concentrations below 500 ppm, which, in

turn, leads to increased operational costs.[138,139] To tackle these limitations, solid-supported adsorbents like MOFs,[140,141] porous polymers,[142–144] and zeolites,[145,146] have gained significant attention due to their non-corrosive nature and inherently low energy demands for regeneration. Despite their potential, the practical deployment of these materials is often restricted by high production costs and limited selectivity.[147–149] As an alternative, researchers used tertiary amine adsorbents, which can interact with SO_2 (even under dry conditions) due to higher acidity of SO_2 compared to CO_2, without reacting with CO_2.[130,150–158] For example, Tailor *et al.*[156] grafted N,N-dimethylpropyl amine onto pore-expanded MCM-41 (TER-PE-MCM-41), which showed exceptional selectivity. This was demonstrated by an immediate CO_2 breakthrough observed when the material was exposed to a gas mixture containing 0.1% SO_2/N_2 and 20% CO_2/He with the same flow rate, under both dry and humid conditions. This finding led to further investigations into alternative tertiary amine systems, such as methylated PEI[155,157] (Figure 1.8), which have been used to selectively adsorb SO_2 from mixed gas streams composed of SO_2, CO_2, and N_2. These materials demonstrated significant potential for deep desulfurization of flue gas due to their low reactivity with CO_2 (Figure 1.9a), strong affinity for SO_2, and robust stability across multiple regeneration cycles (Figure 1.9b). Nevertheless, the methods used in these studies for synthesizing tertiary amines are complex and involve multi-step processes. Moreover, the concentrations of SO_2 used in these studies substantially exceed 20 ppm, raising concerns regarding the deactivation of the amines. In fact, to the best of our knowledge, none of the studies in literature focused on the removal of SO_2 concentrations below 50 ppm. This gap highlights the critical need for further research to adapt these innovative materials for typical environmental conditions and to streamline their production processes, thereby facilitating industrial applications.

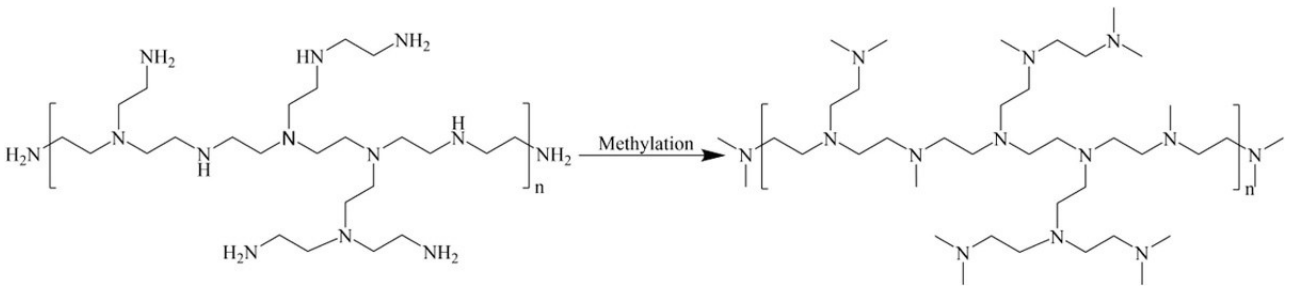

Figure 1.8. Schematic representation of the methylation of polyethylenimine (PEI) to produce methylated PEI with tertiary amine functionalities. Reprinted from ref.[157] with permission from © 2021 Elsevier.

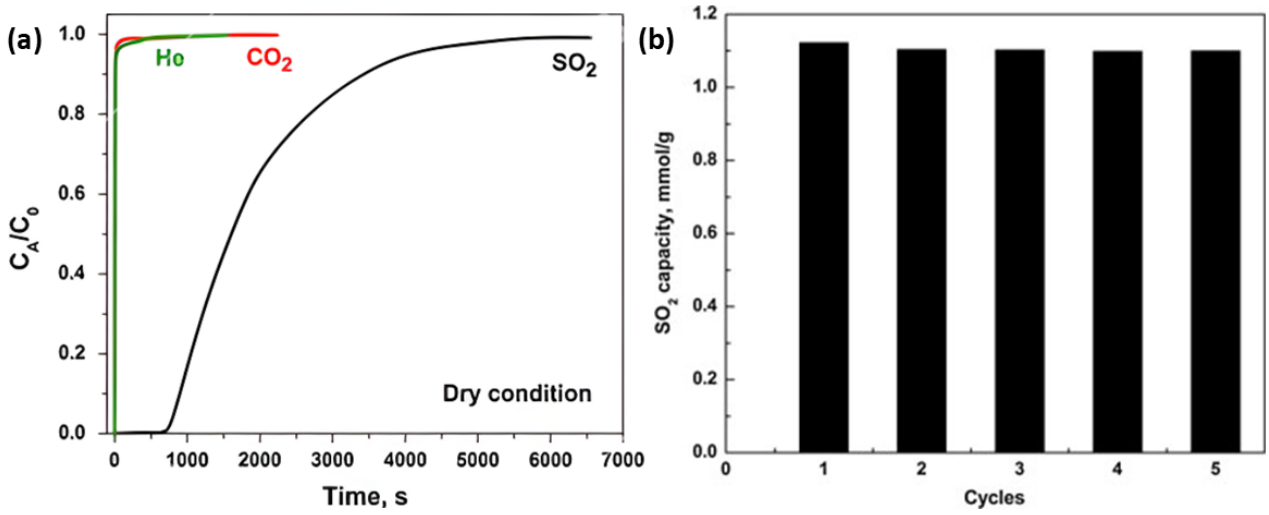

Figure 1.9. (a) Breakthrough curves for TER-PE-MCM-41 in a gas mixture of 0.05% SO_2, 10% CO_2, 49.95% N_2, and 40% He; (b) Regeneration cycles for SO_2 adsorption (0.1% SO_2 in N_2) at 40 °C and regeneration at 130 °C. Reprinted from ref.[156] with permission from © 2014 Elsevier.

1.3.5.2 Oxidative Degradation

Another significant shortcoming of amine-based adsorbents is their vulnerability to oxidative degradation. In a typical cycle of CO_2 adsorption at ambient temperature and CO_2 desorption at elevated temperature (typically at 100 °C or above), these adsorbents are very susceptible to oxidative degradation either during the adsorption when oxygen is present in the feed gas, or during the cooling stage following desorption, where air is used as a cost-effective coolant. The visible evidence of oxidatively degraded adsorbents is the vivid brown color. It is worth mentioning that, during adsorption, the presence of water vapor (H_2O) and CO_2, along with a lower partial pressure of O_2 and

low temperature, significantly reduces the risk of degradation. This stabilizing effect arises primarily from the fast formation of ammonium carbamate and bicarbonate when CO_2 reacts with the amines, effectively protecting them from oxidative degradation. Furthermore, water enhances the oxidative stability of the adsorbents through hydrogen bonding with the amine groups.[159–161]

Two main parameters that control the rate of amine oxidation are the temperature and the oxygen concentration. Oxidative degradation accelerates significantly when flowing air (21% O_2/N_2) is used to cool the adsorbent following the regeneration step, to bring it to the starting point of the adsorption-desorption cycle. The fact that the adsorbent temperature as its highest, *i.e.* about 110 °C, when the material is exposed to air, exacerbates the oxidation process. As demonstrated by Yogo *et al.*,[162] for TEPA loaded mesoporous silica foam (MF), higher loss of CO_2 uptake was observed at higher partial pressure of oxygen or temperature regardless of the TEPA loading on the support, as illustrated in Figure 1.10. For example, for 60% TEPA impregnated MF, increasing the partial pressure of O_2 from 5% (relevant to the typical oxygen content in the feed gas) to 21% O_2/N_2 at 100 °C for 18 h resulted in loss of CO_2 uptake capacity by 27% and 85%, respectively. Further corroborating these results, similar trends were observed in PEI impregnated adsorbents.[159,163] Moreover, the pronounced effect of temperature on oxidative instability was evident, as exposure of the adsorbent to O_2 at 80 °C and 100 °C resulted in decrease in CO_2 uptake capacity by 38 and 88%, respectively.[162] This trend aligns with findings reported in numerous research papers, which suggest that oxidation at higher temperatures leads to more severe degradation of adsorbents.[159,162–165] Empirical studies, such as those by Heydari-Gorji and Sayari[159], further reinforce these observations. They reported the complete oxidative deactivation of PEI-impregnated mesoporous silica when exposed to dry air at 120 °C for 30 h, culminating in a total loss of CO_2 uptake capacity.

These findings underpin the importance of addressing oxidative degradation of amines, which significantly undermines the performance of the adsorbent over extended periods. Otherwise, the need for frequent replacements of the adsorbents not only escalates operational costs but also

negatively impacts the economic viability and sustainability of using amine-based adsorbents in industrial applications[166,167]. Therefore, mitigating this degradation is essential for maintaining efficiency and reducing the lifecycle costs of carbon capture.

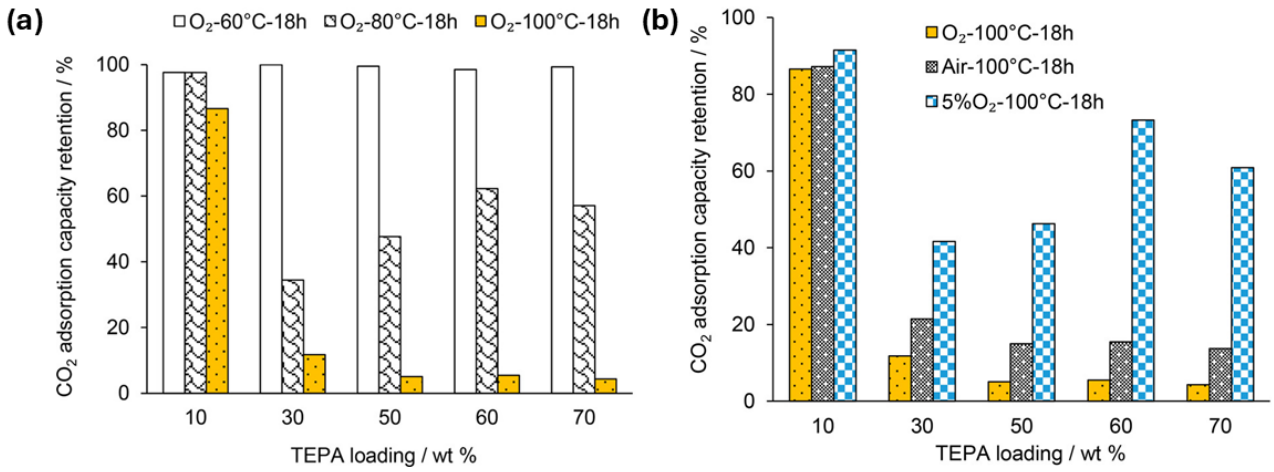

Figure 1.10. Effect of (a) temperature and (b) partial pressure of oxygen on CO_2 adsorption capacity retention of TEPA-loaded MF. Adapted from ref.[162] with permission from © 2019 American Chemical Society.

To counter these adverse effects, several strategies have been explored, including the integration of metal chelators, based on the working hypothesis that transition metal ion initiate and/or catalyze the degradation process.[160,168,169] Another effective strategy is the use of sterically hindered amines.[164] This substitution prevents alpha-hydrogen abstraction, which is believed to be the initial stage of the whole oxidative degradation process, thus enhancing oxidation stability of the adsorbent.[170] Furthermore, the incorporation of hydroxyl-rich additives has gained attention for its protective effects against oxidation.[160,171,172] Of these, hydroxyl-rich additives have proven particularly effective in enhancing the stability of amine adsorbents against oxidative degradation.[160,170,171,173] A widely accepted mechanism says that the presence of hydroxyl groups can facilitate hydrogen bonding with amines, creating a protective barrier that shields the adsorbents from oxidative degradation.[170]

In this context, Chuang and coworkers[171] used polyvinyl alcohol (PVA) as a support for PEI to investigate its potential for enhancing the oxidative stability. The experimental methodology was systematically divided into different stages, starting with pretreatment of the adsorbent. This was followed by the adsorption of CO_2, which was performed at 40 °C for 10 min under 15% CO_2 balanced in air. Subsequently, argon was purged to remove adsorbed gases, followed by temperature-programmed desorption (TPD). Then a degradation test was performed at 130 °C for 30 minutes using 15% CO_2 in air, with the process concluding with a cooling phase. In these adsorption-desorption cycles, PEI-PVA material showed enhanced oxidation stability compared to PEI impregnated silica support (Figure 1.11), which was attributed to hydrogen bonds between amines of PEI and hydroxyl groups of PVA in PEI-PVA adsorbent. However, it is important to note that the conditions used during the degradation stage do not mimic the air-cooling process of practical operations, thereby limiting the direct applicability of these results. Furthermore, the CO_2 adsorption capacity of PVA-PEI (1.31 mmol/g) was 35% less than the silica-supported PEI (2.01 mmol/g). This highlights a common compromise in enhancing the oxidation stability of an adsorbent, which is often achieved at the expense of a reduced CO_2 uptake capacity.

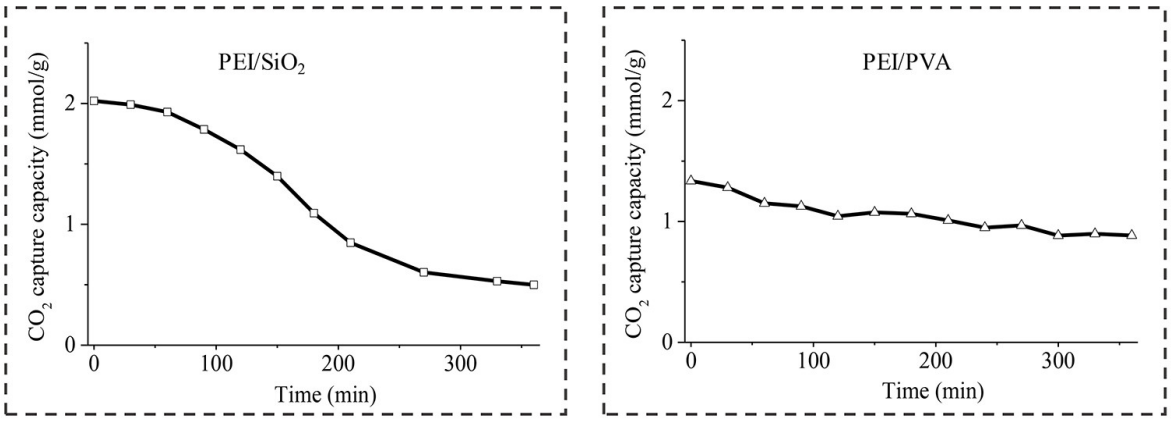

Figure 1.11. Comparison of decline in CO_2 uptake of PEI supported silica and PVA adsorbents over time. Reprinted from ref.[171] with permission from © 2017 American Chemical Society.

In another highly relevant study by Choi *et al.*,[160] their findings indicated the occurrence of similar limitations. Their strategy for enhancing oxidative stability involved the use of chelators to

bind metal ions and simultaneously the functionalization of PEI with epoxides (1,2-butylene oxide, shown in Figure 1.12), which is essentially grafting of the protective hydroxyl group to amine. It is important to note that although this method indeed led to significant improvement in oxidation resistance, it also succumbed to the drastic decrease in CO_2 uptake capacity, by approximately 54.6%. This decrease in CO_2 uptake capacity was primarily attributed to the transformation of more CO_2-reactive primary amines into less reactive secondary and tertiary amines. It is worth commenting that the simulated flue gas employed by Choi *et al*: 3% O_2, 15% CO_2, and 10% H_2O, was considerably mild and thus far from the situation typically encountered in the realistic air-cooling process of adsorbents, where atmospheric oxygen is 21% and the stabilizing effects of CO_2 and H_2O are absent.

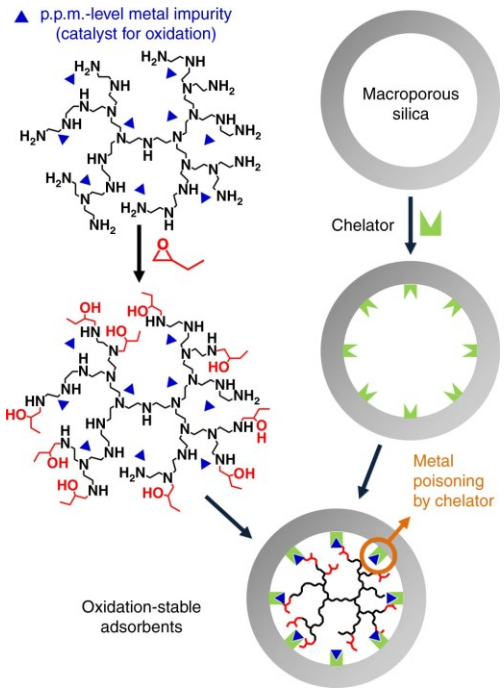

Figure 1.12. Schematic illustration use of metal chelators and functionalization of PEI with epoxy butane to enhance oxidative stability and reduce metal poisoning in adsorbents. Reprinted from ref.[160], according to Creative Commons Attribution 4.0 International (CC BY 4.0).

Meanwhile, a growing body of research on enhancing the oxidative stability of amine-based adsorbents reveals that the incorporation of hydroxyl-containing additives, either through functionalization or use as support, can improve their resistance to oxidation.[160,170,171,173] However, this advancement also highlights the persistent challenges that impede the practical deployment of

these materials. A critical bottleneck is that while the addition or functionalization of PEI with hydroxyl groups does enhance oxidative stability, it frequently results in a diminished CO_2 capture capacity. This reduction underscores the crucial need to develop adsorbents that maintain both high oxidative stability and high CO_2 uptake capacity, pointing to the essential balance required between durability and performance. Moreover, the experimental conditions used in these studies often do not correspond to the severe environments typically encountered during the air cooling of adsorbents in industrial settings. Additionally, there is a lack of consistency in experimental conditions across different studies, which complicates direct comparisons of various methodologies, such as hydroxyl group impregnation and functionalization. This inconsistency hinders a comprehensive evaluation of the relative effectiveness of each approach, creating significant barriers to progress in the field.

1.3.5.3 RH - Pore Size – CO_2 Uptake Relationships

Having explored the effect of SO_2 and O_2 on amine-based adsorbents, it is equally important to consider the impact of other components on adsorbent performance. Interestingly, in contrast to the detrimental effects of SO_2 and O_2 on CO_2 uptake and lifetime of the adsorbent, water vapor—a ubiquitous component of flue gas not only enhances CO_2 uptake[114] but also increase the stability of the adsorbent against urea formation.[126] Researchers propose that the water can act as a lubricant, improving the mobility of amine polymers and allowing better access to active sites.[174,175] Additionally, the presence of water enables the formation of bicarbonate, changing the CO_2–amine chemistry from a 1:2 to a 1:1 stoichiometry. This change allows each CO_2 molecule to interact with one amine molecule instead of two, significantly enhancing the adsorption capacity.[61,115,176–178] Nevertheless, in some cases, excessively high RH levels can reduce efficiency.[114]

Given its positive impact, researchers investigated the effect of RH on CO_2 uptake and found that the adsorbent achieve maximum uptake at a specific RH.[174,179,180] As illustrated in Figure 1.13a, lysine (MOF-808-Lys) and tris(3-aminopropyl)amine (MOF-808-TAPA), covalently bonded separately to MOF-808, showed an increase in CO_2 uptake as the RH increases from 0% to 50%.

Notably, MOF-808-TAPA showed a significant enhancement in CO_2 uptake, rising from 0.454 mmol/g at 0% RH to 0.872 mmol/g at 50% RH when exposed to a 400 ppm CO_2 in N_2 gas stream at 25 °C.[178] Similarly, Figure 1.13b demonstrates that CO_2 uptake of a PEI impregnated adsorbent increases with RH, reaching its maximum at 30% RH, and then decreases thereafter. Nonetheless, H_2O uptake continues to rise with increasing RH. This indicates that at higher relative humidity, more pores are occupied by water molecules, thereby limiting the availability of sites for CO_2 adsorption.[174] Furthermore, Figure 1.14 shows increase in CO_2 uptake by 16, 22, and 74% at RH levels of 27, 61, and 74%, respectively, compared to dry conditions for APTMS grafted pore-expanded MCM-41 support (MONO-PE-MCM-41). Interestingly, there was dramatic increase in CO_2 uptake at 74% RH, which was attributed to water capillary condensation.[61]

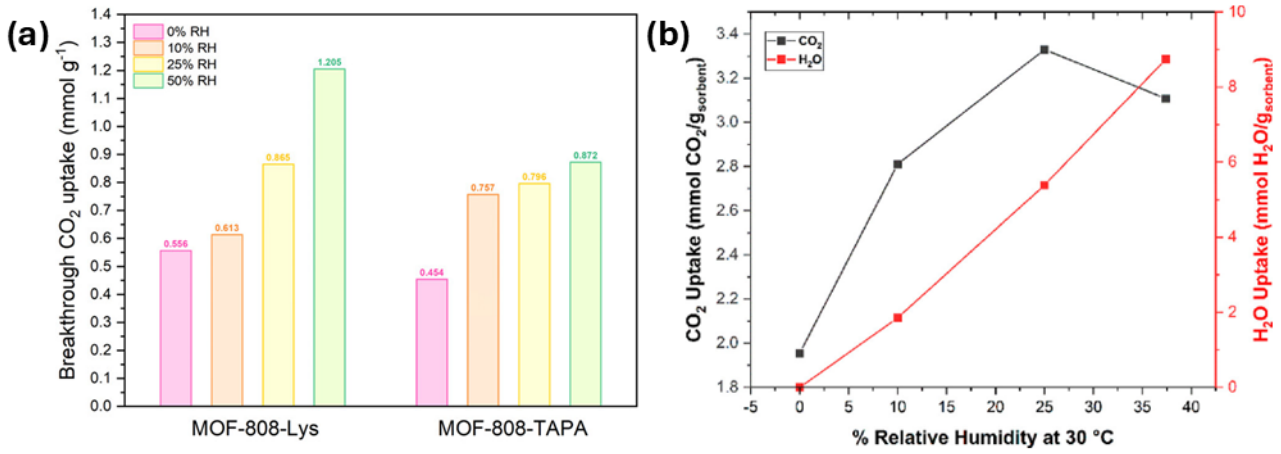

Figure 1.13. CO_2 and H_2O uptake as a function of RH for (a) polyimide COF at 25 °C and (b) PEI impregnated single-walled zeolite at 30 °C. (a) Reprinted from ref.[178] with permission from American Chemical Society (2024). (b) Reprinted from ref.[174], according to Creative Commons Attribution 4.0 International (CC BY 4.0).

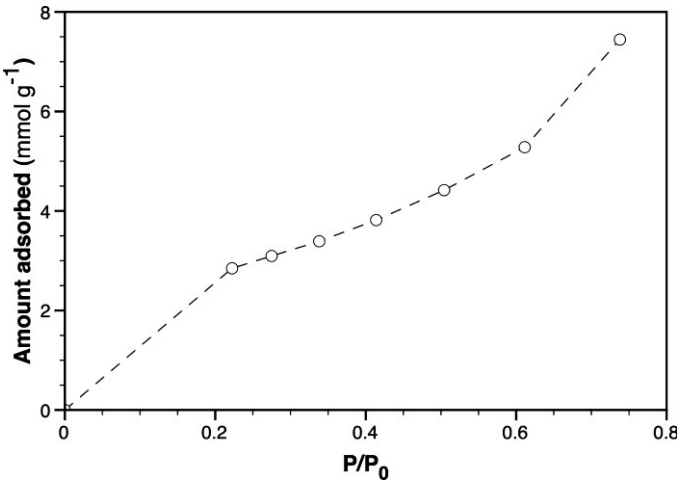

Figure 1.14. H_2O adsorption isotherm for MONO-PE-MCM-41 at 25 °C. Reprinted from ref.[61] with permission from © 2008 American Chemical Society.

Consequently, to achieve optimal CO_2 adsorption, the RH of the feed gas should be adjusted to align with the adsorbent's optimal RH. However, these adjustments may not always be economically feasible. A more practical strategy may lie in tuning the adsorbent itself. For example, MONO-PE-MCM-41 showed a dramatic increase in CO_2 uptake at the partial pressure of water capillary condensation.[61] Given the strong dependence of capillary condensation on pore size, strategically tailoring the pore size of amine-containing adsorbents can offer a means to align the water capillary condensation pressure with the water vapor partial pressure of the feed gas, thereby facilitating optimal CO_2 adsorption. Exploring this interplay between pore size, relative humidity, and CO_2 uptake offers valuable insights for developing adsorbents capable of maximizing CO_2 capture efficiency without requiring energy-intensive humidity control. Nonetheless, to the best of our knowledge, such correlations have not been documented in existing literature. This knowledge gap is critical, as understanding these relationships not only enhances CO_2 capture efficiency but also improves economic feasibility, both of which are essential for achieving effective carbon mitigation. Given that current CO_2 capture efforts do not align with the scale required to meet global mitigation targets[181], bridging this gap is crucial in advancing industrial carbon capture efforts in line with the goals set under the Paris Agreement[182].

1.4. Thesis Structure

This thesis addresses key challenges in optimizing amine-based adsorbents for CO_2 capture, focusing on the effects of SO_2, O_2, and water vapor. By mitigating adverse interactions and leveraging beneficial ones, this work aims to enhance CO_2 uptake. The research is structured around three primary challenges: SO_2 poisoning, oxidative degradation, and the need to maximize CO_2 uptake by tailoring adsorbent properties to specific RH conditions (Figure 1.15). Each challenge is systematically investigated to develop solutions that directly or indirectly improve CO_2 uptake under industrially relevant conditions. The dissertation is organized into five chapters, beginning with an introduction that outlines the research scope and significance, followed by chapters addressing each challenge with proposed solutions, and concluding with findings and future directions for advancing carbon capture technologies.

Chapter 1: Introduction

This chapter provides the necessary background and foundation for the research presented in this thesis. It is divided into two main parts:

Part 1: Background, Challenges and Research Gap

This section discusses the urgency of addressing CO_2 emissions and the role of amine-containing solid adsorbents as a promising CCS solution. It includes the synthesis, support materials, and CO_2–amine interactions critical for optimizing adsorbent performance. Additionally, it highlights the key advantages of amine-based adsorbents, along with the primary challenges limiting their long-term stability and efficiency. These challenges define the existing research gap, emphasizing the need for innovative strategies to enhance adsorbent performance and durability.

Part 2: Instrumentation and Analysis

This section outlines the key analytical techniques used to characterize the synthesized adsorbents, including spectroscopic, thermal, and breakthrough analysis. It explains their role in assessing material structure, stability, and CO_2 uptake, while also addressing important considerations for data interpretation.

Chapter 2: SO_2 Poisoning

This chapter focuses on mitigating SO_2 poisoning in amine-based adsorbents by developing tertiary amine-functionalized materials with high SO_2 selectivity. These adsorbents act as preliminary filters, removing SO_2 and optimizing conditions for efficient CO_2 capture. The study focuses on a simple preparation method to develop effective adsorbents for low SO_2 concentrations, with potential industrial applications.

Chapter 3: Oxidative Degradation

This chapter addresses oxidative degradation in amine-based adsorbents, which reduces CO_2 uptake and lifespan. It explores enhancing oxidation stability using hydroxyl-containing additives like HES to preserve CO_2 capacity and improve resistance under accelerated oxidation conditions, particularly relevant during the cooling phase following adsorbent regeneration.

Chapter 4: Pore Size - RH - CO_2 Uptake Relationships

In this chapter, the relationship between pore size, RH, and CO_2 uptake is explored. By synthesizing supports with different pore sizes, this work aims to determine how these variables interact and influence CO_2 uptake through phenomenon such as water capillary condensation. The objective is to tailor the pore structure to optimize the adsorbent design for flue gas with specific RH levels, enhancing CO_2 uptake efficiency.

Chapter 5: Conclusions and Future Directions

The final chapter summarizes the research findings across all areas studied, emphasizing their contribution to advancing CO_2 capture technologies. It discusses the limitations of current studies, highlights potential improvements, and outlines directions for future research to further enhance amine-based solid adsorbents for carbon capture.

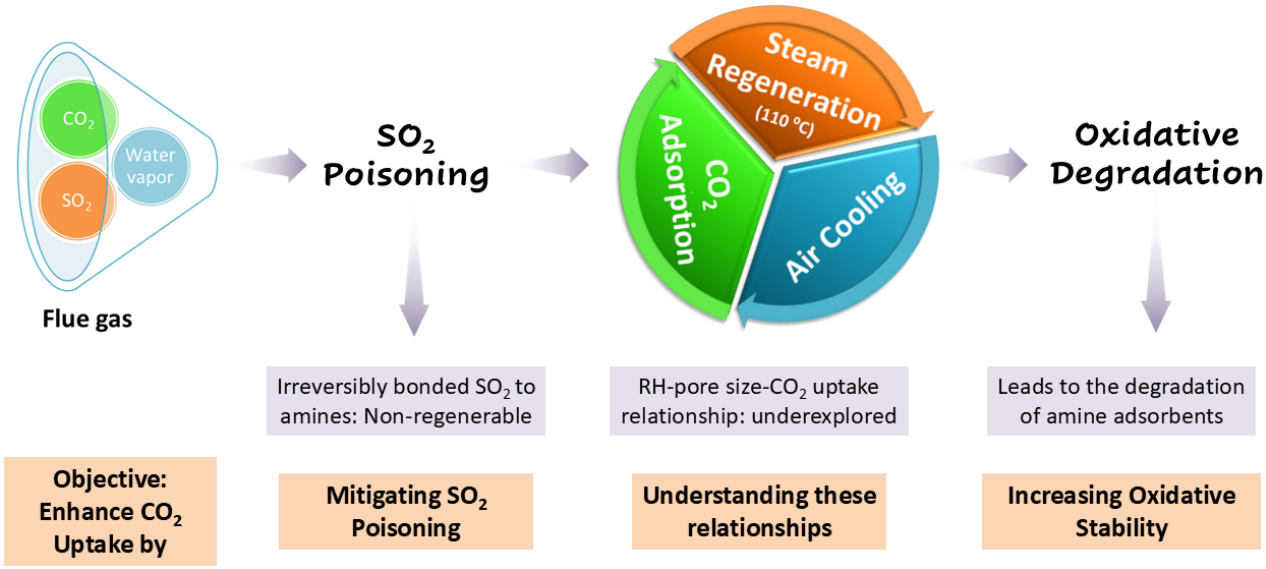

Figure 1.15. Schematic showing the limitations of amine-based adsorbents and the main objective of this study.

Part 2: Instrumentation and Analysis

1.6. Introduction

A range of analytical techniques were used to thoroughly characterize the adsorbent materials and assess their performance. Nuclear Magnetic Resonance (NMR) Spectroscopy offered vital insights into the molecular structure and dynamics of PEI, crucial for determining the functionalization and quantification of amines, as well as for identifying functional groups associated with oxidation. Infrared Spectroscopy (IR) complements this by probing molecular vibrations to confirm the presence and modifications of functional groups, particularly useful for monitoring changes during amine functionalization and oxidation. Nitrogen adsorption analysis was crucial in determining the porosity and textural properties of the materials, offering essential data on their adsorptive capabilities. Thermogravimetric Analysis (TGA) was used to measure CO_2 uptake under dry conditions, determine the nitrogen content, and evaluate the thermal stability of the materials. Dynamic Vapor Sorption (DVS) measured CO_2 uptake under humid conditions and water adsorption capacity of the adsorbents. This analysis facilitated detailed investigations into the relationships between CO_2 uptake, pore size, and relative humidity (RH) within the adsorbent materials. Finally, dynamic column breakthrough experiments using Mass Spectrometry (MS) provided detailed insights into CO_2 adsorption under humid conditions, as well as the identification of fragments formed during amine oxidation. In all, the analytical techniques significantly enhanced understanding of the adsorbent's properties. A detailed description of analytical tools and techniques are presented in the following sections.

1.7. NMR Spectroscopy

1.7.1. Principle

NMR spectroscopy is a powerful analytical technique that provides detailed information about the local chemical environment of molecules, thereby revealing structural changes within a molecule subject to chemical reaction or noncovalent molecular interaction. At the core of NMR spectroscopy

lies the intrinsic property of nuclear spin, which is characterized by the spin quantum number (I). Only nuclei with a nonzero spin ($I \neq 0$) show magnetic properties and can interact with an external magnetic field, making them NMR active. Examples include ^{1}H (proton) and ^{13}C (carbon-13), both of which possess a spin of $I = 1/2$. Put in an oversimplified analogue, these nuclei act like tiny bar magnets and once placed in an external magnetic field (B_0), they either align parallelly or anti-parallelly along the B_0 vector, with a population governed by the Boltzmann distribution. As shown in Figure 1.16, at thermal equilibrium, the lower-energy state is slightly more populated, making this distribution more stable since systems naturally favor lower energy configurations. For an individual nuclear spin, it precess around the B_0 vector. The precession frequency is known as the Larmor frequency and is given by the equation:

$$\nu_0 = \frac{\gamma_m B_0}{2\pi}$$

where:

- ν_0 is the Larmor frequency,
- γ_m is the gyromagnetic ratio.

To generate an NMR signal, a radiofrequency (RF) pulse matching the Larmor frequency is applied perpendicular to B_0. This pulse provides energy to the nuclei, causing some of them to jump from the lower-energy state to the higher-energy state. In returning to the Boltzmann equilibrium, which is also known as relaxation, the collective precession of the ensemble of tiny nuclei magnets induces an electrical response in detection circuit of a coil shape sitting next to the NMR tube in which the sample of interest is contained. Since the intrinsic frequency of the circuit is tuned by a combination of capacitor and inductance, exactly to the Larmor frequency of the nuclei of interest (*e.g.* ^{1}H and ^{13}C), this process is in resonance condition.

As a result of this relaxation of excited nuclear spins to Boltzmann equilibrium, the induced electrical signal known as the free induction decay (FID) is recorded by the NMR spectrometer, which is essentially a voltage response as function of time. Upon Fourier transform, the time-domain signal is converted to a frequency domain spectrum, which conveniently can be used to reveal subtle changes in chemical environment of molecules, particularly the breaking and formation of chemical bonds including covalent and non-covalent ones. This results in variations in chemical shift, multiplicity, and coupling constants, providing detailed insights into molecular structure and dynamics.[182,183]

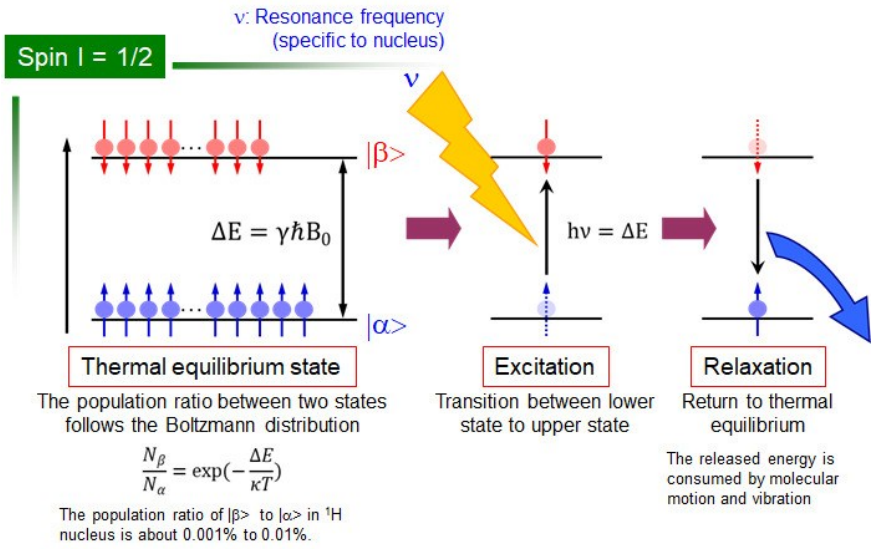

Figure 1.16. Schematic of NMR for a nucleus with spin quantum number *I*=1/2, illustrating the energy level transitions between α and β states. The diagram depicts thermal equilibrium, excitation at the resonance frequency, and relaxation back to equilibrium. Adapted from ref.[183] with permission from © 2025 Toray Research Centre.

1.7.2. Selection of NMR Technique and Solvent

In this study, the Bruker Avance III HD (AVIII) 600 MHz spectrometer was chosen over the AVIII 400 MHz and AVII 300 MHz models due to its superior capabilities. Equipped with a cryogenic probe, the AVIII 600 MHz spectrometer provides enhanced resolution and sensitivity, crucial for the

detailed structural analysis of polymers such as PEI. Its higher operating frequency enhances the resolution of closely overlapping NMR peaks, enabling a precise and detailed characterization of the chemical environment within PEI. Furthermore, cryogenic probe suppresses thermal noise, significantly speeding up the analysis process while ensuring both the reliability and accuracy of the results. Furthermore, liquid-state NMR spectroscopy was selected over solid-state NMR for its superior resolution and signal-to-noise ratio, enhanced by increased molecular motion in the liquid phase. Selecting an appropriate solvent is crucial in liquid-state NMR, as it must be chemically inert toward the analyte and capable of efficiently dissolving the targeted sample to ensure a homogeneous solution for satisfactory spectral resolution. For example, deuterium oxide (D_2O) was chosen for PEI-impregnated samples as the solvent because it extracts and dissolves PEI completely, and the solvent peak does not overlap with the regions of interest.

1.7.3. Analysis

^1H NMR is widely favored for analyses in NMR spectroscopy due to the high natural abundance of ^1H, which constitutes approximately 99.98% of naturally occurring hydrogen isotopes. This abundance coupled with the high gyromagnetic ratio of hydrogen makes ^1H NMR highly sensitive, allowing for the rapid acquisition of high-quality spectra with excellent signal-to-noise ratios. Such attributes make it ideal for detecting even trace amounts of material and obtaining detailed information about molecular structure quickly. However, ^1H NMR has its limitations, particularly when analyzing compounds like PEI where the molecular structure can result in complex spectra. In case of PEI, ^1H NMR spectra of the amines often show extensive peak overlap (Figure 1.17) due to the similarity in the chemical environments of hydrogen atoms within the various amine groups (primary, secondary, and tertiary). This overlapping complicates the clear identification and quantification of each amine type, thus obscuring critical details necessary for a thorough analysis.

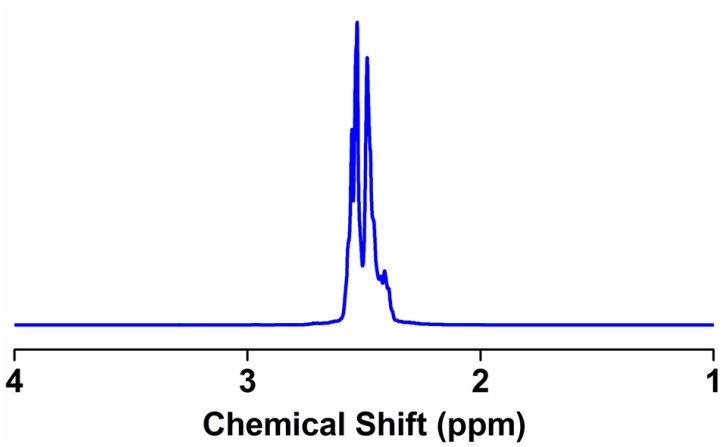

Figure 1.17. ^{1}H NMR of PEI

To overcome these challenges, ^{13}C NMR (Carbon-13) characterization is also performed. Although ^{13}C is naturally less abundant (about 1.1% of carbon) and has a lower sensitivity due to its smaller gyromagnetic ratio compared to ^{1}H, it offers several advantages. The ^{13}C NMR spectra provide a greater range of chemical shifts, which results from the broader variation in the chemical environments surrounding carbon atoms in organic molecules. This wider chemical shift range generally leads to less overlap in the spectra, making ^{13}C NMR particularly useful for distinguishing structurally similar groups within a molecule. In PEI, ^{13}C NMR analysis enables the clear differentiation and quantification of primary, secondary, and tertiary amines. Each type of amine carbon resonates at distinct chemical shifts, allowing for precise integration and ratio determination of the amine types within the sample.

Furthermore, optimization of relaxation delay is a critical factor in obtaining quantitative NMR data. The relaxation delay, which allows nuclei to fully return to thermal equilibrium between scans, was meticulously adjusted to ensure reliable quantification of amine groups in PEI. A 90 s relaxation delay was selected to allow full relaxation of the nuclei, thereby enabling precise quantification. Moreover, to accurately quantify primary, secondary, and tertiary amines in PEI using ^{13}C NMR, it is crucial to use inverse-gated decoupling. This technique reduces interference from the Nuclear Overhauser Effect (NOE)—a phenomenon in which dipolar interactions between nearby nuclear

spins enhance or reduce signal intensities, thereby changing peak intensities and leading to inaccuracies in quantitative analysis. By using inverse-gated decoupling, we ensure that ^{13}C signals are recorded without enhancements from nearby proton spins, thereby improving the accuracy and reproducibility of our data. This method is essential for precise quantification and clear analysis of the amine ratio in PEI. Following spectral acquisition and optimization, a formula from the literature was applied to calculate the ratios of primary, secondary, and tertiary amines. This formula uses integrated peak intensities (A) for calculation, as shown in Eq. 1.5 below.

$$\text{Primary: Secondary: Tertiary} = \left(\frac{A_a+A_b}{1}\right) : \left(\frac{A_c+A_d+A_e}{2}\right) : \left(\frac{A_f+A_g+A_h}{3}\right) \quad \text{Eq. 1.5}$$

1.8. IR Spectroscopy

IR spectroscopy relies on infrared laser to probe molecular vibrations and hence the functional groups present in the targeted samples, providing detailed insights into their chemical composition and structural attributes. This technique is based on the principle that molecular bonds absorb infrared light at specific frequencies that correspond to the energy gaps between quantized vibrational and rotational states. These frequencies are unique to each type of bond within a molecule, resulting in distinctive absorption patterns that reflect the molecular structure.[184] In the study of amine-functionalized materials, IR spectroscopy is essential for confirming the presence and modifications of functional groups.

The presence of amine groups is typically indicated by characteristic vibrational bands in infrared spectroscopy, with C–H stretching and bending observed around 2811[72] and 1458 cm^{-1}, respectively, and N–H stretching and bending around 3297[172] and 1567 cm^{-1},[185] respectively. Functionalization involving hydroxyl groups is evidenced by an increase in the intensity of the hydroxyl absorption band ~3350 cm^{-1} and a simultaneous decrease in the intensity of the N-H bending band.[186] Similarly, introduction of new functional groups is indicated by new band in the

spectrum. Furthermore, the technique is highly effective in monitoring the oxidation of amines, which leads to the formation of amides and/or imines. These compounds exhibit a distinctive absorption band around 1670 cm^{-1}, corresponding to the C=O stretching vibration in amides or C=N stretching in imines, a band that is not present in non-oxidized samples.[72] The appearance of this band in an IR spectrum thus serves as a clear indicator of the oxidative degradation of amines.

1.9. Nitrogen Adsorption Analysis

Nitrogen adsorption analysis at liquid nitrogen temperature, is an indispensable, non-destructive analytical technique for characterizing the porosity of material. This method uses nitrogen as the adsorptive medium, sometime argon, providing precise quantification of critical parameters including pore size distribution, total pore volume, and surface area, all under rigorously controlled experimental conditions.

1.9.1. Principle

The underlying mechanism of this technique is physisorption, driven predominantly by van der Waals interactions, which are sufficiently gentle to preserve the material's structural integrity during analysis. The initial phase involves the formation of a nitrogen monolayer on the accessible internal surfaces of the material, directly correlating with the surface area. As pressure increases, nitrogen molecules fill the pores through capillary condensation, crucial for determining the pore volume and distribution, depicted through an adsorption isotherm.

1.9.2. Experimental Procedure

1.9.2.1. Sample Preparation and Pretreatment

A specific amount of the material was placed in a sample holder and subjected to vacuum pretreatment at a temperature selected based on the thermal stability of the material, ranging from

50 to 300 °C, to eliminate any pre-adsorbed species. Accurate mass measurement post-treatment ensures precision in subsequent adsorption data.

1.9.2.2. Adsorption and Desorption Measurement

The prepared sample is exposed to a known volume of adsorbate (V_i) at an initial pressure (P_i) and temperature (T_i). The initial number of adsorbate molecules (n_i) are calculated using the ideal gas law. Then, the system is allowed to reach thermodynamic equilibrium at a constant temperature. After equilibrium, the final volume (V_f), pressure (P_f), and temperature (T_f) are recorded. The number of molecules adsorbed per gram of material at P_f is calculated using the ideal gas law, making corrections for any temperature variations within different sections of the setup. This procedure is repeated multiple times to gather a set of data across a broad range of pressures. This data collection is crucial for obtaining an adsorption isotherm. Subsequently, a known amount of adsorbate is systematically removed from the sample under controlled conditions to obtain the desorption isotherm.

1.9.2.3. Physical Adsorption Isotherms and Pore Size

The adsorption isotherm represents the amount of nitrogen adsorbed vs. relative pressure (P/P_0) at standard temperature and pressure (STP). Here, P_0 is the saturation pressure of the nitrogen at the adsorption temperature. When experiments are performed at the normal boiling point of the adsorbate, the value of P/P_0 ranges from 0 to 1, allowing for a comprehensive evaluation of adsorption behavior. The resulting isotherms provide key insights into the material's pore structure, surface interactions, and adsorption mechanism. Based on these characteristics, the International Union of Pure and Applied Chemistry (IUPAC) classifies physical adsorption isotherms into six types (Figure 1.18):

- **Type I Isotherm**: Typical for microporous materials, this isotherm shows a steep initial uptake at very low relative pressures ($P/P_0 < 0.05$), indicating rapid pore filling. Once the micropores

are saturated, the adsorption plateaus, reflecting a monolayer formation on high surface area materials with well-defined pore structures. Type I(a) isotherms indicate predominantly narrow micropores (<1 nm), while Type I(b) isotherms are associated with a broader pore distribution, including wider micropores and narrow mesopores (up to ~2.5 nm).

- **Type II Isotherm**: Common in non-porous or macroporous materials, this isotherm has an inflection point that signifies the completion of monolayer coverage and the commencement of multilayer adsorption.
- **Type III Isotherm**: This isotherm is convex to the pressure axis and often indicates weaker adsorbate-adsorbent interactions and is commonly observed in vapor adsorption processes.
- **Type IV Isotherm**: Characteristic of mesoporous materials, featuring a hysteresis loop due to capillary condensation occurring in the mesopores, indicating that the adsorption and desorption processes do not coincide and are therefore not reversible over some range of pressures. In Type IV(a), hysteresis occurs when pore widths exceed a critical value (~4 nm), which depends on the adsorption system and temperature. For materials with narrower mesopores, Type IV(b) isotherms are observed and are generally reversible**.**
- **Type V Isotherm**: Similar to Type IV but typically involves weaker adsorbate-adsorbent interactions and a more pronounced hysteresis loop due to delayed desorption.
- **Type VI Isotherm**: This rare isotherm shows stepwise multilayer adsorption on highly uniform, non-porous surfaces.

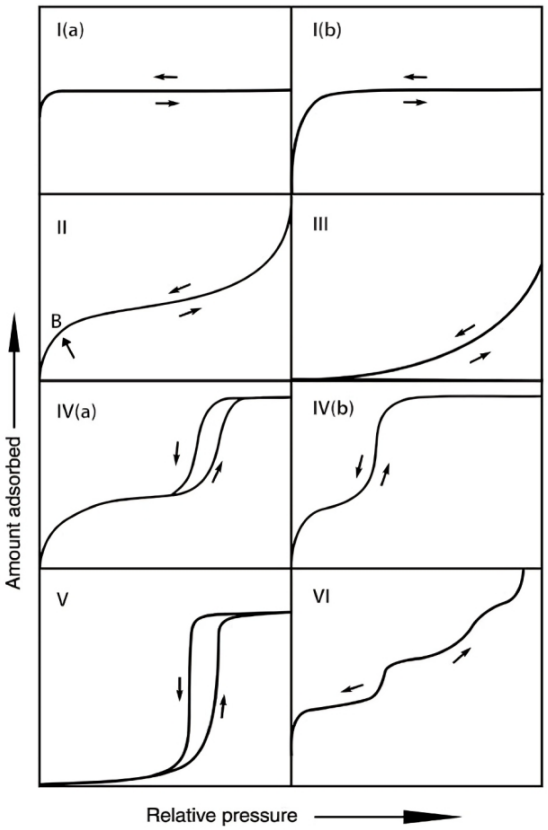

Figure 1.18. Classification of physical adsorption isotherms according to IUPAC. Reprinted from ref.[187] with permission from © 2015 IUPAC & De Gruyter.

Expanding on the classification of isotherms, Type IV isotherms provide valuable insights into adsorption behavior of mesoporous materials. The adsorption process progresses through different stages, each reflecting specific interactions between the adsorbate and the porous material. These stages are shown in Figure 1.19 and are outlined below:

- **Stage 0-A**: This initial stage involves the adsorption of a monolayer of the adsorbate onto the surface and the filling of any micropores present within the material. This occurs at very low pressures.
- **Stage A-B**: Following monolayer formation, multilayer adsorption begins. Unlike the orderly layer-by-layer adsorption seen in some other isotherms, this stage in a Type IV isotherm can involve more complex multilayer adsorption patterns.

- **Stage B-C**: This stage is crucial for understanding mesoporosity and involves capillary condensation occurring within the mesopores. The sharp increase in adsorbed volume observed in this stage results from a gas-to-liquid condensation process, which is facilitated by the mesopore structure conforming to the Kelvin equation (Eq. 1.6). Notably, a sharper hysteresis loop in this stage suggests a narrower pore size distribution.
- **Stage C-D**: Finally, as the relative pressure increases closer to one, regular multilayer adsorption continues on the surface.

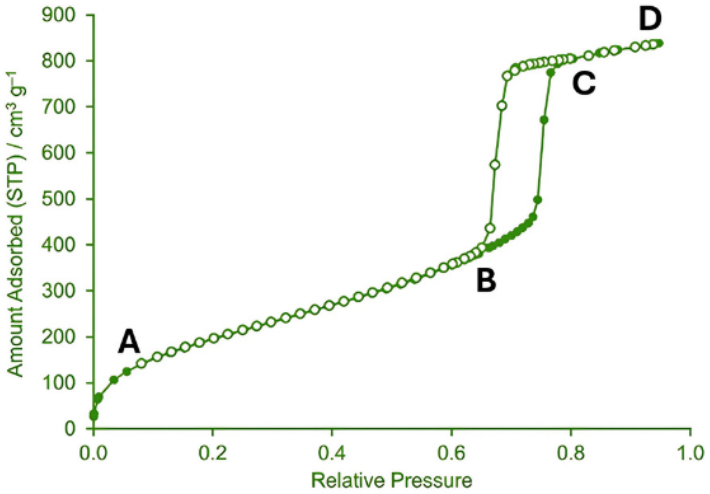

Figure 1.19. Type IV adsorption isotherm illustrating the stages of gas adsorption in mesoporous materials. Adapted from ref.[188], according to Creative Commons Attribution 4.0 International (CC BY 4.0).

In this equation:

- P/P_0 denotes the relative partial pressure of the adsorbate,

$$\ln\frac{P}{P_0} = -\frac{2\gamma_s v_m}{rRT} \qquad \text{Eq. 1.6}$$

- γ_s is the surface tension of the liquid,
- v_m represents the molar volume of the condensing liquid,
- r stands for the radius of curvature of the meniscus in the pore,
- R is the universal gas constant,
- T refers to the absolute temperature.

Kelvin equation is used to measure pore size of the material. It relates the radius of the pores to the pressure at which capillary condensation occurs, providing a method to calculate the pore size by analyzing the meniscus curvature within a pore. The Barret, Joyner, and Halenda (BJH) method uses Kelvin equation to calculate pore size distributions. This method assumes an open-ended cylindrical pore model and accounts for the multilayer adsorption.[189]

1.9.2.4. Total Pore Volume

The total pore volume of a material is calculated by determining the volume of nitrogen adsorbed at a relative pressure (P/P_0) close to 1, measured at STP. This measured volume is then converted to its liquid equivalent using a conversion factor, typically 0.00156 cm^3/g for nitrogen. According to the Gurvitsch rule, this liquid volume is assumed to be independent of the adsorbate type.

1.9.2.5. Surface Area

Brunauer-Emmett-Teller (BET) model is widely used to calculate the surface area of materials. This model extends the simple Langmuir theory to allow for multilayer adsorption, making it applicable to a broader range of conditions, particularly under higher pressures where multilayer adsorption is significant. The BET equation (Eq. 1.7) applies to the linear portion of the isotherm, typically in the relative pressure range of 0.05 to 0.35, and is given as follows:

$$\frac{P}{n(P_0 - P)} = \frac{1}{n_m c} + \frac{c-1}{n_m c}\frac{P}{P_0} \qquad \text{Eq. 1.7}$$

where, n represents the quantity of molecules adsorbed at equilibrium pressure P,

n_m indicates the total molecules that form a complete monolayer,

c is a material-dependent constant.

By plotting the BET equation in its linear form, n_m is determined. Using Avogadro's number (N_A) and the established cross-sectional area of a nitrogen molecule (σ), which is 16 $Å^2$, the total

surface area of the material is calculated using the formula $S=N_A n_m \sigma$.

1.9.2.6. Critical Details and Precautions

Maintaining accurate control over temperature and pressure is crucial to circumvent data misinterpretation. Rigorous calibration of equipment and thorough pretreatment of samples are imperative to avert analytical errors that could skew interpretations of pore structure and size.

1.10. Thermogravimetric Analysis (TGA)

TGA is a gravimetric technique to determine the adsorption capacity, equilibration time, the impact of temperature on adsorption and desorption kinetics, decomposition temperature, and organic content of a material and the material's recyclability. In this method, the sample is placed in a pan, which is suspended from an electronic microbalance and adjacent to a thermocouple. This setup enables simultaneous monitoring of mass changes in the sample in response to controlled temperature variations. To calculate the amount of CO_2 adsorbed, the sample is initially pretreated to eliminate moisture and any residual solvents. The sample is cooled to the desired adsorption temperature before being exposed to a CO_2 gas mixture until equilibrium is achieved, or for a predetermined period if kinetic measurements are required. The resulting increase in weight, recorded in milligrams, is converted to a percentage of the original weight. This value is then used to express the amount of CO_2 adsorbed in millimoles per gram of adsorbent, calculated using the following equation (Eq. 1.8)[190]:

$$\mathrm{CO_2(ads)} = \frac{\text{Weight gain (\%)}}{\mathrm{MW}_{CO_2}} \times 10 \qquad \text{Eq. 1.8}$$

where weight gain (%) = (Final weight (%) – Initial weight (%))/ Initial weight (%) during the adsorption stage and MW_{CO_2} is molecular weight of CO_2.

To determine the organic content in an adsorbent, weight loss is measured from the onset of decomposition of organics to their complete breakdown. For amine-based silica adsorbents, decomposition begins at *ca.* 200 °C and continues up to 700 °C. At 700 °C, the sample is maintained under flowing air for *ca.* 30 minutes to decompose any residual carbonaceous materials, while the silica remains stable.[191] The organic content is calculated by measuring weight loss beyond 200 °C and applying the following formula (Eq. 1.9):

$$\text{Organic Content (\%)} = \frac{\text{Weight loss at 700 °C} - \text{Weight loss at 200 °C}}{\text{Weight loss at 200 °C}} \times 100 \qquad \text{Eq. 1.9}$$

1.11. Dynamic Vapor Gravimetric Sorption (DVS)

DVS is an analytical technique used to quantify the adsorption and desorption of dry or humid gases. Its working principle is similar to TGA in that it involves precise weighing of a sample to determine changes in mass.[192] It is especially useful to obtain water adsorption isotherms, which involve flowing a carrier gas at a predetermined RH over the sample. Figure 1.20 illustrates the experimental setup of the DVS Carbon instrument used to perform H_2O and CO_2 uptake measurements of the adsorbents, as described in detail in Chapter 4. The instrument is equipped with a high-precision microbalance, with a minimum resolution of 0.01 μg, which continuously monitors the mass change of the sample within a temperature-controlled environment. A reference pan ensures the accurate determination of mass changes solely attributed to adsorption phenomena. The gas streams, regulated by mass flow controllers (MFCs), pass through solvent reservoirs to achieve the desired humidity levels, which are monitored by integrated RH sensors. During the experiments, two water reservoirs were used to regulate humidity during different stages of the experiment. Reservoir A was used to humidify nitrogen gas, which was subsequently used to pre-humidify the adsorbent. Reservoir B was used to humidify a CO_2 gas stream before mixing it with the humidified nitrogen, yielding a 5% CO_2/N_2 gas mixture at the same RH as the pre-humidified sample. The total flow rate of the gas mixture delivered to the adsorbent was maintained at 100 mL/min.

To ensure the reliability and precision of data obtained via gravimetric analysis like TGA and DVS, it is imperative to implement several precautionary measures. The sensitivity of DVS measurements to vibrations necessitates a stable experimental environment to mitigate any potential fluctuations in recorded mass. The regular calibration of mass and temperature are essential to maintain the accuracy of measurements.

Analytical techniques such as DVS and TGA offer substantial advantages in characterizing sorption behaviors, notably their ability to operate effectively with minimal sample sizes, typically as small as 10 mg. However, while these techniques proficiently measure the total mass changes associated with the adsorption processes, they do not possess the intrinsic ability to discriminate between different adsorbed species, such as CO_2 and H_2O. To circumvent this limitation, a common approach involves pre-humidifying the sample with water, followed by the introduction of CO_2 under the assumption of non-competitive adsorption between the two gases. While this assumption is generally valid, it may not hold in all cases, particularly when the adsorption sites show a preference for one molecule over the other. In such scenarios, these instruments are coupled with a mass spectrometer or FTIR.[114,193]

Important to Note:

It is important to note that in flue gas compositions, water content is typically expressed as volume percent (e.g., 6–18 vol %, as shown in Table 1.1), representing post-combustion conditions. However, here the water content of the gas phase is often referred to in terms of relative humidity (RH). RH is defined as the ratio of the actual partial pressure of water vapor to the saturation vapor pressure of water at a given temperature. Unlike volume percent, RH inherently incorporates the temperature dependence of water vapor saturation, thereby providing a more relevant measure for adsorption studies involving humidity.

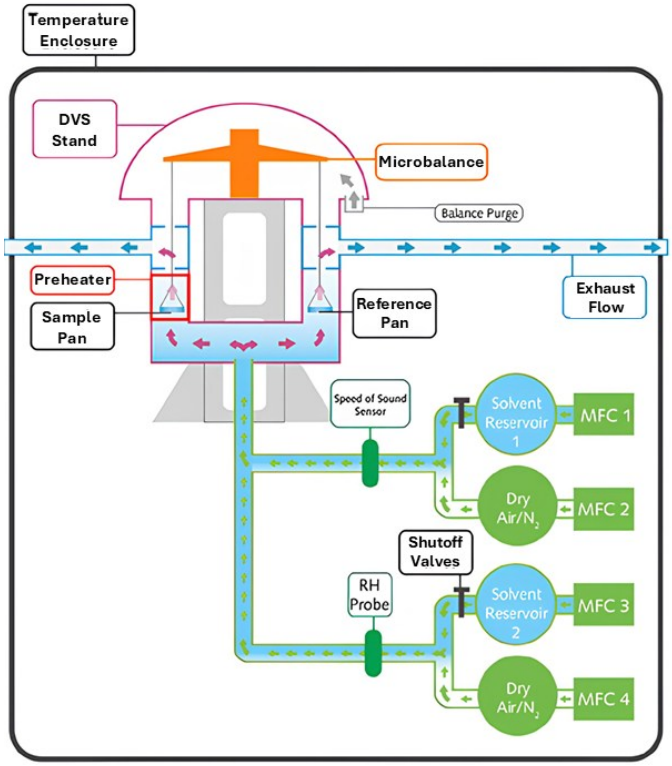

Figure 1.20. Schematic of the DVS Carbon setup used for humidity-controlled gas adsorption measurements. Printed with permission from Surface Measurement Systems, Limited.

1.12. Column Breakthrough Analysis – Mass Spectrometry

Column breakthrough analysis is used to analyze the separation and quantification of gases in a multicomponent gas mixture as it moves through an adsorbent. This process starts by loading an adsorbent into a column and then passing the gas mixture through it under controlled conditions. Initially, as the gas mixture enters the column, the adsorbent selectively adsorbs the target gas while allowing the carrier gas to pass to the detector. Over time, as the adsorbent approaches saturation, the adsorbate breaks through the column and starts getting detected, indicating the onset of the breakthrough. Continuous monitoring of the eluted gas is essential and is typically performed using techniques such as mass spectrometry or a thermal conductivity detector (TCD). This monitoring helps in obtaining a breakthrough curve by plotting the ratio of the outlet concentration to the inlet concentration against time, as illustrated in Figure 1.21. The breakthrough point is identified when the adsorbate concentration at the column outlet exceeds 5-10% of the feed gas stream concentration.

As the adsorption process continues, the concentration of the adsorbate in the column progressively increases until it approaches the inlet concentration. At this stage, typically when the outlet concentration reaches 90-95% of the inlet concentration, the column is considered fully saturated, marking the endpoint of the process. Another critical aspect of this analysis is determining the "dead time," which is the time taken by the adsorbates to travel from the source to the column outlet and all the way up to the detector when column is not packed with adsorbent. This is often measured using non-adsorptive gas like helium. A common approach to account for dead volume effects is to perform a blank run under the same flow, pressure, and temperature conditions as the actual experiment, substituting the adsorption column with a low-volume tube or connector. The resulting blank curve is then subtracted point-by-point from the breakthrough profile obtained with the adsorbent, allowing accurate determination of the adsorption capacity from the corrected data (Figure 1.21).[194] This approach assumes that the total system response is a linear sum of the blank and column contributions. However, this assumption becomes invalid at high adsorbate concentrations, where the adsorption process significantly alters the outlet flow rate, making the linear additivity approximation unreliable.[195]

Important to Note:

1. To reduce the pressure-drop across the column, the adsorbent is typically pelletized before it is loaded. Alternatively, in industrial applications, adsorbents are densified into different structured adsorbents such as monoliths, beads, etc. to reduce pressure drop while operating at higher flow rates.[196–198]
2. In the experimental setup, a carrier gas is systematically introduced alongside the feed gas to ensure a stable flow through the detector. This technique is followed generally to ensure repeatability of the results in adsorption studies.
3. Due to the slow formation of bicarbonate, the adsorption experiments are performed for long time to ensure prolonged contact time during the adsorption of humid CO_2.

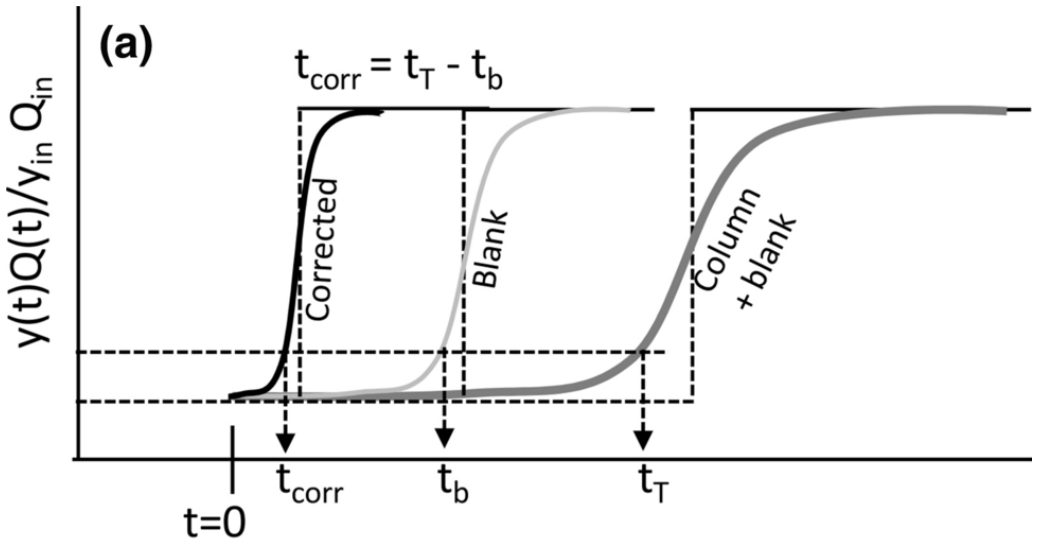

Figure 1.21. Schematic representation of stepwise blank response correction. Reprinted from ref.[194] with permission from © 2021 Springer Nature.

1.13. References

(1) Ritchie, H.; Roser, M.; Rosado, P. *CO_2 and Greenhouse Gas Emissions*. Our World in Data. https://ourworldindata.org/CO2-and-greenhouse-gas-emissions (accessed 2024-12-24).

(2) International Energy Agency. *Electricity*; 2025. https://www.iea.org/reports/electricity-2025/emissions (accessed 2025-04-16).

(3) NASA. *Carbon Dioxide*. https://climate.nasa.gov/vital-signs/carbon-dioxide/?intent=121 (accessed 2025-04-15).

(4) Global Monitoring Laboratory. *Trends in Atmospheric Carbon Dioxide*. https://gml.noaa.gov/ccgg/trends/weekly.html (accessed 2024-08-19).

(5) NASA. *The Effects of Climate Change*. https://science.nasa.gov/climate-change/effects/?utm_source (accessed 2024-12-24).

(6) Intergovernmental Panel on Climate Change (IPCC). *Climate change 2023: Synthesis report*. https://www.ipcc.ch/report/ar6/syr/downloads/report/IPCC_AR6_SYR_LongerReport.pdf (accessed 2024-03-11).

(7) Climate Action Tracker. *2100 Warming Projections: Emissions and expected warming based on pledges and current policies*. https://climateactiontracker.org/global/temperatures/ (accessed 2024-12-24).

(8) Lyons, M.; Durrant, P.; Kochhar, K. *Reaching Zero with Renewables: Capturing Carbon*; International Renewable Energy Agency (IRENA), 2021.

(9) *What is CCS and how does it work*. https://www.nationalgrid.com/stories/energy-explained/what-is-ccs-how-does-it-work (accessed 2024-12-25).

(10) Hekmatmehr, H.; Esmaeili, A.; Pourmahdi, M.; Atashrouz, S.; Abedi, A.; Ali Abuswer, M.;

Nedeljkovic, D.; Latifi, M.; Farag, S.; Mohaddespour, A. Carbon Capture Technologies: A Review on Technology Readiness Level. *Fuel* **2024**, *363*, 130898.

(11) Chao, C.; Deng, Y.; Dewil, R.; Baeyens, J.; Fan, X. Post-Combustion Carbon Capture. *Renew. Sustain. Energy Rev.* **2021**, *138*, 110490.

(12) Kolle, J. M. Mesoporous Organosilicas for CO_2 Capture and Utilization: Reaction Insight and Material Development, Ph.D. Dissertation, University of Ottawa, Canada, 2020. https://ruor.uottawa.ca/server/api/core/bitstreams/e537ce98-0ac2-4b09-b5ce-5830ebd59342/content (accessed 2025-02-11).

(13) Gulzar, A.; Gulzar, A.; Ansari, M. B.; He, F.; Gai, S.; Yang, P. Carbon Dioxide Utilization: A Paradigm Shift with CO_2 Economy. *Chem. Eng. J. Adv.* **2020**, *3*, 100013.

(14) Raganati, F.; Ammendola, P. CO_2 Post-Combustion Capture: A Critical Review of Current Technologies and Future Directions. *Energy Fuels* **2024**, *38*, 13858–13905.

(15) Lashaki M.J.; Khiavi, S.; Sayari, A. Stability of Amine-Functionalized CO_2 Adsorbents: A Multifaceted Puzzle. *Chem. Soc. Rev.* **2019**, *48*, 3320–3405.

(16) Pyo, S.-H.; Park, J. H.; Chang, T.-S.; Hatti-Kaul, R. Dimethyl Carbonate as a Green Chemical. *Curr. Opin. Green Sustain. Chem.* **2017**, *5*, 61–66.

(17) Wang, M.; Lawal, A.; Stephenson, P.; Sidders, J.; Ramshaw, C. Post-Combustion CO_2 Capture with Chemical Absorption: A State-of-the-Art Review. *Chem. Eng. Res. Des.* **2011**, *89*, 1609–1624.

(18) Raganati, F.; Miccio, F.; Ammendola, P. Adsorption of Carbon Dioxide for Post-Combustion Capture: A Review. *Energy Fuels* **2021**, *35*, 12845–12868.

(19) Hou, R.; Fong, C.; Freeman, B. D.; Hill, M. R.; Xie, Z. Current Status and Advances in Membrane Technology for Carbon Capture. *Sep. Sci. Technol.* **2022**, *300*, 121863.

(20) Song, C.; Liu, Q.; Deng, S.; Li, H.; Kitamura, Y. Cryogenic-Based CO_2 Capture Technologies: State-of-the-Art Developments and Current Challenges. *Renew. Sustain. Energy Rev.* **2019**, *101*, 265–278.

(21) *Global Status of CCS 2024: Collaborating for a Net-Zero Future*. https://www.globalccsinstitute.com/wp-content/uploads/2024/10/2024-GSR_20241015.pdf (accessed 2024-12-30).

(22) Global Cement and Concrete Association. *Amine-based post-combustion capture*. https://gccassociation.org/cement-and-concrete-innovation/carbon-capture-and-utilisation/amine-based-post-combustion-capture/?utm_source (accessed 2024-12-30).

(23) KAMINSKI, J. Technologies and Costs of SO_2-Emissions Reduction for the Energy Sector. *Appl. Energy* **2003**, *75*, 165–172.

(24) Zhou, S.; Wang, S.; Chen, C. Thermal Degradation of Monoethanolamine in CO_2 Capture with Acidic Impurities in Flue Gas. *Ind. Eng. Chem. Res.* **2012**, *51*, 2539–2547.

(25) Reynolds, A. J.; Verheyen, T. V.; Adeloju, S. B.; Meuleman, E.; Feron, P. Towards Commercial Scale Postcombustion Capture of CO_2 with Monoethanolamine Solvent: Key

Considerations for Solvent Management and Environmental Impacts. *Environ. Sci. Technol.* **2012**, *46*, 3643–3654.

(26) Bui, M.; Adjiman, C. S.; Bardow, A.; Anthony, E. J.; Boston, A.; Brown, S.; Fennell, P. S.; Fuss, S.; Galindo, A.; Hackett, L. A.; Hallett, J. P.; Herzog, H. J.; Jackson, G.; Kemper, J.; Krevor, S.; Maitland, G. C.; Matuszewski, M.; Metcalfe, I. S.; Petit, C.; Puxty, G.; Reimer, J.; Reiner, D. M.; Rubin, E. S.; Scott, S. A.; Shah, N.; Smit, B.; Trusler, J. P. M.; Webley, P.; Wilcox, J.; Mac Dowell, N. Carbon Capture and Storage (CCS): The Way Forward. *Energy Environ. Sci.* **2018**, *11*, 1062–1176.

(27) Zanco, S. E.; Pérez-Calvo, J. F.; Gasós, A.; Cordiano, B.; Becattini, V.; Mazzotti, M. Postcombustion CO_2 Capture: A Comparative Techno-Economic Assessment of Three Technologies Using a Solvent, an Adsorbent, and a Membrane. *ACS Eng. Au* **2021**, *1*, 50–72.

(28) Gao, W.; Liang, S.; Wang, R.; Jiang, Q.; Zhang, Y.; Zheng, Q.; Xie, B.; Toe, C. Y.; Zhu, X.; Wang, J.; Huang, L.; Gao, Y.; Wang, Z.; Jo, C.; Wang, Q.; Wang, L.; Liu, Y.; Louis, B.; Scott, J.; Roger, A.-C.; Amal, R.; He, H.; Park, S.-E. Industrial Carbon Dioxide Capture and Utilization: State of the Art and Future Challenges. *Chem. Soc. Rev.* **2020**, *49*, 8584–8686.

(29) Kolle, J. M.; Fayaz, M.; Sayari, A. Understanding the Effect of Water on CO_2 Adsorption. *Chem. Reviews* **2021**, *121*, 7280–7345.

(30) Jaffar, M. M.; Rolfe, A.; Brandoni, C.; Martinez, J.; Snape, C.; Kaldis, S.; Santos, A.; Lysiak, B.; Lappas, A.; Hewitt, N.; Huang, Y. A Technical and Environmental Comparison of Novel Silica PEI Adsorbent-Based and Conventional MEA-Based CO_2 Capture Technologies in the Selected Cement Plant. *Carbon Capture Sci. Technol.* **2024**, *10*, 100179.

(31) Choi, S.; Drese, J. H.; Jones, C. W. Adsorbent Materials for Carbon Dioxide Capture from Large Anthropogenic Point Sources. *ChemSusChem* **2009**, *2*, 796–854.

(32) Hack, J.; Maeda, N.; Meier, D. M. Review on CO_2 Capture Using Amine-Functionalized Materials. *ACS Omega* **2022**, *7*, 39520–39530.

(33) Santiago, R. G.; Siqueira, R. M.; Alves, C. A.; Vilarrasa-García, E.; Maia, D. A. S.; Bastos-Neto, M.; de Azevedo, D. C. S. Evaluation of the Thermal Regeneration of an Amine-Grafted Mesoporous Silica Used for CO_2/N_2 Separation. *Adsorption* **2020**, *26*, 203–215.

(34) Zhao, P.; Zhang, G.; Hao, L. A Novel Blended Amine Functionalized Porous Silica Adsorbent for Carbon Dioxide Capture. *Adsorption* **2020**, *26*, 749–764.

(35) Hiyoshi, N.; Yogo, K.; Yashima, T. Adsorption of Carbon Dioxide on Amine Modified SBA-15 in the Presence of Water Vapor. *Chem. Lett.* **2004**, *33*, 510–511.

(36) Yue, M. B.; Sun, L. B.; Cao, Y.; Wang, Z. J.; Wang, Y.; Yu, Q.; Zhu, J. H. Promoting the CO_2 Adsorption in the Amine-Containing SBA-15 by Hydroxyl Group. *Microporous Mesoporous Mater.* **2008**, *114*, 74–81.

(37) Lin, L.; Han, S.; Meng, F.; Li, J.; Chen, K.; Hu, E.; Jiang, J. The Influence of Pore Size and Pore Structure of Silica-Based Material on the Amine-Modified Adsorbent for CO_2 Capture. *Sep. Purif. Technol.* **2024**, *340*, 126735.

(38) Kishor, R.; Ghoshal, A. K. Amine-Modified Mesoporous Silica for CO_2 Adsorption: The Role of Structural Parameters. *Ind. Eng. Chem. Res.* **2017**, *56*, 6078–6087.

(39) Yan, H.; Zhang, G.; Liu, J.; Li, G.; Zhao, Y.; Wang, Y.; Wu, C.; Wu, W. Amine-Functionalized Disordered Hierarchical Porous Silica Derived from Blast Furnace Slag with High Adsorption Capability and Cyclic Stability for CO_2 Adsorption. *Chem. Eng. J.* **2023**, *478*.

(40) Anyanwu, J. T.; Wang, Y.; Yang, R. T. Tunable Amine Loading of Amine Grafted Mesoporous Silica Grafted at Room Temperature: Applications for CO_2 Capture. *Chem. Eng. Sci.* **2022**, *254*, 117626.

(41) Rosu, C.; Pang, S. H.; Sujan, A. R.; Sakwa-Novak, M. A.; Ping, E. W.; Jones, C. W. Effect of Extended Aging and Oxidation on Linear Poly (propylenimine)-Mesoporous Silica Composites for CO_2 Capture from Simulated Air and Flue Gas Streams. *ACS Appl. Mater. Interfaces* **2020**, *12*, 38085–38097.

(42) Wadi, B.; Li, C.; Manovic, V.; Moghadam, P.; Nabavi, S. A. Contributions of CH_4-Amine Interactions by Primary, Secondary, and Tertiary Amines on CO_2/CH_4 Separation Efficiency. *Chem. Eng. J.* **2023**, *463*, 142117.

(43) Pacheco, M.; Bordonhos, M.; Sardo, M.; Afonso, R.; Gomes, J. R. B.; Mafra, L.; Pinto, M. L. Moisture Effect on the Separation of CO_2/CH_4 Mixtures with Amine-Functionalised Porous Silicas. *Chem. Eng. J.* **2022**, *443*, 136271.

(44) Kumar, R.; Bandyopadhyay, M.; Pandey, M.; Tsunoji, N. Amine-Impregnated Nanoarchitectonics of Mesoporous Silica for Capturing Dry and Humid 400 Ppm Carbon Dioxide: A Comparative Study. *Microporous Mesoporous Mater.* **2022**, *338*, 111956.

(45) Sneddon, G.; McGlynn, J. C.; Neumann, M. S.; Aydin, H. M.; Yiu, H. H. P.; Ganin, A. Y. Aminated Poly (Vinyl Chloride) Solid State Adsorbents with Hydrophobic Function for Post-Combustion CO_2 Capture. *J. Mater. Chem. A. Mater.* **2017**, *5*, 11864–11872.

(46) Hahn, M. W.; Steib, M.; Jentys, A.; Lercher, J. A. Mechanism and Kinetics of CO_2 Adsorption on Surface Bonded Amines. *J. Phys. Chem. C* **2015**, *119*, 4126–4135.

(47) Jing, Y.; Wei, L.; Wang, Y.; Yu, Y. Synthesis, Characterization and CO_2 Capture of Mesoporous SBA-15 Adsorbents Functionalized with Melamine-Based and Acrylate-Based Amine Dendrimers. *Microporous Mesoporous Mater.* **2014**, *183*, 124–133.

(48) Xue, Q.; Liu, Y. Mixed-Amine Modified SBA-15 as Novel Adsorbent of CO_2 Separation for Biogas Upgrading. *Sep. Sci. Technol.* **2011**, *46*, 679–686.

(49) Zhang, G.; Zhao, P.; Xu, Y.; Yang, Z.; Cheng, H.; Zhang, Y. Structure Property–CO_2 Capture Performance Relations of Amine-Functionalized Porous Silica Composite Adsorbents. *ACS Appl. Mater. Interfaces* **2018**, *10*, 34340–34354.

(50) Harlick, P. J. E.; Sayari, A. Applications of Pore-Expanded Mesoporous Silica. 5. Triamine Grafted Material with Exceptional CO_2 Dynamic and Equilibrium Adsorption Performance. *Ind. Eng. Chem. Res.* **2007**, 46, 446–458.

(51) Serna-Guerrero, R.; Belmabkhout, Y.; Sayari, A. Modeling CO_2 Adsorption on Amine-Functionalized Mesoporous Silica: 1. A Semi-Empirical Equilibrium Model. *Chem. Eng. J.* **2010**, *161*, 173–181.

(52) Tian, H.; Du, J.; Lu, P.; Xu, S.; Guo, Y.; Tang, J.; Wu, M.; Guo, Q. Bi-Amine Functionalized

Mesostructured Silica Nanospheres for Enhanced CO_2 Adsorption Performance and Fast Desorption Kinetics. *Appl. Surf. Sci.* **2022**, *606*.

(53) Gao, F.; Ji, C.; Wang, S.; Wang, W.; Dong, J.; Guo, C.; Gao, Y.; Chen, G. Sterically Hindered Amine-Functionalized MCM-41 Composite for Efficient Carbon Dioxide Capture. *Korean J. Chem. Eng.* **2022**, *39*, 1981–1988.

(54) Muchan, P.; Saiwan, C.; Nithitanakul, M. Carbon Dioxide Adsorption/Desorption Performance of Single-and Blended-Amines-Impregnated MCM-41 Mesoporous Silica in Post-Combustion Carbon Capture. *Clean Energy* **2022**, *6*, 424–437.

(55) Ahmed, S.; Ramli, A.; Yusup, S. CO_2 Adsorption Study on Primary, Secondary and Tertiary Amine Functionalized Si-MCM-41. *Int. J. Greenh. Gas Control* **2016**, *51*, 230–238.

(56) de Carvalho, L. S.; Silva, E.; Andrade, J. C.; Silva, J. A.; Urbina, M.; Nascimento, P. F.; Carvalho, F.; Ruiz, J. A. Low-Cost Mesoporous Adsorbents Amines-Impregnated for CO_2 Capture. *Adsorption* **2015**, *21*, 597–609.

(57) Liu, Z.; Teng, Y.; Zhang, K.; Chen, H.; Yang, Y. CO_2 Adsorption Performance of Different Amine-Based Siliceous MCM-41 Materials. *J. Energy Chem.* **2015**, *24*, 322–330.

(58) Choi, S.; Bae, H.-K. Adsorption of CO_2 on Amine-Impregnated Mesoporous MCM41 Silica. *KSCE J. Civ. Eng.* **2014**, *18*, 1977–1983.

(59) Klinthong, W.; Huang, C. H.; Tan, C. S. Polyallylamine and NaOH as a Novel Binder to Pelletize Amine-Functionalized Mesoporous Silicas for CO_2 Capture. *Microporous Mesoporous Mater.* **2014**, *197*, 278–287.

(60) Belmabkhout, Y.; Sayari, A. Effect of Pore Expansion and Amine Functionalization of Mesoporous Silica on CO_2 Adsorption over a Wide Range of Conditions. *Adsorption* **2009**, *15*, 318–328.

(61) Serna-Guerrero, R.; Da'na, E.; Sayari, A. New Insights into the Interactions of CO_2 with Amine-Functionalized Silica. *Ind. Eng. Chem. Res.* **2008**, *47*, 9406–9412.

(62) Sayari, A.; Hamoudi, S. Periodic Mesoporous Silica-Based Organic−Inorganic Nanocomposite Materials. *Chem. Mater.* **2001**, *13*, 3151–3168.

(63) Franchi, R. S.; Harlick, P. J. E.; Sayari, A. Applications of Pore-Expanded Mesoporous Silica. 2. Development of a High-Capacity, Water-Tolerant Adsorbent for CO_2. *Ind. Eng. Chem. Res.* **2005**, *44*, 8007–8013.

(64) Ziaei-Azad, H.; Kolle, J. M.; Al-Yasser, N.; Sayari, A. One-Pot Synthesis of Large-Pore AlMCM-41 Aluminosilicates with High Stability and Adjustable Acidity. *Microporous Mesoporous Mater.* **2018**, *262*, 166–174.

(65) Jahandar Lashaki, M.; Ziaei-Azad, H.; Sayari, A. Unprecedented Improvement of the Hydrothermal Stability of Amine-Grafted MCM-41 Silica for CO_2 Capture via Aluminum Incorporation. *Chem. Eng. J.* **2022**, *450*, 138393.

(66) Jahandar Lashaki, M.; Sayari, A. CO_2 Capture Using Triamine-Grafted SBA-15: The Impact of the Support Pore Structure. *Chem. Eng. J.* **2018**, *334*, 1260–1269.

(67) Chon, H.; Woo, S. Ihl.; Park, S.-E. Recent Advances and New Horizons in Zeolite Science and Technology; Chon, H. (Hakze), Woo, S. Ihl., Park, S.-E. (Sang E., International Zeolite Conference (11th : 1996 : Taejŏn-si, K., Eds.; Studies in surface science and catalysis ; vol. 102; Elsevier: Amsterdam ;, 1996.

(68) Sayari, A.; Yang, Y. Highly Ordered MCM-41 Silica Prepared in the Presence of Decyltrimethylammonium Bromide. *J. Phys. Chem. B* **2000**, *104*, 4835–4839.

(69) Sayari, A.; Han, B.-H. H.; Yang, Y. Simple Synthesis Route to Monodispersed SBA-15 Silica Rods. *J. Am. Chem. Soc.* **2004**, *126*, 14348–14349.

(70) Hermani, M.; Abdollahi-Esfahlani, H.; Sadeghi, A.; Sharabiani, A. S.; Shafaati, E.; Imani, A.; Amjadi, A.; Daneshvar, A. Enhanced Nanofiltration Performance of the PVC/PVA Thin Film Membranes for Treatment of Petroleum Refinery Wastewater through Incorporation of Amino-Functionalized SBA-15 Nanoparticles. *J. Polym. Environ.* **2024**, *32*, 5195–5211.

(71) Kaur, C.; Sayari, A. Enhancing Oxidation Stability of Amine-Containing CO_2 Adsorbents Using Hydroxyethyl Starch. *Chem. Eng. J.* **2024**, *496*, 153756.

(72) Carneiro, J. S. A.; Innocenti, G.; Moon, H. J.; Guta, Y.; Proaño, L.; Sievers, C.; Sakwa-Novak, M. A.; Ping, E. W.; Jones, C. W. Insights into the Oxidative Degradation Mechanism of Solid Amine Sorbents for CO_2 Capture from Air: Roles of Atmospheric Water. *Angew. Chem., Int. Ed.* **2023**, *62*, e202302887.

(73) Mohamad, N. F.; Rani, N. H. A.; Onn, M.; Jamaludin, S. I. S.; Shafiq, A. S. I. A.; Yeit, W. M. Y. W.; Zulkifli, N. A. Synthesis and Characterization of Amine-Impregnated Silica Gel for Potential Carbon Dioxide (CO_2) Absorption. In *Journal of Physics: Conference Series*; IOP Publishing, 2019; Vol. 1349, p 012100.

(74) Manianglung, C.; Pacia, R. M.; Ko, Y. S. Synergistic Effect of Blended Primary and Secondary Amines Functionalized onto the Silica on CO_2 Capture Performance. *Korean J. Chem. Eng.* **2019**, *36*, 1267–1273.

(75) Ayub, A.; Ahsan, S.; Meeroff, D.; Lashaki, M. J. Amine-Grafted Mesoporous Silica Materials for Single-Stage Biogas Upgrading to Biomethane. *Chem. Eng. J.* **2022**, *445*, 136497.

(76) Kolle, J. M.; Sayari, A. Dry Gel Grafting of Mesoporous Silica: Application to Amine-Based CO_2 Adsorbents. *Microporous Mesoporous Mater.* **2022**, *343*, 112195.

(77) Minju, N.; Nair, B. N.; Peer Mohamed, A.; Ananthakumar, S. Surface Engineered Silica Mesospheres – A Promising Adsorbent for CO_2 Capture. *Sep. Purif. Technol.* **2017**, *181*, 192–200.

(78) Sayari, A.; Heydari-Gorji, A.; Yang, Y. CO_2-Induced Degradation of Amine-Containing Adsorbents: Reaction Products and Pathways. *J. Am. Chem. Soc.* **2012**, *134*, 13834–13842.

(79) Fang, Q.; Huang, W.; Wang, H. Role of Additives in Silica-Supported Polyethylenimine Adsorbents for CO_2 Adsorption. *Mater. Res. Express* **2020**, *7*, 035026.

(80) Qadir, S.; Su, H.; Li, D.; Gu, Y.; Zhao, S.; Wang, S.; Wang, S. Low-Cost Preferential Different Amine Grafted Silica Spheres Adsorbents for DAC CO_2 Removal. *J. Energy Chem.* **2022**, *75*, 494–503.

(81) Hiyoshi, N.; Yogo, K.; Yashima, T. Adsorption Characteristics of Carbon Dioxide on Organically Functionalized SBA-15. *Microporous Mesoporous Mater.* **2005**, *84*, 357–365.

(82) Cogswell, C. F.; Jiang, H.; Ramberger, J.; Accetta, D.; Willey, R. J.; Choi, S. Effect of Pore Structure on CO_2 Adsorption Characteristics of Aminopolymer Impregnated MCM-36. *Langmuir* **2015**, *31*, 4534–4541.

(83) Zhao, P.; Yin, Y.; Xu, X.; Yang, D.; Wang, J.; Yang, F.; Zhang, G. Facile Fabrication of Mesoporosity Silica as Support for Solid Amine CO_2 Adsorbents with Enhanced Adsorption Capacity and Kinetics. *Energy* **2022**, *253*.

(84) Yan, W.; Tang, J.; Bian, Z.; Hu, J.; Liu, H. Carbon Dioxide Capture by Amine-Impregnated Mesocellular-Foam-Containing Template. *Ind. Eng. Chem. Res.* **2012**, *51*, 3653–3662.

(85) Bahadur, J.; Mehta, S.; Singh, S.; Das, A.; Maity, A.; Youngs, T.; Sen, D.; Polshettiwar, V. Interlocking Dendritic Fibrous Nanosilica into Microgranules by Polyethylenimine Assisted Assembly: In Situ Neutron Diffraction and CO_2 Capture Studies. *Mater. Adv.* **2022**.

(86) Erans, M.; Arencibia, A.; Sanz-Pérez, E. S.; Sanz, R. Amine-Bridged Periodic Mesoporous Organosilica Adsorbents for CO_2 Capture. *J. Environ. Chem. Eng.* **2023**, *11*, 111590.

(87) Zhang, Y.; Zhao, S.; Li, L.; Feng, J.; Qiu, W.; Wei, Z.; Li, X.; Huang, Z.; Lin, H. Revealing the Correlation between the Performance of Silica-Based DAC Adsorbents and Their Pore Natures. *Gas Sci. Eng.* **2024**, *123*, 205251.

(88) Taheri, F. S.; Ghaemi, A.; Maleki, A.; Shahhosseini, S. High CO_2 Adsorption on Amine-Functionalized Improved Mesoporous Silica Nanotube as an Eco-Friendly Nanocomposite. *Energy Fuels* **2019**, *33*, 5384–5397.

(89) Zhao, Y.; Zhou, J.; Fan, L.; Chen, L.; Li, L.; Xu, Z. P.; Qian, G. Indoor CO_2 Control through Mesoporous Amine-Functionalized Silica Monoliths. *Ind. Eng. Chem. Res.* **2019**, *58*, 19465–19474.

(90) Huang, J.; Yu, L.; Fan, Q.; Yao, J.; Huang, Y.; Luo, H.; Liu, B.; Wang, H.; Xia, Q. Effective Adsorptive Removal of Trace CO_2 from Olefin Using Alkanolamine-Polyethylenimine-Functionalized Fumed Silica. *AIChE Journal* **2024**, *70*.

(91) Li, C.; Wang, X.; Yang, A.; Chen, P.; Zhao, T.; Liu, F. Polyethyleneimine-Modified Amorphous Silica for the Selective Adsorption of CO_2/N_2 at High Temperatures. *ACS Omega* **2021**, *6*, 35389–35397.

(92) Ojeda, M.; Mazaj, M.; Garcia, S.; Xuan, J.; Maroto-Valer, M. M.; Logar, N. Z. Novel Amine-Impregnated Mesostructured Silica Materials for CO_2 Capture. *Energy Procedia* **2017**, *114*, 2252–2258.

(93) Lou, F.; Zhang, A.; Zhang, G.; Ren, L.; Guo, X.; Song, C. Enhanced Kinetics for CO_2 Sorption in Amine-Functionalized Mesoporous Silica Nanosphere with Inverted Cone-Shaped Pore Structure. *Appl. Energy* **2020**, *264*.

(94) Chen, Y.; Wu, J.; Wang, X.; Liu, M.; Liu, Y. Synthesis, Characterization and Application of Amine-Functionalized Hierarchically Micro-Mesoporous Silicon Composites for CO_2 Capture in Flue Gas. *Molecules* **2022**, *27*.

(95) Huang, W.; Liu, J.; Rao, N.; Fan, G.; Yan, J.; Cheng, Q.; Song, G. Influence of Surfactant on CO_2 Adsorption of Amine-Functionalized MCM-41. *Environ. Technol.* **2022**, *43*, 4545–4553.

(96) Sayari, A.; Belmabkhout, Y.; Serna-Guerrero, R. Flue Gas Treatment via CO_2 Adsorption. *Chem. Eng. J.* **2011**, *171*, 760–774.

(97) Cogswell, C. F.; Nigl, T. P.; Stavola, A.; Wolek, A.; Wang, Y.; Zummo, J.; Lin, Y.; Dukaye, L.; Chinn, R.; Choi, S. Generation and Use of a Pure Titanium Pillared MCM-36 Structure as a High Efficiency Carbon Dioxide Capture Platform and Amine Loaded Solid Adsorbent. *Microporous Mesoporous Mater.* **2019**, *280*, 151–156.

(98) Jiao, J.; Lv, P.; Wang, L.; Dan, S.; Qi, L.; Cui, Y. CO_2 Capture of Amino Functionalized Three-Dimensional Worm-Hole Mesostructured MSU-J Silica. *J. Porous Mater.* **2014**, *21*, 775–781.

(99) Jiao, J.; Cao, J.; Xia, Y.; Zhao, L. Improvement of Adsorbent Materials for CO_2 Capture by Amine Functionalized Mesoporous Silica with Worm-Hole Framework Structure. *Chem. Eng. J.* **2016**, *306*, 9–16.

(100) Zhao, P.; Zhang, G.; Xu, Y.; Lv, Y. Amine Functionalized Hierarchical Bimodal Mesoporous Silicas as a Promising Nanocomposite for Highly Efficient CO_2 Capture. *J. CO_2 Util.* **2019**, *34*, 543–557.

(101) Zhao, P.; Zhang, G.; Xu, Y.; Lv, Y. K.; Yang, Z.; Cheng, H. Development of Amine-Functionalized Silica Foams with Hierarchical Pore Structure for CO_2 Capture. *Energy Fuels* **2019**, *33*, 3357–3369.

(102) Qi, L.; Yang, W.; Zhang, L.; Liu, Q.; Fei, Z.; Chen, X.; Zhang, Z.; Tang, J.; Cui, M.; Qiao, X. Reinforced CO_2 Capture on Amine-Impregnated Organosilica with Double Brush-like Additives Modified. *Ind. Eng. Chem. Res.* **2022**, *61*, 14859–14867.

(103) Li, X.; Li, H.; Zhao, X.; Zhao, Y.; Zhang, B.; Zhao, K.; Peng, K. Synergy Tetraethylenepentamine and Diethanolamine Impregnated within Silica Nanotubes Derived from Natural Halloysite for Efficient CO_2 Capture. *J. Clean Prod.* **2024**, *434*.

(104) Thakkar, H.; Eastman, S.; Al-Mamoori, A.; Hajari, A.; Rownaghi, A. A.; Rezaei, F. Formulation of Aminosilica Adsorbents into 3D-Printed Monoliths and Evaluation of Their CO_2 Capture Performance. *ACS Appl. Mater. Interfaces* **2017**, *9*, 7489–7498.

(105) Rahim, A. R. A.; Hao, T. T.; Azhari, A. A. W.; Saman, N.; Mat, H.; Johari, K. Synthesis and Characterization of Secondary Amine-Functionalized Silica for CO_2 Capture. In *IOP Conference Series: Earth and Environmental Science*; IOP Publishing, 2021; Vol. 765, p 012091.

(106) Vu, Q. T.; Yamada, H.; Yogo, K. Effects of Amine Structures on Oxidative Degradation of Amine-Functionalized Adsorbents for CO_2 Capture. *Ind. Eng. Chem. Res.* **2021**, *60*, 4942–4950.

(107) Lai, Q.; Diao, Z.; Kong, L.; Adidharma, H.; Fan, M. Amine-Impregnated Silicic Acid Composite as an Efficient Adsorbent for CO_2 Capture. *Appl. Energy* **2018**, *223*, 293–301.

(108) Wu, X.; Liu, M.; Shi, R.; Yu, X.; Liu, Y. CO_2 Adsorption/Regeneration Kinetics and Regeneration Properties of Amine Functionalized SBA-16. *J. Porous Mater.* **2018**, *25*, 1219–

1227.

(109) Liu, Y.; Lin, X.; Wu, X.; Liu, M.; Shi, R.; Yu, X. Pentaethylenehexamine Loaded SBA-16 for CO_2 Capture from Simulated Flue Gas. *Powder Technol.* **2017**, *318*, 186–192.

(110) Estévez-Jácome, J.; Argáez, C.; Ramírez-Zamora, R. M.; Alcántar-Vázquez, B. CO_2 Adsorption on PEHA-Functionalized Geothermal Silica Waste: A Kinetic Study and Quantum Chemistry Approach. *React. Chem. Eng.* **2022**, *7*, 2025–2034.

(111) Yan, H.; Zhang, G.; Liu, J.; Li, G.; Zhao, Y.; Wang, Y.; Wu, C.; Zhang, Y.; Xu, Y. Investigation of CO_2 Adsorption Performance of Amine Impregnated Adsorbents Using Amine-Support Matching Strategies. *Sep. Purif. Technol.* **2023**, *310*.

(112) Gelles, T.; Lawson, S.; Rownaghi, A. A.; Rezaei, F. Recent Advances in Development of Amine Functionalized Adsorbents for CO_2 Capture. *Adsorption* **2020**, *26*, 5–50.

(113) Samanta, A.; Zhao, A.; Shimizu, G. K. H.; Sarkar, P.; Gupta, R. Post-Combustion CO_2 Capture Using Solid Sorbents: A Review. *Ind. Eng. Chem. Res.* **2012**, *51*, 1438–1463.

(114) Kolle, J. M.; Fayaz, M.; Sayari, A. Understanding the Effect of Water on CO_2 Adsorption. *Chem. Rev.* **2021**, *121*, 7280–7345.

(115) Sardo, M.; Afonso, R.; Juźków, J.; Pacheco, M.; Bordonhos, M.; Pinto, M. L.; Gomes, J. R. B.; Mafra, L. Unravelling Moisture-Induced CO_2 Chemisorption Mechanisms in Amine-Modified Sorbents at the Molecular Scale. *J. Mater. Chem. A* **2021**, *9*, 5542–5555.

(116) Said, R. Ben; Kolle, J. M.; Essalah, K.; Tangour, B.; Sayari, A. A Unified Approach to CO_2–Amine Reaction Mechanisms. *ACS Omega* **2020**, *5*, 26125–26133.

(117) Szego, A. E.; Jaworski, A.; Hedin, N. Chemisorption of CO_2 on Diaminated Silica as Bicarbonates and Different Types of Carbamate Ammonium Ion Pairs. *Mater. Adv.* **2021**, *2*, 448.

(118) Lee, J. J.; Chen, C.-H.; Shimon, D.; Hayes, S. E.; Sievers, C.; Jones, C. W. Effect of Humidity on the CO_2 Adsorption of Tertiary Amine Grafted SBA-15. *J. Phys. Chem. C* **2017**, *121*, 23480–23487.

(119) Choi, S.; Gray, M. L.; Jones, C. W. Amine-Tethered Solid Adsorbents Coupling High Adsorption Capacity and Regenerability for CO_2 Capture from Ambient Air. *ChemSusChem* **2011**, *4*, 628–635.

(120) Pang, S. H.; Lively, R. P.; Jones, C. W. Oxidatively-Stable Linear Poly(propylenimine)-Containing Adsorbents for CO_2 Capture from Ultradilute Streams. *ChemSusChem* **2018**, *11*, 2628–2637.

(121) Kong, Y.; Jiang, G.; Wu, Y.; Cui, S.; Shen, X. Amine Hybrid Aerogel for High-Efficiency CO_2 Capture: Effect of Amine Loading and CO_2 Concentration. *Chem. Eng. J.* **2016**, *306*, 362–368.

(122) Rim, G.; Priyadarshini, P.; Song, M.; Wang, Y.; Bai, A.; Realff, M. J.; Lively, R. P.; Jones, C. W. Support Pore Structure and Composition Strongly Influence the Direct Air Capture of CO_2 on Supported Amines. *J. Am. Chem. Soc.* **2023**, *145*, 7190–7204.

(123) Min, K.; Choi, W.; Kim, C.; Choi, M. Rational Design of the Polymeric Amines in Solid Adsorbents for Postcombustion Carbon Dioxide Capture. *ACS Appl. Mater. Interfaces* **2018**, *10*, 23825–23833.

(124) Elfving, J.; Kauppinen, J.; Jegoroff, M.; Ruuskanen, V.; Järvinen, L.; Sainio, T. Experimental Comparison of Regeneration Methods for CO_2 Concentration from Air Using Amine-Based Adsorbent. *Chem. Eng. J.* **2021**, *404*, 126337.

(125) Grossmann, Q.; Mazzotti, M. Mass Transfer of CO_2 in Amine-Functionalized Structured Contactors in Ultra-Dilute Conditions. *Ind. Eng. Chem. Res.* **2025**.

(126) Sayari, A.; Belmabkhout, Y. Stabilization of Amine-Containing CO_2 Adsorbents: Dramatic Effect of Water Vapor. *J. Am. Chem. Soc.* **2010**, *132*, 6312–6314.

(127) Sayari, A.; Belmabkhout, Y.; Da'na, E. CO_2 Deactivation of Supported Amines: Does the Nature of Amine Matter? *Langmuir* **2012**, *28*, 4241–4247.

(128) US Department of Energy. *Cement Kiln Flue Gas Recovery Scrubber Project: A DOE Assessment*. https://digital-library-unt-edu.proxy.bib.uottawa.ca/ark:/67531/metadc721230/ (accessed 2025-01-25).

(129) Zevenhoven, R.; Kilpinen, P. *Control of Pollutants in Flue Gases and Fuel Gases*; 2001. www.hut.fi/~rzevenho/gasbook.

(130) Rezaei, F.; Jones, C. W. Stability of Supported Amine Adsorbents to SO_2 and NO_x in Postcombustion CO_2 Capture. 1. Single-Component Adsorption. *Ind. Eng. Chem. Res.* **2013**, *52*, 12192–12201.

(131) Belmabkhout, Y.; Sayari, A. Isothermal versus Non-Isothermal Adsorption−Desorption Cycling of Triamine-Grafted Pore-Expanded MCM-41 Mesoporous Silica for CO_2 Capture from Flue Gas. *Energy Fuels* **2010**, *24*, 5273–5280.

(132) Hallenbeck, A. P.; Kitchin, J. R. Effects of O_2 and SO_2 on the Capture Capacity of a Primary-Amine Based Polymeric CO_2 Sorbent. *Ind. Eng. Chem. Res.* **2013**, *52*, 10788–10794.

(133) Environmental Protection Agency. *Sulfur Dioxide Basics*. https://www.epa.gov/so2-pollution/sulfur-dioxide-basics (accessed 2025-01-26).

(134) Diaf, A.; Garcia, J. L.; Beckman, E. J. Thermally Reversible Polymeric Sorbents for Acid Gases: CO_2, SO_2, and NO_x. *J. Appl. Polym. Sci.* **1994**, *53*, 857–875.

(135) Wang, M.; Yao, L.; Wang, J.; Zhang, Z.; Qiao, W.; Long, D.; Ling, L. Adsorption and Regeneration Study of Polyethylenimine-Impregnated Millimeter-Sized Mesoporous Carbon Spheres for Post-Combustion CO_2 Capture. *Appl. Energy* **2016**, *168*, 282–290.

(136) Li, X.; Han, J.; Liu, Y.; Dou, Z.; Zhang, T. Summary of Research Progress on Industrial Flue Gas Desulfurization Technology. *Sep. Purif. Technol.* **2022**, *281*, 119849.

(137) Gu, S.; Yang, Z.; Chen, Z.; You, C. Dissolution Reactivity and Kinetics of Low-Grade Limestone for Wet Flue Gas Desulfurization. *Ind. Eng. Chem. Res.* **2020**, *59*, 14242–14251.

(138) Liu, Y.; Ye, Q.; Shen, M.; Shi, J.; Chen, J.; Pan, H.; Shi, Y. Carbon Dioxide Capture by Functionalized Solid Amine Sorbents with Simulated Flue Gas Conditions. *Environ. Sci.*

Technol. **2011**, *45*, 5710–5716.

(139) Srivastava, R. K.; Jozewicz, W. Flue Gas Desulfurization: The State of the Art. *J. Air Waste Manage. Assoc.* **2001**, *51*, 1676–1688.

(140) Li, W.; Cheng, C.; Gao, G.; Xu, H.; Huang, W.; Qu, Z.; Yan, N. Trace SO2 Capture within the Engineered Pore Space Using a Highly Stable SnF_6^{2-}-Pillared MOF. *Mater. Horiz.* **2024**, *11*, 1889–1898.

(141) Brandt, P.; Nuhnen, A.; Lange, M.; Möllmer, J.; Weingart, O.; Janiak, C. Metal–Organic Frameworks with Potential Application for SO_2 Separation and Flue Gas Desulfurization. *ACS Appl. Mater. Interfaces* **2019**, *11*, 17350–17358.

(142) Fu, Y.; Wang, Z.; Li, S.; He, X.; Pan, C.; Yan, J.; Yu, G. Functionalized Covalent Triazine Frameworks for Effective CO_2 and SO_2 Removal. *ACS Appl. Mater. Interfaces* **2018**, *10*, 36002–36009.

(143) An, X. C.; Li, Z. M.; Zhou, Y.; Zhu, W.; Tao, D. J. Rapid Capture and Efficient Removal of Low-Concentration SO_2 in Simulated Flue Gas by Hypercrosslinked Hollow Nanotube Ionic Polymers. *Chem. Eng. J.* **2020**, *394*, 124859.

(144) Jia, J.; Bhatt, P. M.; Tavares, S. R.; Abou-Hamad, E.; Belmabkhout, Y.; Jiang, H.; Mallick, A.; Parvatkar, P. T.; Maurin, G.; Eddaoudi, M. Porous Organic Polymers for Efficient and Selective SO_2 Capture from CO_2-rich Flue Gas. *Angew. Chem. Int. Ed.* **2024**, *63*, e202318844-n/a.

(145) Yi, H.; Deng, H.; Tang, X.; Yu, Q.; Zhou, X.; Liu, H. Adsorption Equilibrium and Kinetics for SO_2, NO, CO_2 on Zeolites FAU and LTA. *J. Hazard. Mater.* **2012**, *203*, 111–117.

(146) Ivanova, E.; Koumanova, B. Adsorption of Sulfur Dioxide on Natural Clinoptilolite Chemically Modified with Salt Solutions. *J. Hazard. Mater.* **2009**, *167*, 306–312.

(147) Fan, Y. L.; Zhang, H. P.; Yin, M. J.; Krishna, R.; Feng, X. F.; Wang, L.; Luo, M. B.; Luo, F. High Adsorption Capacity and Selectivity of SO_2 over CO_2 in a Metal-Organic Framework. *Inorg. Chem.* **2021**, *60*, 4–8.

(148) Zhang, Y.; Zhang, P.; Yu, W.; Zhang, J.; Huang, J.; Wang, J.; Xu, M.; Deng, Q.; Zeng, Z.; Deng, S. Highly Selective and Reversible Sulfur Dioxide Adsorption on a Microporous Metal–Organic Framework via Polar Sites. *ACS Appl. Mat. Interfaces* **2019**, *11*, 10680–10688.

(149) Smith, G. L.; Eyley, J. E.; Han, X.; Zhang, X.; Li, J.; Jacques, N. M.; Godfrey, H. G. W.; Argent, S. P.; McCormick McPherson, L. J.; Teat, S. J.; Cheng, Y.; Frogley, M. D.; Cinque, G.; Day, S. J.; Tang, C. C.; Easun, T. L.; Rudić, S.; Ramirez-Cuesta, A. J.; Yang, S.; Schröder, M. Reversible Coordinative Binding and Separation of Sulfur Dioxide in a Robust Metal-Organic Framework with Open Copper Sites. *Nat. Mater.* **2019**, *18*, 1358–1365.

(150) Tailor, R.; Sayari, A. Grafted Propyldiethanolamine for Selective Removal of SO_2 in the Presence of CO_2. *Chem. Eng. J* **2016**, *289*, 142–149.

(151) Kim, C.; Choi, W.; Choi, M. SO_2 -Resistant Amine-Containing CO_2 Adsorbent with a Surface Protection Layer. *ACS Appl. Mater. Interfaces* **2019**, *11*, 16586–16593.

(152) Vasilieva, L. L.; Dultsev, F. N.; Milekhin, A. K. IR Spectral Study of SO_2 Adsorption on Polysiloxane Layers Containing Tertiary Amino Groups. *J. Struct. Chem.* **1996**, *37*, 142–145.

(153) Zhu, G.; Carrillo, J.-M. Y.; Sujan, A.; Okonkwo, C. N.; Park, S.; Sumpter, B. G.; Jones, C. W.; Lively, R. P. Molecular Blends of Methylated-Poly(ethylenimine) and Amorphous Porous Organic Cages for SO_2 Adsorption. *J. Mater. Chem. A* **2018**, *6*, 22043–22052.

(154) Buijs, W. Molecular Modeling Study of the SO_2 Deactivation of an Amine Resin and a Procedure to Avoid SO_2 Deactivation Using a Polyethylene Glycol/Tertiary Amine System. *Ind. Eng. Chem. Res.* **2020**, *59*, 13388–13395

(155) Tailor, R.; Abboud, M.; Sayari, A. Supported Polytertiary Amines: Highly Efficient and Selective SO_2 Adsorbents. *Environ. Sci. Technol.* **2014**, *48*, 2025–2034.

(156) Tailor, R.; Ahmadalinezhad, A.; Sayari, A. Selective Removal of SO_2 over Tertiary Amine-Containing Materials. *Chem. Eng. J.* **2014**, *240*, 462–468.

(157) Lan, H. C.; Zhang, J. Y.; Dai, Q. J.; Ye, H.; Mao, X. Y.; Wang, Y. C.; Peng, H. L.; Du, J.; Huang, K. Highly Efficient, Selective and Reversible Capture of Sulfur Dioxide by Methylated-Polyethylenimine Supported on Graphitic Carbon Nitride. *Chem. Eng. J.* **2021**, *409*.

(158) Lan, H. C.; Zou, Y. T.; Wang, Y. C.; Cheng, N. N.; Xu, W. L.; Peng, H. L.; Huang, K.; Kong, L. Y.; Du, J. Meso-Macroporous Polymer Densely Functionalized with Tertiary Amine Groups as Effective Sorbents for SO_2 Capture. *Chem. Eng. J.* **2021**, *422*.

(159) Heydari-Gorji, A.; Sayari, A. Thermal, Oxidative, and CO_2-Induced Degradation of Supported Polyethylenimine Adsorbents. *Ind. Eng. Chem. Res.* **2012**, *51*, 6887–6894.

(160) Min, K.; Choi, W.; Kim, C.; Choi, M. Oxidation-Stable Amine-Containing Adsorbents for Carbon Dioxide Capture. *Nat. Commun.* **2018**, *9*, 726.

(161) Vu, Q. T.; Yamada, H.; Yogo, K. Stability of Polyamine Based Adsorbents to Gas Impurities for CO_2 Capture. *ISIJ Int.* **2022**, *62*, 2442–2445.

(162) Vu, Q. T.; Yamada, H.; Yogo, K. Oxidative Degradation of Tetraethylenepentamine-Impregnated Silica Sorbents for CO_2 Capture. *Energy Fuels* **2019**, *33*, 3370–3379.

(163) Bali, S.; Chen, T. T.; Chaikittisilp, W.; Jones, C. W. Oxidative Stability of Amino Polymer-Alumina Hybrid Adsorbents for Carbon Dioxide Capture. *Energy Fuels* **2013**, *27*, 1547–1554.

(164) Lee, J. J.; Yoo, C. J.; Chen, C. H.; Hayes, S. E.; Sievers, C.; Jones, C. W. Silica-Supported Sterically Hindered Amines for CO_2 Capture. *Langmuir* **2018**, *34*, 12279–12292.

(165) Guo, M.; Liang, S.; Liu, J.; Jin, J.; Mi, J. Epoxide-Functionalization of Grafted Tetraethylenepentamine on the Framework of an Acrylate Copolymer as a CO_2 Sorbent with Long Cycle Stability. *ACS Sustainable Chem. Eng.* **2020**, *8*, 3853–3864.

(166) Holmes, H. E.; Banerjee, S.; Vallace, A.; Lively, R. P.; Jones, C. W.; Realff, M. J. Tuning Sorbent Properties to Reduce the Cost of Direct Air Capture. *Energy Environ. Sci.* **2024**, *17*, 4544–4559.

(167) Panda, D.; Kulkarni, V.; Singh, S. K. Evaluation of Amine-Based Solid Adsorbents for Direct

Air Capture: A Critical Review. *React. Chem. Eng.* **2022**, *8*, 1–4.

(168) Choi, W.; Park, J.; Choi, M. Cation Effects of Phosphate Additives for Enhancing the Oxidative Stability of Amine-Containing CO_2 Adsorbents. *Ind. Eng. Chem. Res.* **2021**, *60*, 6147–6152.

(169) Choi, W.; Min, K.; Kim, C.; Ko, Y. S.; Jeon, J. W.; Seo, H.; Park, Y. K.; Choi, M. Epoxide-Functionalization of Polyethyleneimine for Synthesis of Stable Carbon Dioxide Adsorbent in Temperature Swing Adsorption. *Nat. Commun.* **2016**, *7*, 12640.

(170) Yan, C.; Sayari, A. Spectroscopic Investigation into the Oxidation of Polyethylenimine for CO_2 Capture: Mitigation Strategies and Mechanism. *Chem. Eng. J.* **2024**, *479*, 147498.

(171) Zhai, Y.; Chuang, S. S. C. Enhancing Degradation Resistance of Polyethylenimine for CO_2 Capture with Cross-Linked Poly(vinyl alcohol). *Ind. Eng. Chem. Res.* **2017**, *56*, 13766–13775.

(172) Srikanth, C. S.; Chuang, S. S. C. Spectroscopic Investigation into Oxidative Degradation of Silica-Supported Amine Sorbents for CO_2 Capture. *ChemSusChem* **2012**, *5*, 1435–1442.

(173) Li, S.; Andrade, M. F.; Varni, A. J.; Russell-Parks, G. A.; Braunecker, W. A.; Hunter-Sellars, E.; Marple, M. A.; Pang, S. H. Enhanced Hydrogen Bonding via Epoxide-Functionalization Restricts Mobility in Poly(ethylenimine) for CO_2 Capture. *Chem. Commun.* **2023**, *59*, 10737–10740.

(174) Short, G. N.; Burentugs, E.; Proaño, L.; Moon, H. J.; Rim, G.; Nezam, I.; Korde, A.; Nair, S.; Jones, C. W. Single-Walled Zeolitic Nanotubes: Advantaged Supports for Poly(ethylenimine) in CO_2 Separation from Simulated Air and Flue Gas. *JACS Au* **2023**, *3*, 62–69.

(175) Zerze, H.; Tipirneni, A.; McHugh, A. J. Reusable Poly(allylamine)-Based Solid Materials for Carbon Dioxide Capture under Continuous Flow of Ambient Air. *Sep. Sci. Technol.* **2017**, *52*, 2513–2522.

(176) Chen, C.-H.; Shimon, D.; Lee, J. J.; Mentink-Vigier, F.; Hung, I.; Sievers, C.; Jones, C. W.; Hayes, S. E. The "Missing" Bicarbonate in CO_2 Chemisorption Reactions on Solid Amine Sorbents. *J. Am. Chem. Soc.* **2018**, *140*, 8648–8651.

(177) Chen, C.-H.; Sesti, E. L.; Lee, J. J.; Mentink-Vigier, F.; Sievers, C.; Jones, C. W.; Hayes, S. E. NMR Reveals Two Bicarbonate Environments in SBA 15-Solid-Amine CO_2 Sorbents. *J. Phys. Chem. C* **2021**, *125*, 16759–16765.

(178) Chen, O. I. F.; Liu, C. H.; Wang, K.; Borrego-Marin, E.; Li, H.; Alawadhi, A. H.; Navarro, J. A. R.; Yaghi, O. M. Water-Enhanced Direct Air Capture of Carbon Dioxide in Metal-Organic Frameworks. *J. Am. Chem. Soc.* **2024**, *146*, 2835–2844.

(179) Veldhuizen, H.; Butt, S. A.; van Leuken, A.; van der Linden, B.; Rook, W.; van der Zwaag, S.; van der Veen, M. A. Competitive and Cooperative CO_2–H_2O Adsorption through Humidity Control in a Polyimide Covalent Organic Framework. *ACS Appl. Mater. Interfaces* **2023**, *15*, 29186–29194.

(180) Holmes, H. E.; Ghosh, S.; Li, C.; Kalyanaraman, J.; Realff, M. J.; Weston, S. C.; Lively, R. P. Optimum Relative Humidity Enhances CO_2 Uptake in Diamine-Appended M_2(Dobpdc). *Chem. Eng. J.* **2023**, *477*, 147119.

(181) International Energy Agency. *Carbon Capture, Utilisation, and Storage*. https://www.iea.org/energy-system/carbon-capture-utilisation-and-storage?utm_source (accessed 2025-01-29).

(182) United Nations Framework Convention on Climate Change. *The Paris Agreement*. https://unfccc.int/process-and-meetings/the-paris-agreement (accessed 2025-01-29).

(183) Technology Networks. *NMR Spectroscopy Principles, Interpreting an NMR Spectrum, and Common Problems*. https://www.technologynetworks.com/analysis/articles/nmr-spectroscopy-principles-interpreting-an-nmr-spectrum-and-common-problems-355891 (accessed 2025-02-07).

(184) Kemp, W. *Organic Spectroscopy*, Third Edition.; Macmillan Education UK, 1991.

(185) Yan, X.; Zhang, L.; Zhang, Y.; Yang, G.; Yan, Z. Amine-Modified SBA-15: Effect of Pore Structure on the Performance for CO_2 Capture. *Ind. Eng. Chem. Res.* **2011**, *50*, 3220–3226.

(186) Kaur, C.; Sayari, A. Glycidol-Modified PEI: A Highly Selective Adsorbent for SO_2 in the Presence of CO_2. *J. Mater. Chem. A* **2024**, *12*, 31526–31532.

(187) Thommes, M.; Kaneko, K.; Neimark, A. V.; Olivier, J. P.; Rodriguez-Reinoso, F.; Rouquerol, J.; Sing, K. S. W. Physisorption of Gases, with Special Reference to the Evaluation of Surface Area and Pore Size Distribution (IUPAC Technical Report). *Pure Appl. Chem.* **2015**, *87*, 1051–1069.

(188) Calzaferri, G.; Gallagher, S. H.; Lustenberger, S.; Walther, F.; Brühwiler, D. Multiple Equilibria Description of Type H1 Hysteresis in Gas Sorption Isotherms of Mesoporous Materials. *Mater. Chem. Phys.* **2023**, *296*, 127121.

(189) Barrett, E. P.; Joyner, L. G.; Halenda, P. P. The Determination of Pore Volume and Area Distributions in Porous Substances. I. Computations from Nitrogen Isotherms. *J. Am. Chem. Soc.* **1951**, *73*, 373–380.

(190) Gutierrez-Ortega, A.; Nomen, R.; Sempere, J.; Parra, J. B.; Montes-Morán, M. A.; Gonzalez-Olmos, R. A Fast Methodology to Rank Adsorbents for CO_2 Capture with Temperature Swing Adsorption. *Chem. Eng. J.* **2022**, *435*, 134703.

(191) Ahsan, S.; Ayub, A.; Meeroff, D.; Jahandar Lashaki, M. A Comprehensive Comparison of Zeolite-5A Molecular Sieves and Amine-Grafted SBA-15 Silica for Cyclic Adsorption-Desorption of Carbon Dioxide in Enclosed Environments. *Chem. Eng. J.* **2022**, *437*, 135139.

(192) Surface Measurement Systems. *Dynamic Vapor Sorption*. https://surfacemeasurementsystems.com/solutions/dynamic-vapor-sorption/#:~:text=Dynamic%20Vapor%20Sorption%20rapidly%20measures,sensitive%20recording%20microbalance%2C%20the%20patented (accessed 2025-01-17).

(193) Dods, M. N.; Weston, S. C.; Long, J. R. Prospects for Simultaneously Capturing Carbon Dioxide and Harvesting Water from Air. *Adv. Mater.* **2022**, *34*, 2204277.

(194) Wilkins, N. S.; Rajendran, A.; Farooq, S. Dynamic Column Breakthrough Experiments for Measurement of Adsorption Equilibrium and Kinetics. *Adsorption* **2021**, *27*, 397–422.

(195) Rajendran, A.; Kariwala, V.; Farooq, S. Correction Procedures for Extra-Column Effects in

Dynamic Column Breakthrough Experiments. *Chem. Eng. Sci.* **2008**, *63*, 2696–2706.

(196) Darunte, L. A.; Terada, Y.; Murdock, C. R.; Walton, K. S.; Sholl, D. S.; Jones, C. W. Monolith-Supported Amine-Functionalized Mg_2(Dobpdc) Adsorbents for CO_2 Capture. *ACS Appl. Mater. Interfaces* **2017**, *9*, 17042–17050.

(197) Sujan, A. R.; Pang, S. H.; Zhu, G.; Jones, C. W.; Lively, R. P. Direct CO_2 Capture from Air Using Poly(ethylenimine)-Loaded Polymer/Silica Fiber Sorbents. *ACS Sustainable Chem. Eng.* **2019**, *7*, 5264–5273.

(198) DeWitt, S. J. A.; Sinha, A.; Kalyanaraman, J.; Zhang, F.; Realff, M. J.; Lively, R. P. Critical Comparison of Structured Contactors for Adsorption-Based Gas Separations. *Annu. Rev. Chem. Biomol. Eng.* **2018**, *9*, 129–152.

CHAPTER 2 GLYCIDOL-MODIFIED PEI: A HIGHLY SELECTIVE ADSORBENT FOR SO_2 IN THE PRESENCE OF CO_2

2.1. Abstract

Amine-containing CO_2 adsorbents are highly sensitive to the presence of SO_2 in the feed gas, even in minute amounts. It is thus necessary to remove SO_2 quantitatively prior to CO_2 capture. To this end, we developed a silica-supported polyethylenimine (GD-PEI/S) adsorbent containing only tertiary amines via quantitative glycidol functionalization. The novel material was characterized by infra-red (IR) and nuclear magnetic resonance (NMR) spectroscopy, and by thermogravimetric analysis (TGA). In the presence of a gas mixture containing 5 ppm SO_2 and more than $2x10^4$ higher concentration of CO_2, the GD-PEI/S material adsorbed SO_2 quantitatively until near saturation, with no CO_2 uptake, indicating that the adsorbent exhibits 100% SO_2 selectivity versus CO_2, even in the presence of very high CO_2/SO_2 ratios. Furthermore, the SO_2 uptake of the adsorbent almost doubled in the presence of humidity, possibly due to increased diffusion of SO_2. Under recycling conditions, GD-PEI/S showed good reversibility in the presence of both dry and humid SO_2 at low and high SO_2 concentration.

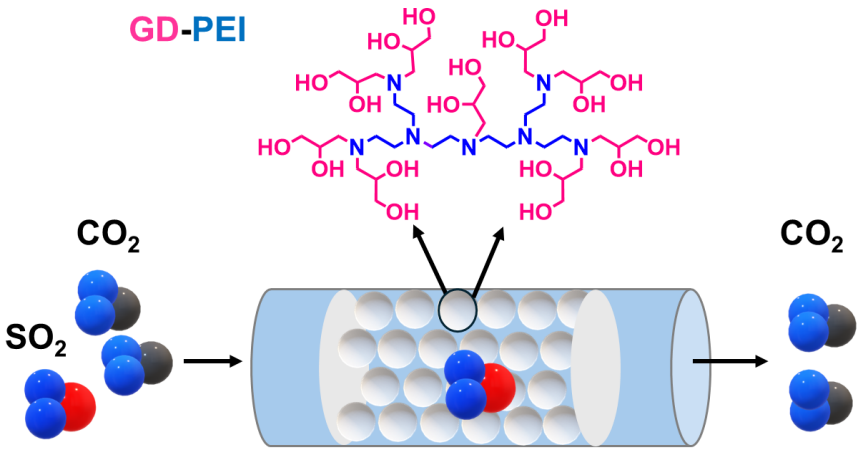

2.2. Introduction

As the main contributor to the greenhouse gas effect, CO_2 plays a predominant role in global warming.[1] The National Oceanic and Atmospheric Administration (NOAA) reported increasing levels of CO_2 in the atmosphere reaching 422 ppm in 2024.[2] Rising levels of CO_2 in the atmosphere were correlated with the increase in earth's temperature.[3] CO_2 capture and sequestration from flue gas and directly from air, is recognized as a key strategy for reducing CO_2 emissions, from stationary and distributed sources.[4,5]

Regarding CO_2 capture, solid amine adsorbents received significant attention due to their excellent selectivity, high adsorption capacity and low energy regeneration.[6–8] Nevertheless, there are challenges in using solid amine adsorbents, including the deleterious effect of harmful acidic gas impurities, such as SO_x and NO_x, that may occur in flue gas. Such species do not only cause environmental and health issues but are detrimental to CO_2 capture due to their strongly competitive adsorption.[9] Notice that, due to the potential health risks and environmental impact associated with elevated concentrations of SO_2 in the atmosphere[10], limits are imposed on sulfur emissions from large power facilities. Typical mandatory limits for SO_2 in exhaust gases are set to 120 ppm in the US, 75 to 300 ppm in China, and 50 to 250 ppm in Europe.[11] However, no matter how low the residual SO_2 content in the feed gas, amines in CO_2 adsorbents will be irreversibly deactivated.[12–14] For example, Jones and co-workers[14] reported that when PEI-impregnated silica support was exposed to a mixture of 20 ppm SO_2, 10% CO_2 balance N_2 at 35 °C, adsorbent lost 41% of CO_2 uptake after first cycle of adsorption. Therefore, before adsorbing CO_2 on amine-containing materials, it is crucial to remove SO_2 quantitatively from the feed gas.

Although there are numerous technologies for flue gas desulfurization, particularly liquid phase scrubbing[15], work on selective removal of traces of SO_2 in the presence of much higher CO_2 partial pressures is more pertinent for carbon capture over amine-containing adsorbents. More specifically, meeting this objective using adsorption would be easier to streamline with processes of CO_2 capture by adsorption. Many candidate materials were proposed for SO_2 removal, including

metal organic frameworks (MOFs),[16,17] zeolites,[18,19] porous polymers[20–22] and activated carbons.[23,24] Nonetheless, they have limitations, for example, activated carbons showed very limited selectivity and efficiency[25] in the presence of O_2 and H_2O, as they deactivated, producing H_2SO_4[26]. A number of MOFs with SO_2 vs CO_2 selectivity between 28 and 44 were reported in the literature.[27–29] However, not only such selectivities are not high enough, but the SO_2 concentration used was somewhat high (≥ 2000 ppm).

Adsorbents containing only tertiary amines seem to be the most selective for SO_2 vs CO_2. Tertiary amines adsorb SO_2 readily, but do not interact with CO_2, at least under dry condition.[14,30–39] For instance, when Tailor and Sayari[32] exposed propyldiethanolamine grafted on a pore-expanded MCM-41 support to a 50:50 mixture of 0.1% SO_2 balance N_2 and 20% CO_2 balance He at room temperature, they found that the presence of CO_2 had no effect on the adsorbent's ability to adsorb SO_2. Also, adsorbent could be fully regenerated after 11 adsorption-desorption cycles, which indicates high stability of material against heat and SO_2.

However, achieving complete functionalization of PEI protic amines into tertiary amines was found to be either difficult[33], or tedious[30,35,36,38]. Moreover, the majority of reported studies focused on removing high levels of SO_2 in gas mixtures[30–32,35,36] and to the best of our knowledge, none of the studies dealt with SO_2 concentrations below 50 ppm. Furthermore, in some cases, the working capacity of the adsorbent was found to decrease significantly in the presence of humid SO_2.[32]

The objective of this work was to develop a novel polytertiary amine adsorbent to selectively and quantitatively remove SO_2 at concentrations as low as 5 ppm in the presence of typical flue gas CO_2 concentration of 10-15%. To this end, complete functionalization of PEI with GD was achieved as shown in Scheme 2.1. In addition to its straightforward preparation, the glycidol-functionalized amine adsorbent exhibited stable working capacity in the presence of both dry and humid SO_2 at low and high SO_2 concentration. It is noteworthy that in addition to tertiary amines being highly selective to SO_2 adsorption, it was reported that the occurrence of hydroxyethylene groups decreases the energy for regeneration and increases the reversibility of the adsorbent.[33,40]

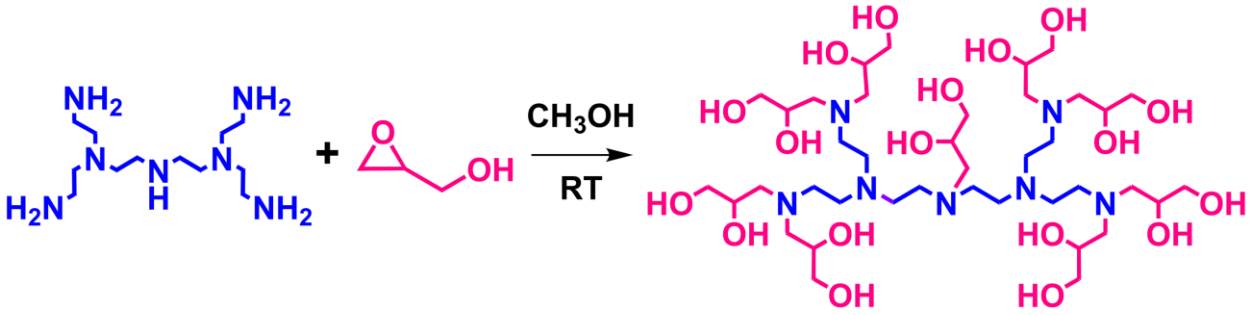

Scheme 2.1. Schematic of synthesis of GD-PEI.

2.3. Experimental Section

2.3.1. Materials

Polyethylenimine (PEI, Mw 1200), glycidol (GD, 96%), fumed silica (Cab-O-Sil, M5), tetramethylammonium hydroxide (TMAOH, 25 wt% solution), cetyltrimethylammonium bromide (CTAB, 98%), N,N-dimethyldodecyl amine (DMDA, 97%), tetraethyl orthosilicate (TEOS, 98%) and deuterium oxide (D_2O, 99.9 %) were obtained from Sigma-Aldrich. Sodium aluminate ($NaAlO_2$, 92%) was obtained from Strem Chemicals. Anhydrous methanol (99.8%) and ammonia solution (30 wt%) were obtained from Fischer. Chemicals were used as obtained. Ultrahigh purity (99.999%) nitrogen, 15% or 20% CO_2 in nitrogen and gas cylinders containing 20, 100 and 1000 ppm SO_2 in N_2, were purchased from Messer Canada.

2.3.2. Preparation of GD-PEI

Pore-expanded aluminosilica (PE-$AlSiO_2$) support was prepared as reported elsewhere,[41] and further details are included in the Supplementary Information (Figure A2.1). Functionalization of primary and secondary amines of PEI with GD was carried out as reported by Fan *et al.*[42] with slight modification. Briefly, 2 g of PEI (44 mmol of N) was dissolved in 20 mL of anhydrous methanol under nitrogen atmosphere. Then, 3.55 g (47.96 mmol) of GD was added dropwise, and the solution was stirred for 4 h. After removing excess of methanol using a rotary evaporator, the product was precipitated with acetone, then separated and dried in a vacuum oven at 70 °C,

overnight. The functionalized PEI, designated GD-PEI was impregnated onto PE-$AlSiO_2$ as follows. The obtained GD-PEI compound was dissolved in 30 mL of anhydrous methanol and stirred until complete dissolution. After that, 5.5 g of PE-$AlSiO_2$ was slowly added into the solution and the mixture stirred until the solvent evaporated. The final material was dried in an oven at 80 °C for 3 h and referred to as GD-PEI/S. 0.5 g of PEI was dissolved in 15 mL of methanol. After that, 0.5 g of PE-$AlSiO_2$ was added and mixture was stirred overnight followed by evaporation of solvent in oven at 70 °C for 6 h to obtain PEI/S. The overall loading of PEI/S and GD-PEI/S was fixed to 50 wt% with respect to adsorbent.

2.3.3. Characterization

The pore structure of PE-$AlSiO_2$ was investigated by N_2 adsorption measurements at −196 °C using a 3Flex instrument (Micromeritics). The sample was pretreated in flowing N_2 at 120 °C for 4 h. The specific surface area was determined using the Brunauer-Emmett-Teller (BET) method at relative pressures ranging from 0.06 to 0.2. The total pore volume was measured at $P/P_0 = 0.99$, whereas the pore size distribution was calculated using the Kruk-Jaroniec-Sayari method.[43]

PEI and GD-PEI were dissolved in D_2O and their ^{13}C nuclear magnetic resonance (NMR) spectra were obtained using an AVIII 600 spectrometer set to 45° pulse, 40 scans, 90 second relaxation delay and an acquisition time of 0.999 second. Inverse-gated proton decoupling was used to avoid the nuclear Overhauser effect. Fourier transform infrared spectroscopy (FTIR) spectra were obtained using a Cary 630 FTIR instrument by Agilent.

2.3.4. Adsorption Measurements

SO_2 adsorption measurements were carried out in a fixed bed reactor as shown in Figure 2.1. In a typical experiment, 0.5-1 g of sample was loaded into a 1 cm long stainless steel column with 0.42 cm inner diameter, and placed in a temperature-controlled oven. The material was pretreated under N_2 (40 mL/min) at 110 °C for 2 h. After cooling to 23 °C, it was exposed to SO_2 in N_2 gas mixture (40 mL/min) with different compositions. As for experiments under humid condition, N_2 was

bubbled through a water saturator placed in a thermostatic bath maintained at 20 °C, then combined with the SO_2 containing N_2. The gas mixture exiting from the column was constantly analyzed by a MKS Cirrus 3 mass spectrometer (MS), and breakthrough curves were obtained using MS data obtained for 64 amu. The SO_2 adsorption capacity (mmol/g) of GD-PEI/S at different partial pressures, was calculated using Eq. 2.1:

$$q = \frac{C_0 F t_q}{m} \qquad \text{Eq. 2.1}$$

where C_0 is the inlet concentration of SO_2, F is the flowrate of the gas mixture, m is the mass of the adsorbent and t_q is the stoichiometric time, which was evaluated from the column breakthrough curve using Eq. 2.2:

$$t_q = \int_0^\infty \left(1 - \frac{C_A}{C_0}\right) dt \qquad \text{Eq. 2.2}$$

where C_A represents the downstream concentration of SO_2.

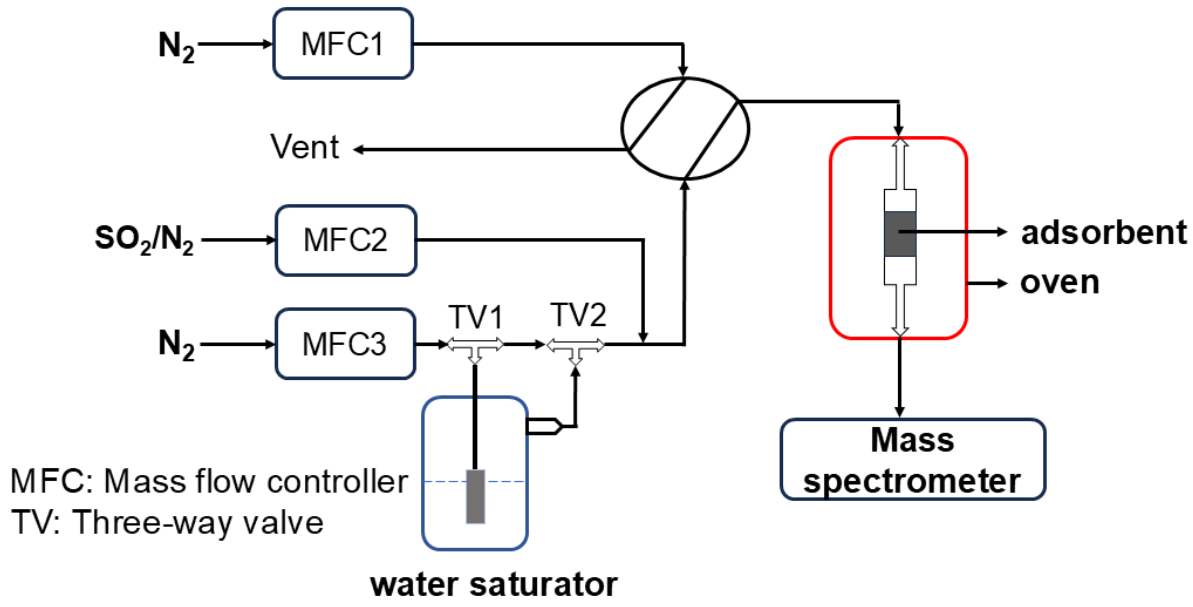

Figure 2.1. Schematic of the column breakthrough setup.

The CO_2 uptake and organic content of GD-PEI/S were measured using a thermogravimetric analyzer (TGA 550, TA Instruments). The sample (ca. 20 mg) was pretreated under N_2 for 60 min at 110 °C, followed by cooling to 25 °C, and then the gas stream was switched to 15% CO_2 balance N_2 for 30 min. After removal of adsorbed CO_2, if any, at 110 °C for 10 min under flowing N_2, the adsorbent was cooled down to 75 °C, and the gas stream was switched to 15% CO_2/N_2 for 30 min. Then, the temperature was increased to 700 °C at a rate of 10 °C min^{-1} under flowing N_2, before switching the gas to air for 25 min. The organic content was determined as the weight loss of the material beyond 200 °C.

2.4. Results and Discussion

2.4.1. Characterization of the adsorbent

The surface area, pore volume and average pore size of PE-$AlSiO_2$ were found to be 818 m^2/g, 1.66 cm^3/g and 8.13 nm. According to IUPAC nomenclature, the nitrogen adsorption-desorption isotherm of the support (Figure 2.2) belongs to Type IV, with an H1 hysteresis loop, indicating that the support is mesoporous. This is further confirmed by the pore size distribution shown in Figure 2.3, where the majority of pores fall within the range of 3-15 nm, with a maximum at 7 nm. The total polymer content of GD-PEI/S was 55 wt% with respect to the weight of the adsorbent (Figure A2.2).

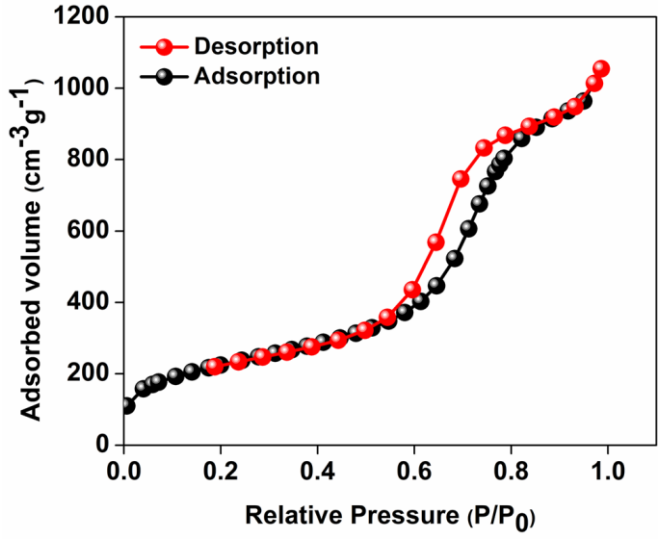

Figure 2.2. N_2 adsorption-desorption isotherm.

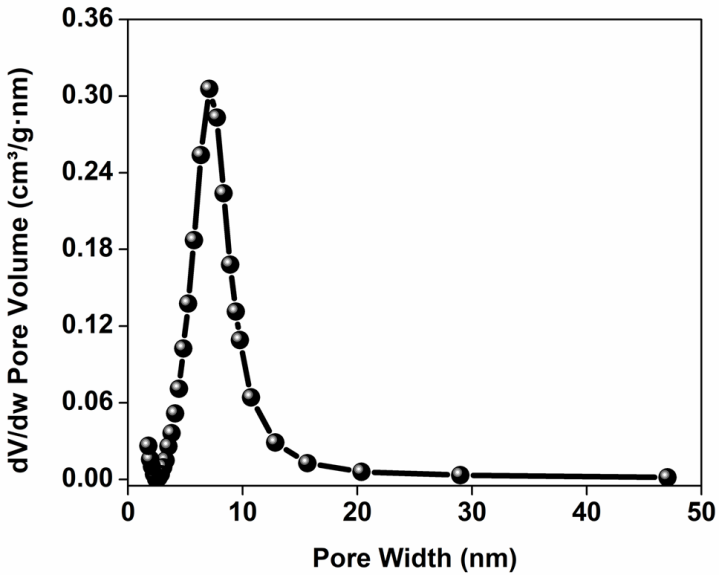

Figure 2.3. Pore size distribution of PE-$AlSiO_2$.

The FTIR spectra in Figure 2.4 showed that the band at 1567 cm^{-1} in PEI/S corresponding to N-H bending[44] disappeared completely upon functionalization with GD. Moreover, the higher intensity hydroxyl band at 3347 cm^{-1} in GD-PEI/S compared to PEI/S is consistent with the significant increase of hydroxyl groups. Functionalization of PEI with GD was further confirmed using ^{13}C NMR measurements as shown in Figure 2.5. The carbon peaks were assigned as outlined in the literature.[45,46] Using the intensity of NMR peaks of carbon atoms adjacent to primary, secondary and tertiary amines in PEI, the percentage of such amines was found to be 36:37:27.

Upon functionalization of PEI with GD, the NMR peaks corresponding to carbons neighboring primary and secondary amines disappeared, and new peaks attributable to carbons neighboring tertiary amines and to added GD, developed (Scheme 2.1). This finding confirmed the incorporation of GD with complete conversion of primary and secondary amines into tertiary amines.

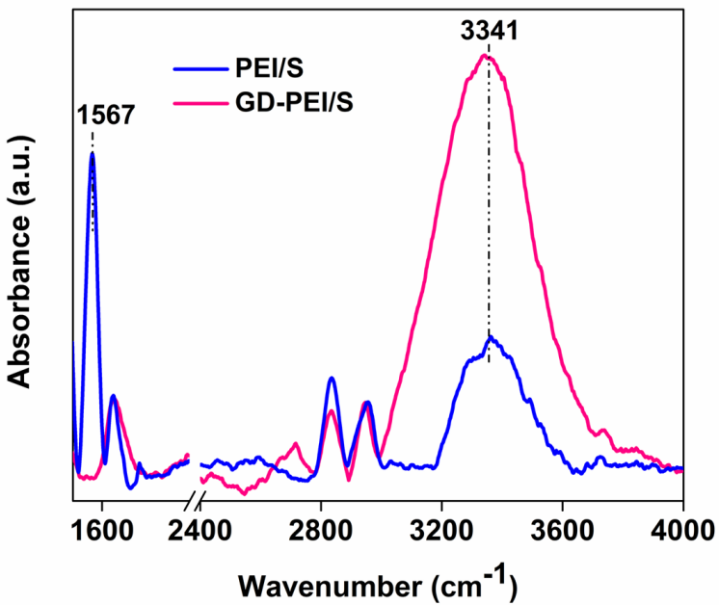

Figure 2.4. FT-IR spectra of PEI/S and GD-PEI/S.

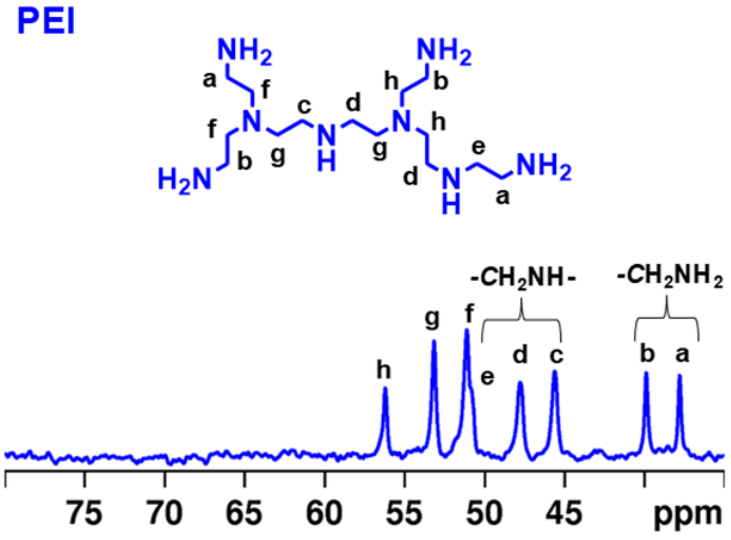

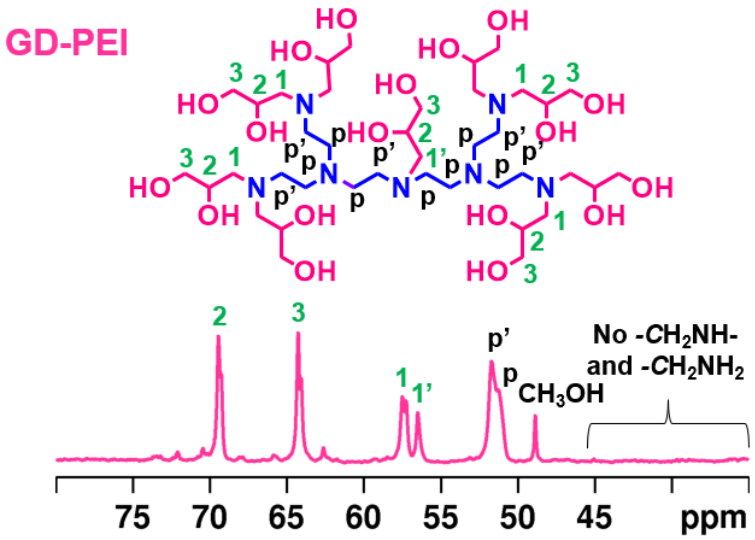

Figure 2.5. ^{13}C NMR spectra of PEI and GD-PEI.

2.4.2. SO_2 adsorption isotherm

Figure 2.6 shows the SO_2 uptake of GD-PEI/S at 23 °C at different concentrations. The different gas compositions were achieved by diluting premixed 20, 100 or 1000 ppm SO_2/N_2 with pure N_2, at different flowrates, while maintaining the overall flowrate at 40 mL/min. The shape of this isotherm is consistent with chemisorption. At low concentrations, the adsorption capacity rises steeply with increasing concentration, indicating the high sensitivity of tertiary amine groups toward SO_2. The uptake reaches a plateau at ca. 1000 ppm SO_2, presumably because most of the accessible adsorption sites are occupied. The actual SO_2 uptakes versus partial pressure are listed in Table A2.1. The breakthrough curves of GD-PEI/S under different partial of SO_2 are shown in Figure A2.3.

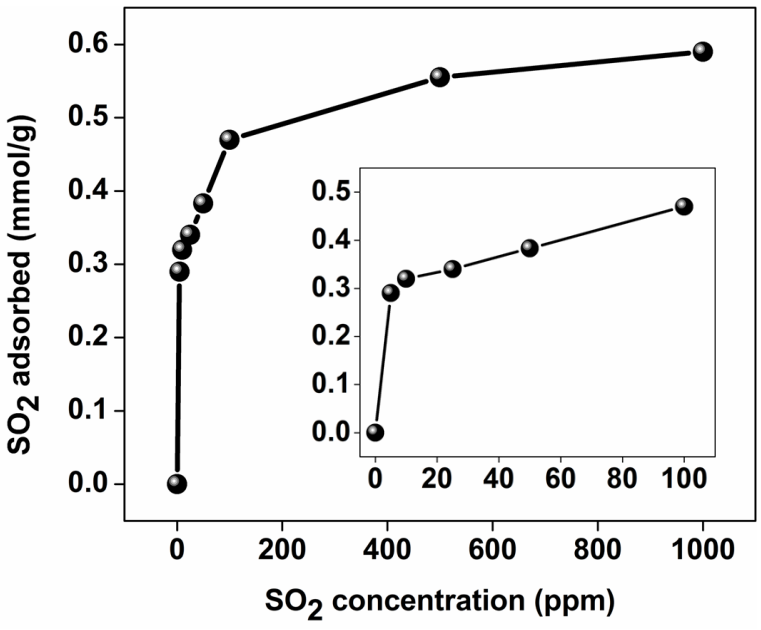

Figure 2.6. SO_2 adsorption isotherms for GD-PEI/S.

2.4.3. Selectivity towards SO_2 versus CO_2

Figure 2.7 depicts the column-breakthrough data over GD-PEI/S in the presence of 5 to 50 ppm SO_2 in 10% or 11% CO_2, as indicated. The gas compositions were achieved by mixing different concentrations of SO_2 in N_2 with 15% or 20% premixed CO_2 in N_2, while maintaining the overall flowrate at 40 mL/min. Column breakthrough curves showed that CO_2 comes out of the column within few seconds of passing the gas mixture. Furthermore, regardless of the presence of CO_2, the SO_2 uptake (Figure A2.4), breakthrough time, and equilibrium time remained the same at any given SO_2 concentration. This is consistent with TGA measurements (Figure A2.5), which showed that the CO_2 uptake of GD-PEI/S was only 0.08 and 0.01 mmol/g at 25 and 75°C, respectively. These results indicate that no CO_2 was chemisorbed by GD-PEI/S, which is in line with the fact that under dry conditions, only protic amines interact with CO_2 to afford ammonium carbamate.[47]

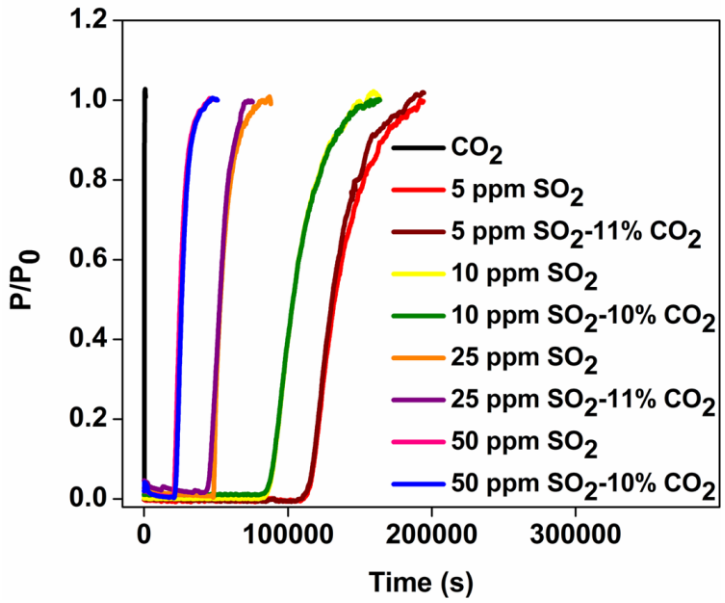

Figure 2.7. Breakthrough curves of GD-PEI/S in the presence of different concentrations of SO_2 with and without CO_2.

2.4.4. Stability of the adsorbent under cyclic conditions

To investigate the stability of SO_2 working capacity over GD-PEI/S or the lack thereof, a series of SO_2 adsorption-desorption was carried out, with adsorption at 23 °C in the presence of dry 100 ppm SO_2 in N_2, and desorption at 110 °C in N_2. SO_2 uptake of GD-PEI/S decreased by 7 and 5% during the first and second cycles, then remained stable thereafter (Figure 2.8). Moreover, breakthrough and equilibrium times remained the same after the second adsorption cycle, as seen in Figure A2.6. Zhu *et al.*[38] observed a similar trend and attributed the decrease in SO_2 uptake during the first cycle to the adsorption of SO_2 onto basic sites that were not completely regenerated.

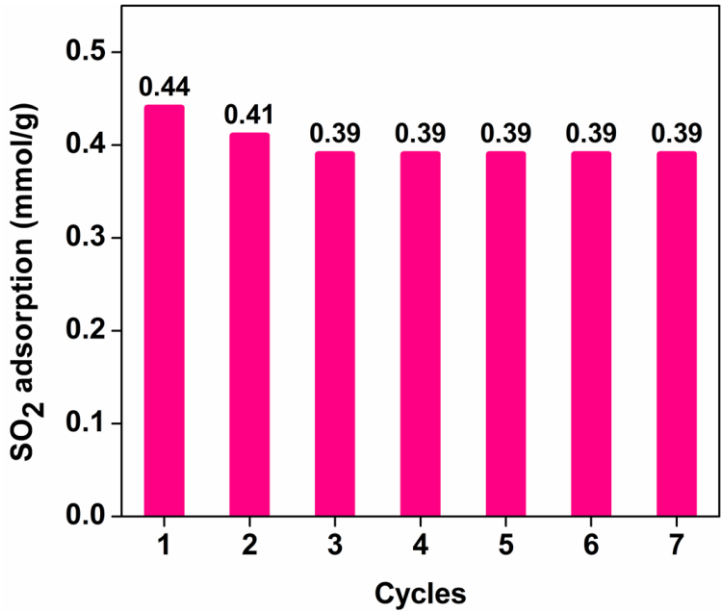

Figure 2.8. Regeneration cycles of GD-PEI/S under dry 100 ppm SO_2 balance N_2.

Adsorption-desorption cycles were also performed under dry and humid 500 ppm SO_2 balance N_2 as shown in Figure A2.7 and 2.9 respectively. In the absence of moisture, the adsorbent lost 17% SO_2 uptake after the first two regeneration cycles, and it remained almost stable in subsequent cycles. However, adsorbent deactivated more in 500 ppm SO_2 in N_2 than 100 ppm SO_2 in N_2. This could be a result of elevated SO_2 concentration, which increases the interaction of SO_2 with adsorption sites and subsequently the likelihood of their deactivation. In agreement with other studies,[30–32] SO_2 adsorption capacity of GD-PEI/S increased by 64% under humid (42% RH) 500 ppm SO_2 in N_2, from 0.55 to 0.90 mmol/g, which may be because water can act as a lubricant, reducing the diffusion resistance for incoming SO_2. Tailor *et al.*[30] proposed that this improvement may be due to the formation of ammonium bisulfite salt[48,49] in humid environment as shown in equation 3. Overall, the decrease in SO_2 uptake before stabilization was similar under dry and wet conditions *i.e.* ~ 23%. The corresponding breakthrough curves are shown in Figure A2.8.

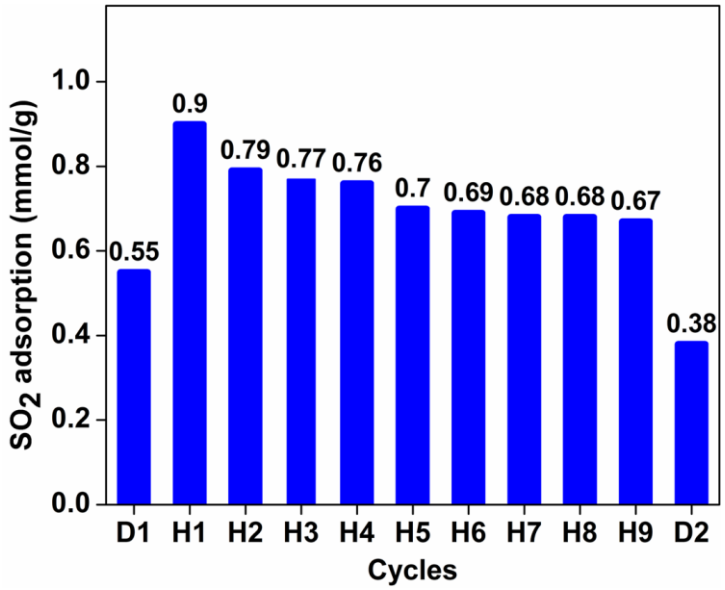

Figure 2.9. Working capacity over GD-PEI/S of humid 500 ppm SO_2 in N_2. D1 and D2 indicate data under dry condition before and after experiment in humid condition.

$$R_3N + SO_2 \rightleftharpoons R_3N\cdots SO_2 \overset{+H_2O}{\underset{-H_2O}{\rightleftharpoons}} R_3NH^+HSO_3^- \qquad \text{Eq. 2.3}$$

2.5. Conclusions

GD-PEI/S was synthesized by converting all protic amines in PEI into tertiary amines using glycidol functionalization, followed by impregnation onto pore-expanded $AlSiO_2$. The adsorbent showed SO_2 capacity of 0.29 mmol/g when exposed to 5 ppm SO_2/N_2, with a positive correlation with increasing SO_2 concentration. The selectivity of the adsorbent towards SO_2 was investigated in the presence of different concentrations of SO_2 in CO_2/N_2 mixtures. GD-PEI/S was found to be 100% selective for SO_2 at concentration as low as 5 ppm in the presence of 11% CO_2, corresponding to CO_2/SO_2 ratio of 22,000. The presence of only tertiary amines with no interaction with CO_2 is at the origin of the high selectivity toward SO_2 versus CO_2. Moreover, the adsorbent showed more than two times increase in SO_2 uptake under humid conditions. The adsorbent was also found to be stable during adsorption-desorption cycling in the presence of dry and wet SO_2/N_2 mixtures. Therefore, GD-PEI/S may be used as a filter for extensive desulfurization before CO_2 capture on amine-containing adsorbents.

2.6. References

(1) Crippa, M., Guizzardi, D., Pagani, F., Banja, M., Muntean, M., Schaaf E., Becker, W., Monforti-Ferrario, F., Quadrelli, R., Risquez Martin, A., Taghavi-Moharamli, P., Köykkä, J., Grassi, G., Rossi, S., Brandao De Melo, J., Oom, D., Branco, A., San-Miguel, E. *GHG Emissions of All World Countries*; 2023.

(2) *Trends in Atmospheric Carbon Dioxide*, https://gml.noaa.gov/ccgg/trends/weekly.html (accessed 2024-08-18).

(3) www.climate.nasa.gov (accessed 2024-08-18).

(4) Markewitz, P.; Kuckshinrichs, W.; Leitner, W.; Linssen, J.; Zapp, P.; Bongartz, R.; Schreiber, A.; Müller, T. E. Worldwide Innovations in the Development of Carbon Capture Technologies and the Utilization of CO_2. *Energy Environ. Sci.* **2012**, *5*, 7281–7305.

(5) Zhu, X.; Xie, W.; Wu, J.; Miao, Y.; Xiang, C.; Chen, C.; Ge, B.; Gan, Z.; Yang, F.; Zhang, M.; O'Hare, D.; Li, J.; Ge, T.; Wang, R. Recent Advances in Direct Air Capture by Adsorption. *Chem. Soc. Rev.* **2022**, *51*, 6574–6651.

(6) Jaffar, M. M.; Rolfe, A.; Brandoni, C.; Martinez, J.; Snape, C.; Kaldis, S.; Santos, A.; Lysiak, B.; Lappas, A.; Hewitt, N.; Huang, Y. A Technical and Environmental Comparison of Novel Silica PEI Adsorbent-Based and Conventional MEA-Based CO_2 Capture Technologies in the Selected Cement Plant. *Carbon Capture Sci. Technol.* **2024**, *10*, 100179.

(7) Kolle, J. M.; Fayaz, M.; Sayari, A. Understanding the Effect of Water on CO_2 Adsorption. *Chem. Rev.iews* **2021**, *121*, 7280–7345.

(8) Choi, S.; Drese, J. H.; Jones, C. W. Adsorbent Materials for Carbon Dioxide Capture from Large Anthropogenic Point Sources. *ChemSusChem* **2009**, *2*, 796–854.

(9) Lashaki, M. J.; Khiavi, S.; Sayari, A. Stability of Amine-Functionalized CO_2 Adsorbents: A Multifaceted Puzzle. *Chem. Soc. Rev.* **2019**, *48*, 3320–3405.

(10) https://www.epa.gov/criteria-air-pollutants/naaqs-table (accessed 2024-08-18).

(11) https://thundersaidenergy.com/downloads/air-quality-sulphur-nox-and-particulate-emissions/ (accessed 2024-08-18).

(12) Wang, M.; Yao, L.; Wang, J.; Zhang, Z.; Qiao, W.; Long, D.; Ling, L. Adsorption and Regeneration Study of Polyethylenimine-Impregnated Millimeter-Sized Mesoporous Carbon Spheres for Post-Combustion CO_2 Capture. *Appl. Energy* **2016**, *168*, 282–290.

(13) Belmabkhout, Y.; Sayari, A. Isothermal versus Non-Isothermal Adsorption−Desorption Cycling of Triamine-Grafted Pore-Expanded MCM-41 Mesoporous Silica for CO_2 Capture from Flue Gas. *Energy Fuels* **2010**, *24*, 5273–5280.

(14) Fateme Rezaei; Christopher W. Jones. Stability of Supported Amine Adsorbents to SO_2 and NOx in Postcombustion CO_2 Capture. 1. Single-Component Adsorption. *Ind. Eng. Chem. Res.* **2013**, *52*, 12192–12201.

(15) Kumar, L.; Jana, S. K. Advances in Absorbents and Techniques Used in Wet and Dry FGD: A Critical Review. *Rev. Chem. Eng.* **2022**, *38*, 843–880.

(16) Li, W.; Cheng, C.; Gao, G.; Xu, H.; Huang, W.; Qu, Z.; Yan, N. Trace SO_2 Capture within the Engineered Pore Space Using a Highly Stable SnF_6^{2-}-Pillared MOF. *Mater. Horiz.* **2024**, *11*, 1889–1898.

(17) Brandt, P.; Nuhnen, A.; Lange, M.; Möllmer, J.; Weingart, O.; Janiak, C. Metal–Organic Frameworks with Potential Application for SO_2 Separation and Flue Gas Desulfurization. *ACS Appl. Mater. Interfaces* **2019**, *11*, 17350–17358.

(18) Yi, H.; Deng, H.; Tang, X.; Yu, Q.; Zhou, X.; Liu, H. Adsorption Equilibrium and Kinetics for SO_2, NO, CO_2 on Zeolites FAU and LTA. *J. Hazard. Mater.* **2012**, *203*, 111–117.

(19) Ivanova, E.; Koumanova, B. Adsorption of Sulfur Dioxide on Natural Clinoptilolite Chemically Modified with Salt Solutions. *J. Hazard. Mater.* **2009**, *167*, 306–312.

(20) Fu, Y.; Wang, Z.; Li, S.; He, X.; Pan, C.; Yan, J.; Yu, G. Functionalized Covalent Triazine Frameworks for Effective CO_2 and SO_2 Removal. *ACS Appl. Mater. Interfaces* **2018**, *10*, 36002–36009.

(21) An, X. C.; Li, Z.-M.; Zhou, Y.; Zhu, W.; Tao, D.-J. Rapid Capture and Efficient Removal of Low-Concentration SO_2 in Simulated Flue Gas by Hypercrosslinked Hollow Nanotube Ionic Polymers. *Chem. Eng. J.* **2020**, *394*, 124859.

(22) Jia, J.; Bhatt, P. M.; Tavares, S. R.; Abou-Hamad, E.; Belmabkhout, Y.; Jiang, H.; Mallick, A.; Parvatkar, P. T.; Maurin, G.; Eddaoudi, M. Porous Organic Polymers for Efficient and Selective SO_2 Capture from CO_2-rich Flue Gas. *Angew. Chem., Int. Ed.* **2024**, *63*, e202318844.

(23) Jacobs, J. H.; Chou, N.; Lesage, K. L.; Xiao, Y.; Hill, J. M.; Marriott, R. A. Investigating Activated Carbons for SO_2 Adsorption in Wet Flue Gas. *Fuel* **2023**, *353*, 129239.

(24) Bell, J. G.; Benham, M. J.; Thomas, K. M. Adsorption of Carbon Dioxide, Water Vapor, Nitrogen, and Sulfur Dioxide on Activated Carbon for Capture from Flue Gases: Competitive Adsorption and Selectivity Aspects. *Energy Fuels* **2021**, *35*, 8102–8116.

(25) Abdulrasheed, A. A.; Jalil, A. A.; Triwahyono, S.; Zaini, M. A. A.; Gambo, Y.; Ibrahim, M. Surface Modification of Activated Carbon for Adsorption of SO_2 and NO_X: A Review of Existing and Emerging Technologies. *Renewable Sustainable Energy Rev.* **2018**, *94*, 1067–1085.

(26) Yang, F. H.; Yang, R. T. Ab Initio Molecular Orbital Study of the Mechanism of SO_2 Oxidation Catalyzed by Carbon. *Carbon* **2003**, *41*, 2149–2158.

(27) Fan, Y. L.; Zhang, H. P.; Yin, M. J.; Krishna, R.; Feng, X. F.; Wang, L.; Luo, M. B.; Luo, F. High Adsorption Capacity and Selectivity of SO_2 over CO_2 in a Metal-Organic Framework. *Inorg. Chem.* **2021**, *60*, 4–8.

(28) Zhang, Y.; Zhang, P.; Yu, W.; Zhang, J.; Huang, J.; Wang, J.; Xu, M.; Deng, Q.; Zeng, Z.; Deng, S. Highly Selective and Reversible Sulfur Dioxide Adsorption on a Microporous Metal–Organic Framework via Polar Sites. *ACS Appl. Mat. Interfaces* **2019**, *11*, 10680–10688.

(29) Smith, G. L.; Eyley, J. E.; Han, X.; Zhang, X.; Li, J.; Jacques, N. M.; Godfrey, H. G. W.; Argent, S. P.; McCormick McPherson, L. J.; Teat, S. J.; Cheng, Y.; Frogley, M. D.; Cinque, G.; Day, S. J.; Tang, C. C.; Easun, T. L.; Rudić, S.; Ramirez-Cuesta, A. J.; Yang, S.; Schröder, M. Reversible Coordinative Binding and Separation of Sulfur Dioxide in a Robust Metal-Organic Framework with Open Copper Sites. *Nat. Mater.* **2019**, *18*, 1358–1365.

(30) Tailor, R.; Abboud, M.; Sayari, A. Supported Polytertiary Amines: Highly Efficient and Selective SO_2 Adsorbents. *Environ. Sci. Technol.* **2014**, *48*, 2025–2034.

(31) Tailor, R.; Ahmadalinezhad, A.; Sayari, A. Selective Removal of SO_2 over Tertiary Amine-Containing Materials. *Chem. Eng. J* **2014**, *240*, 462–468.

(32) Tailor, R.; Sayari, A. Grafted Propyldiethanolamine for Selective Removal of SO_2 in the Presence of CO_2. *Chem. Eng. J* **2016**, *289*, 142–149.

(33) Kim, C.; Choi, W.; Choi, M. SO_2 -Resistant Amine-Containing CO_2 Adsorbent with a Surface Protection Layer. *ACS Appl. Mater. Interfaces* **2019**, *11*, 16586–16593.

(34) Diaf, A.; Garcia, J. L.; Beckman, E. J. Thermally Reversible Polymeric Sorbents for Acid Gases: CO_2, SO_2, and NOx. *J. Appl. Polym. Sci.* **1994**, *53*, 857–875.

(35) Lan, H. C.; Zhang, J. Y.; Dai, Q. J.; Ye, H.; Mao, X. Y.; Wang, Y. C.; Peng, H. L.; Du, J.; Huang, K. Highly Efficient, Selective and Reversible Capture of Sulfur Dioxide by Methylated-Polyethylenimine Supported on Graphitic Carbon Nitride. *Chem. Eng. J.* **2021**, *409*, 127378.

(36) Lan, H. C.; Zou, Y. T.; Wang, Y. C.; Cheng, N. N.; Xu, W. L.; Peng, H. L.; Huang, K.; Kong, L. Y.; Du, J. Meso-Macroporous Polymer Densely Functionalized with Tertiary Amine Groups as Effective Sorbents for SO_2 Capture. *Chem. Eng. J.* **2021**, *422*, 129699.

(37) Vasilieva, L. L.; Dultsev, F. N.; Milekhin, A. K. IR Spectral Study of SO_2 Adsorption on Polysiloxane Layers Containing Tertiary Amino Groups. *J. Struct. Chem.* **1996**, *37*, 142–145.

(38) Zhu, G.; Carrillo, J.-M. Y.; Sujan, A.; Okonkwo, C. N.; Park, S.; Sumpter, B. G.; Jones, C. W.; Lively, R. P. Molecular Blends of Methylated-Poly(ethylenimine) and Amorphous Porous Organic Cages for SO_2 Adsorption. *J. Mater. Chem. A* **2018**, *6*, 22043–22052.

(39) Buijs, W. Molecular Modeling Study of the SO_2 Deactivation of an Amine Resin and a Procedure to Avoid SO_2 Deactivation Using a Polyethylene Glycol/Tertiary Amine System. *Ind. Eng. Chem. Res.* **2020**, *59*, 13388–13395.

(40) Zhi, Y.; Zhou, Y.; Su, W.; Sun, Y.; Zhou, L. Selective Adsorption of SO_2 from Flue Gas on Triethanolamine-Modified Large Pore SBA-15. *Ind. Eng. Chem. Res.* **2011**, *50*, 8698–8702.

(41) Ziaei-Azad, H.; Kolle, J. M.; Al-Yasser, N.; Sayari, A. One-Pot Synthesis of Large-Pore AlMCM-41 Aluminosilicates with High Stability and Adjustable Acidity. *Microporous and Mesoporous Mat.* **2018**, *262*, 166–174.

(42) Fan, Y.; Cai, Y. Q.; Fu, X. Bin; Yao, Y.; Chen, Y. Core-Shell Type Hyperbranched Grafting Copolymers: Preparation, Characterization and Investigation on Their Intrinsic Fluorescence Properties. *Polymer* **2016**, *107*, 154–162.

(43) Kruk, M.; Jaroniec, M.; Sayari, A. Application of Large Pore MCM-41 Molecular Sieves to Improve Pore Size Analysis Using Nitrogen Adsorption Measurements. *Langmuir* **1997**, *13*, 6267–6273.

(44) Yan, X.; Zhang, L.; Zhang, Y.; Yang, G.; Yan, Z. Amine-Modified SBA-15: Effect of Pore Structure on the Performance for CO_2 Capture. *Ind. Eng. Chem. Res.* **2011**, *50*, 3220–3226.

(45) von Harpe, A.; Petersen, H.; Li, Y.; Kissel, T. Characterization of Commercially Available and Synthesized Polyethylenimines for Gene Delivery. *J. Control. Release* **2000**, *69*, 309–322.

(46) Holycross, D. R.; Chai, M. Comprehensive NMR Studies of the Structures and Properties of PEI Polymers. *Macromolecules* **2013**, *46*, 6891–6897.

(47) Sayari, A.; Belmabkhout, Y.; Da'na, E. CO_2 Deactivation of Supported Amines: Does the Nature of Amine Matter? *Langmuir* **2012**, *28*, 4241–4247.

(48) Vo, H. T.; Cho, S. H.; Lee, U.; Jae, J.; Kim, H.; Lee, H. Reversible Absorption of SO_2 with Alkyl-Anilines: The Effects of Alkyl Group on Aniline and Water. *J. Ind. Eng. Chem.* **2019**, *69*, 338–344.

(49) Lim, S. R.; Lee, K. I.; Soo, C.; Kim, H. S.; Choi, J. S.; Lee, S. D. *US Pat.*, US8894956, **2014**.

Appendix A2 Supplementary Information for Chapter 2

Preparation and Characterization of PE-$AlSiO_2$ Support

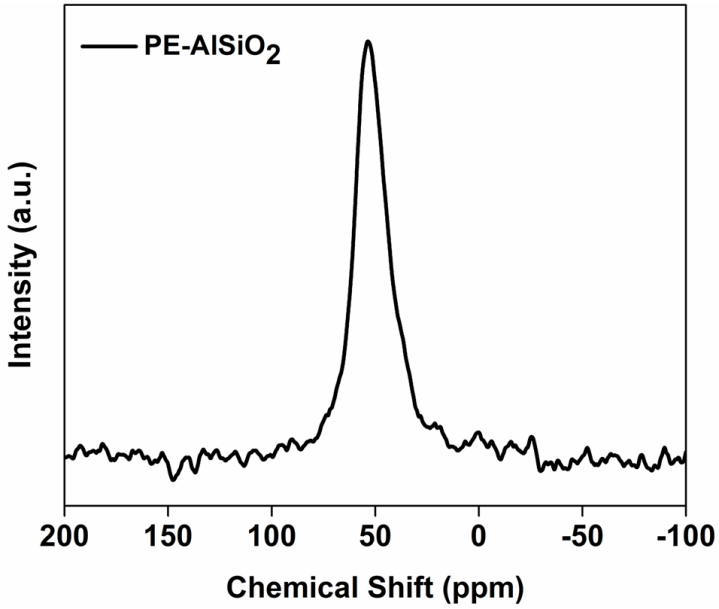

Figure A2.1 ^{27}Al MAS NMR spectra of PE-$AlSiO_2$.

TGA data

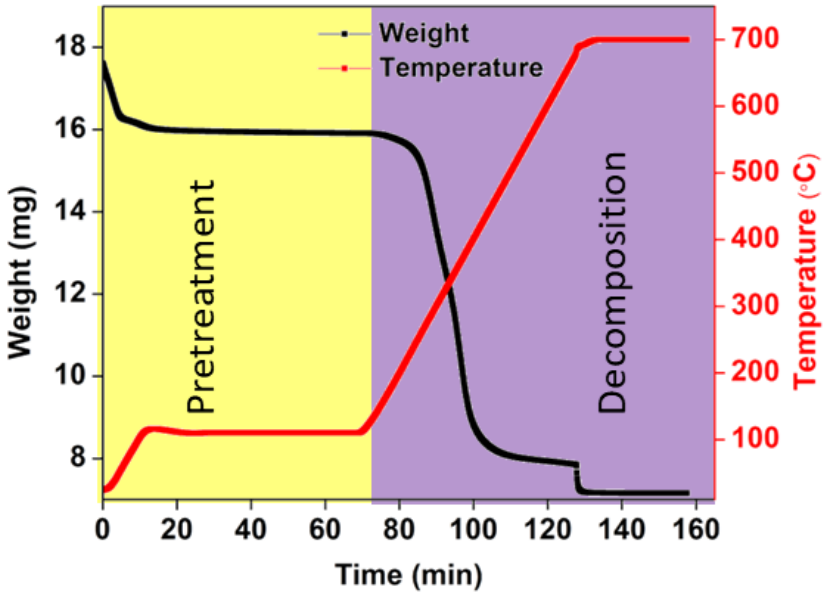

Figure A2.2. TGA graph for decomposition of organic material in GD-PEI/S.

SO_2 uptake of GD-PEI/S

Table A2.1: SO_2 uptake of GD-PEI/S when exposed to various concentrations of SO_2.

Concentration (ppm)	5	10	25	50	100	500	1000
SO_2 uptake (mmol/g)	0.29	0.32	0.34	0.38	0.47	0.55	0.59

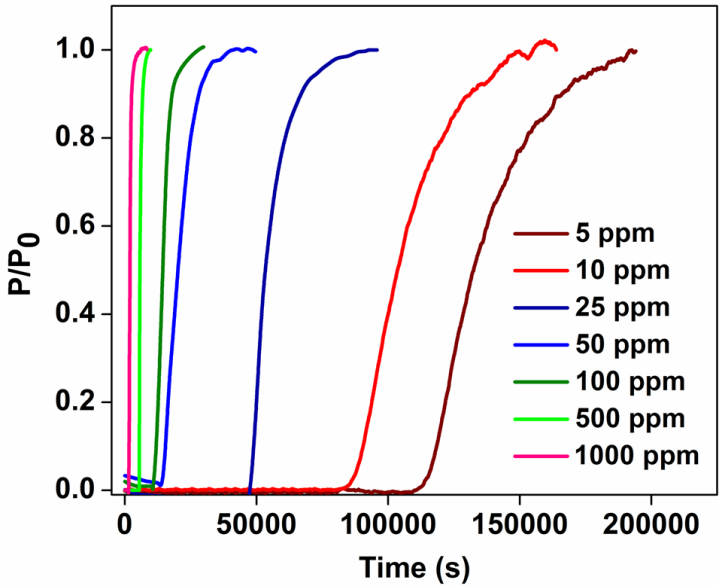

Figure A2.3. Breakthrough curves of GD-PEI/S under different concentrations of SO_2 in N_2.

Selectivity of adsorbent towards SO_2 versus CO_2

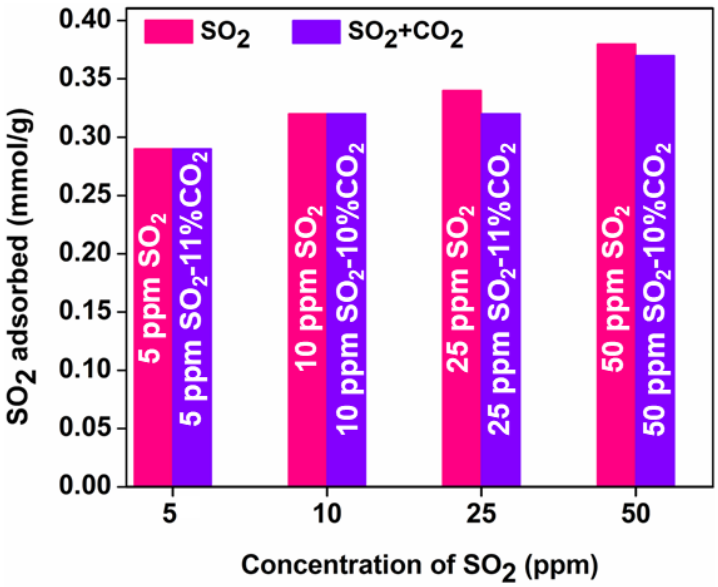

Figure A2.4. SO_2 uptake of GD-PEI/S under different concentrations of SO_2 with and without CO_2.

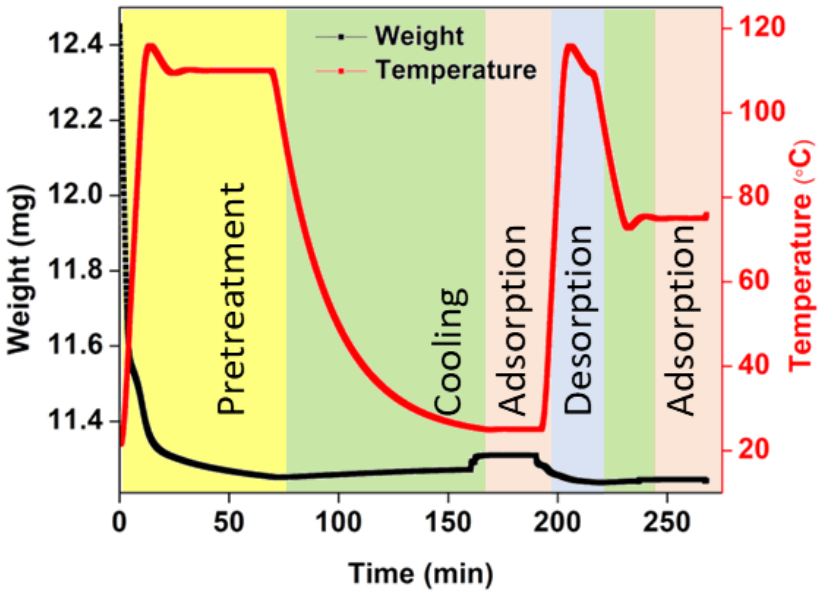

Figure A2.5. TGA graph for CO_2 uptake measurements for GD-PEI/S at 25 °C and 75 °C.

Stability of adsorbent under cyclic conditions

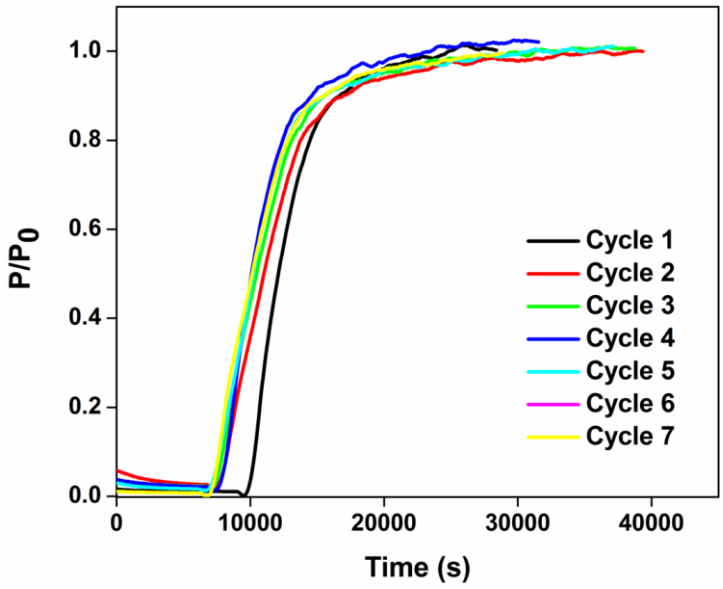

Figure A2.6. Column breakthrough curves of GD-PEI/S for regeneration cycles under dry 100 ppm SO_2 balanced N_2.

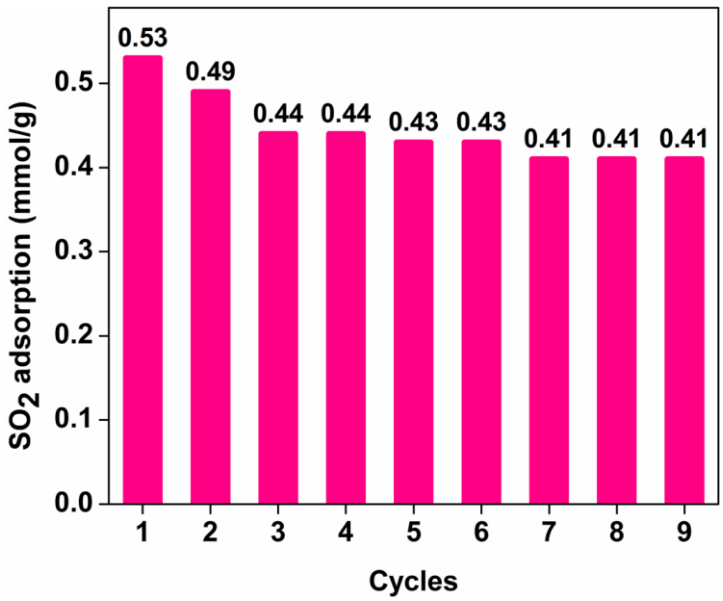

Figure A2.7. Regeneration cycles of GD-PEI/S under dry 500 ppm SO_2 balanced in N_2.

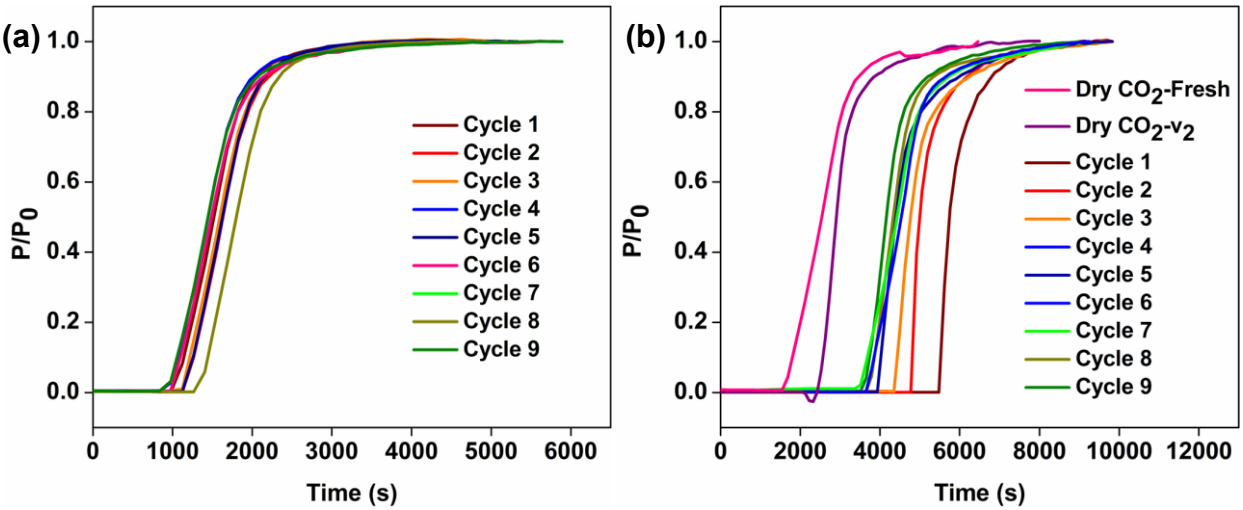

Figure A2.8. (a) Column breakthrough curves for regeneration cycles of GD-PEI/S under (a) dry and (b) humid 500 ppm SO_2 balanced in N_2.

CHAPTER 3 ENHANCING OXIDATION STABILITY OF AMINE-CONTAINING CO_2 ADSORBENTS USING HYDROXYETHYL STARCH

3.1. Abstract

Amine-based adsorbents are widely used for CO_2 capture. However, one of the biggest hurdles for their further development is their limited oxidation stability. Moreover, methods developed to improve the oxidation stability often lead to significant decrease in their CO_2 uptake. Here, we investigated the effect of hydroxyethyl starch (HES) on the CO_2 uptake and oxidation stability of impregnated polyethylenimine (PEI) adsorbents. Performance of HES-PEI co-impregnated materials was evaluated under different oxidation conditions using CO_2 uptake measurements, and mass spectrometry. The effect of HES was compared with other hydroxyl-containing additives such as PVA and PEG, as well as to epoxide functionalization of PEI (EB-PEI). The oxidation stability of PEI upon addition of HES was found to be comparable to EB-PEI containing adsorbent; however, its CO_2 uptake, based on PEI, was twice as high. In addition, oxidation stability of supported HES-PEI was significantly higher than unmodified PEI as well as PVA-PEI and PEG-PEI co-impregnated adsorbents.

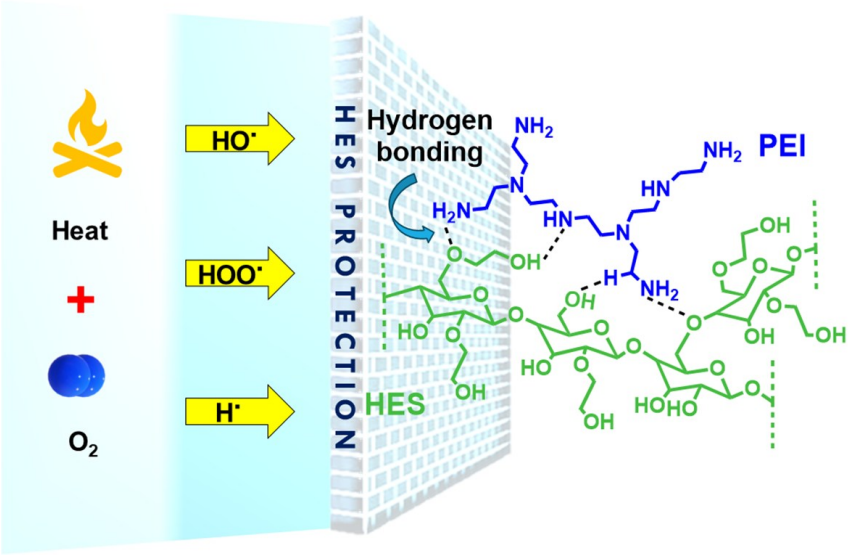

3.2.Introduction

Carbon dioxide is a major heat-trapping gas. Although, it is not the most potent greenhouse gas (GHG), because of its exceedingly high emissions, anthropogenic CO_2 is the largest contributor to global warming.[1] According to the National Oceanic and Atmospheric Administration (NOAA)[2], the concentration of CO_2 in air reached the alarming level of 424 ppm in 2023. The resulting global warming has been correlated with increased risks for people, economies, and ecosystems, including rising sea level and extreme weather events.[3] Mitigating such effects requires immediate and effective measures to reduce GHG emissions.[4] Among a wide range of strategies, carbon capture from large point sources and directly from the atmosphere is recognized as a key technology for large-scale reduction of CO_2 emissions.[5]

Supported amines have garnered substantial attention due to their ability to adsorb CO_2 selectively and reversibly[31] and to their lower energy requirements compared to amine solutions.[7,8] This makes such materials economically viable for large-scale CO_2 capture, as evidenced by many commercial and near-commercial operations throughout the world.[9] Because polyethylenimine (PEI) is affordable, readily available in different molecular weights, and has a high amine content, impregnated PEI materials are among the most popular CO_2 adsorbents.[10] However, one of the most intractable drawbacks of amine-based adsorbents is their high propensity to oxidative degradation.[11–14] In a typical temperature swing adsorption-desorption cycle, the material is exposed to a CO_2-rich gas stream, commonly at 25-50 °C, then regenerated at ca. 110 °C, before it is cooled to the adsorption temperature. To reduce cost, it is desirable that the cooling step takes place in flowing air. However, repetitive exposure of amines to air (21% O_2) at the highest temperature of the process, leads to its gradual oxidative deactivation.[12–16] Amine oxidation may also occur during the adsorption stage as many feed gases contain different levels of oxygen. Nonetheless, this possibility is quite remote since the oxygen content of most feed gases is typically below 10%, and the adsorption temperature is the lowest in the cycle, i.e., typically below 50 °C. Moreover, the presence of CO_2 strongly prevents the amine oxidation.[13,17] In direct air capture,

although the adsorbent is exposed to high oxygen partial pressure (21% O_2/N_2), adsorption is also carried out at ambient temperature.

The high vulnerability of branched PEI to oxidation has been vastly documented.[13–16,18–21] As illustrated in the following examples, there is ample evidence that the extent of amine oxidative deactivation is directly dependent on the temperature and time of exposure as well as the oxygen partial pressure. Heydari-Gorji and Sayari[13] found that in the presence of dry air at 120 °C for 30 h, the deterioration of PEI-impregnated mesoporous silica was quantitative, with 100% loss of CO_2 uptake. Choi and coworkers reported that 50% PEI-impregnated silica lost 81% of its working capacity when exposed to 20% O_2/N_2 at 120 °C for 24 h.[18] Jones' group found that 35% PEI impregnated on SBA-15 lost 58% amine efficiency upon exposure to air at 120 °C for only 4.5 h.[15] Moreover, the structure of amines was found to play a crucial role in determining their relative oxidation stability. Branched PEI (BPEI) with different types of amine groups (primary, secondary, tertiary), was found to be more prone to oxidation than linear PEI (LPEI), consisting of only secondary amines.[16] Likewise, adsorbents containing ethylenediamine units are less stable toward oxidation than materials containing amines with propylene[22–25] and butylene[26] linkages. Sterically hindered amines with fewer alpha-hydrogen atoms, also exhibit higher oxidation stability.[27] Furthermore, it was found that isolated primary amines such as grafted propylamine[10,11] and impregnated polyallylamine (PAA)[19] are particularly stable against oxidation. Upon exposure to air at 110 °C for 20 h, PAA lost only 8% of CO_2 uptake, whereas BPEI lost 70%.[19] Likewise, when exposed to air at 120 °C for 30 h, grafted propylamine lost only 7.5% of CO_2 uptake; however, grafted triamine (with primary and secondary amines) lost 94% under the same conditions.[12] The effect of the two recurrent components in feed gases, namely CO_2 and H_2O, on amine oxidation was also scrutinized. Heydari-Gorji and Sayari[13] investigated the oxidation of PEI-impregnated SBA-15 over a 30 h period, in the presence of different $CO_2/O_2/N_2$ gas mixtures containing 1-20% CO_2, 10.5-17% O_2, balance N_2 at temperatures ranging from 50 to 120 °C. They found that the loss in CO_2 uptake decreased significantly as the CO_2 content of the feed gas increased, presumably due

to the faster formation of ammonium carbamate compared to amine oxidation. In contrast, Guta *et al.*[28] reported that under DAC conditions (0.04% CO_2), CO_2 accelerated amine oxidation. It was hypothesized that the formation of bound CO_2 species such as carbamic acids, catalyzes C-N cleavage, thus enhancing the amine oxidative degradation. Likewise, depending on the actual conditions, the presence of water vapor was reported to either exacerbate the oxidative deactivation[15,28] or enhance the sorbent stability against oxidation.[13,17,29]

Using a combination of NMR and FTIR spectroscopy, along with solvent extraction and CO_2 uptake measurements, Sayari's group[16,30,31] and Carneiro *et al.*[15] identified several imine, amide and formamide containing fragments in air-oxidized adsorbents. Moreover, different low molecular weight compound, such as NH_3, H_2O and hydrocarbon fragments were detected in the gas phase.[30,32] These findings provided clear indication that the formation of unsaturated fragments within the oxidized adsorbents involves the abstraction of hydrogen from the alpha position with respect to nitrogen atoms. Similar to amine solutions,[33,34] the oxidation of supported amines is widely believed to follow a radical mechanism.[15,20,23,28,30] The occurrence of radical species was recently confirmed by electron paramagnetic resonance measurements.[30]

Owing to the importance of the oxidative degradation of amine-containing materials, many studies focussed on mitigating its adverse effect through different strategies. This includes the use of specific amines with increased oxidation stability such as isolated primary amines,[11,12,19] polyamines with propylene or butylene linkers between amines as opposed to ethylene,[22–26,31] and amines with fewer alpha-hydrogen atoms,[27] as well as addition of oxidation inhibitors, oxygen/radical scavengers and chelators.[17,36] Interestingly, occurrence of hydrogen bonding through addition of hydroxyl-containing polymers (HCP), such as polyethylene glycol (PEG)[37], polyvinyl alcohol (PVA)[30,38] or through direct functionalization of PEI with epoxides[17,18,21] was particularly rewarding. The beneficial effect of hydrogen bonding toward the oxidation stability of amine-based adsorbents was confirmed by NMR and computational studies.[30,39] Further improvement was achieved by addition of chelators, presumably to sequester iron impurities in

commercial PEI that may accelerate the generation of radical species.[17,40] 1,2-epoxybutane-functionalized PEI (EB-PEI) was found to be significantly stable at 110 °C in the presence of 3% O_2, 15% CO_2, 10% H_2O in N_2.[17] However, even after adding 4 wt% chelators, the material degraded under air at 110 °C.[21]

Though, none of the adsorbents reported in the literature was stable enough under conditions relevant to the adsorbent cooling stage, addition of hydroxyl groups seems to be the most effective method to enhance the oxidation stability of amine-based materials.[17,30,38,39] So far, direct hydroxyl incorporation through PEI reaction with epoxides was found to be particularly promising.[17,18,21,41] However, not only epoxide functionalization requires additional preparation steps, but it also transforms primary amines, into less active secondary amines, leading to lower amine efficiency and higher than expected decrease in CO_2 uptake, based on the reduced amine content upon epoxide functionalization. For example, Min *et al.*[17] found that under the same conditions, 50%(EB-PEI)/SiO_2 adsorbed 1.84 mmol CO_2/g, versus 4.05 mmol/g for 50%PEI/SiO_2, corresponding to 54.6% decrease, whereas the actual decrease in PEI content was only 37.5%.

As far as hydroxyl-containing polymers are concerned, hydroxyethyl starch (HES), a highly stable polymer with abundant hydroxyl and ether groups for hydrogen bonding with amine groups, provides a straightforward rational to investigate its effect on the oxidation stability of supported PEI, if any. The oxidation stability of HES-PEI co-impregnated material was compared to supported EB-PEI and other HCP-PEI containing CO_2 adsorbents, under conditions pertinent to the cooling stage using air. Accelerated oxidation experiments were carried out in flowing air at *ca.* 110 °C.

3.3. Experimental

3.3.1. Materials

Polyethylenimine (PEI, Mw 1200), hydroxyethyl starch (HES), soluble starch (Starch), tetramethylammonium hydroxide (TMAOH, 25 wt% solution), poly(vinyl alcohol) (PVA, Mw 89,000 Da, 99+% hydrolyzed), polyethylene glycol (PEG, Mw 200 Da), tetraethyl orthosilicate (TEOS, 98%), fumed silica (Cab-O-Sil, M5), cetyltrimethylammonium bromide (CTAB, 98%), N,N-dimethyldodecyl amine (DMDA, 97%) and deuterium oxide (D_2O, 99.9%) were obtained from Sigma-Aldrich and 1,2-epoxy butane (EB, 99%) from Thermo Scientific. Sodium aluminate ($NaAlO_2$, 92%) was purchased from Strem Chemicals. Methanol (99%) and ammonia solution (28 wt%) were obtained from Fischer. Chloroform-d ($CDCl_3$, 99.9% D) was purchased from Cambridge Isotope Laboratories. All chemicals were used without further purification. Ultrahigh purity (99.999%) nitrogen, carbon-free air (21% O_2), 15% CO_2 in nitrogen gas cylinders were purchased from Messer Canada.

3.3.2. Material Preparation

Pore-expanded aluminosilica (PE-$AlSiO_2$)[42] was used as support throughout this investigation. Details about the preparation, characterization and properties of PE-$AlSiO_2$ may be found in the Supplementary Information (Figure A3.1 and Table A3.1). To impregnate PEI on PE-$AlSiO_2$, 0.4 g of PEI was dissolved in 15 mL methanol under stirring. Thereafter, 0.5 g of PE-$AlSiO_2$ was slowly added, and the mixture was stirred overnight, while the solvent evaporated. The resulting material was further dried in a vacuum oven at 80 °C for 2 h. It will be referred to as PEI/S. As for HCP-PEI co-impregnated materials, 0.20 g of HCP was added in 50 mL of water and heated at 80 °C for 15 min. Then, the temperature was increased to 110 °C and the solution stirred for 5 more minutes (Solution A). In another beaker, 0.34 g of PEI was added in 20 mL of H_2O and stirred till complete dissolution (Solution B). Solution A was then added to solution B dropwise and 0.5 g of PE-$AlSiO_2$ was added into it. The resultant mixture was stirred at room temperature overnight and

further dried at 80 °C for 24 h. The adsorbent was designated as HCP-PEI/S. 1,2-epoxybutane-functionalized PEI (EB-PEI/S) was prepared as reported elsewhere with slight modification.[17] In a typical synthesis, 6 g of EB was added dropwise to 30 g of methanolic solution of PEI (10 g PEI + 20 g methanol). EB to nitrogen in PEI was 0.37. The mixture was stirred for 12 h at room temperature and thereafter impregnated on 15 g of PE-$AlSiO_2$ support.

3.3.3. Material Characterization

All materials were characterized by ^{1}H and ^{13}C NMR spectroscopy. Quantification of amines in unsupported PEI and EB-PEI was carried out using suspensions in $CDCl_3$. As for Nuclear Magnetic Resonance (NMR) measurements for impregnated materials, D_2O extraction was used. ^{13}C NMR spectra were collected on a AVIII 600 spectrometer using the following conditions, a 45-degree pulse, 90 second relaxation delay, a 0.99 second acquisition time, and 520 transients. To prevent the nuclear Overhauser effect, all ^{13}C NMR spectra used for quantitative analysis were recorded using inverse-gated proton decoupling. For ^{1}H NMR, relaxation delay of 2 second was used and 32 scans were performed. FTIR spectra (4000–400 cm^{-1}) of samples were recorded using an Agilent Technologies Cary 630 FTIR.

3.3.4. Oxidation Experiments

Oxidation of the adsorbents was carried out in a packed-bed column as shown in Figure 3.1. A 14 cm long stainless-steel column with an inner diameter of 1.1 cm was filled with 0.4-0.5 g of adsorbent pellets sized between 20 and 40 mesh. The column was then placed in a temperature-controlled oven, and the adsorbent was pretreated under flowing nitrogen (80 mL/min) at 100 °C for 60 min. Thereafter, the gas was switched to flowing air (40 mL/min) at ca. 110 °C for different time intervals. After each oxidation step, the oven was cooled to room temperature and a sample was collected for CO_2 uptake measurements using a thermogravimetric analyzer (Q550 TGA, TA Instruments). 20–30 mg samples were preheated under flowing nitrogen for 60 min at 110 °C, then cooled to 75 °C, before switching the gas stream to 15% CO_2 in N_2 for 60 min. Volatile compounds

formed during oxidation were investigated by mass spectrometry using a MKS Cirrus 3 instrument. The organic content of fresh and oxidized materials was determined by combustion using TGA. Typically, the sample was pretreated under flowing nitrogen for 1 h at 110 °C, then heated to 700 °C at a rate of 10 °C min^{-1}, followed by exposure to air at 700 °C for 20 minutes to eliminate any remaining carbonaceous species. The organic content was calculated as the weight loss beyond 200 °C. CO_2 adsorption-desorption cycles were performed using TGA. CO_2 adsorption was carried out at 75 °C under flowing 15% CO_2 in N_2 for 1 h, and desorption under nitrogen at 110 °C for 20 min. The H_2O uptake of materials was performed using gravimetric sorption analyzer (DVS Carbon, Surface Measurement Systems).

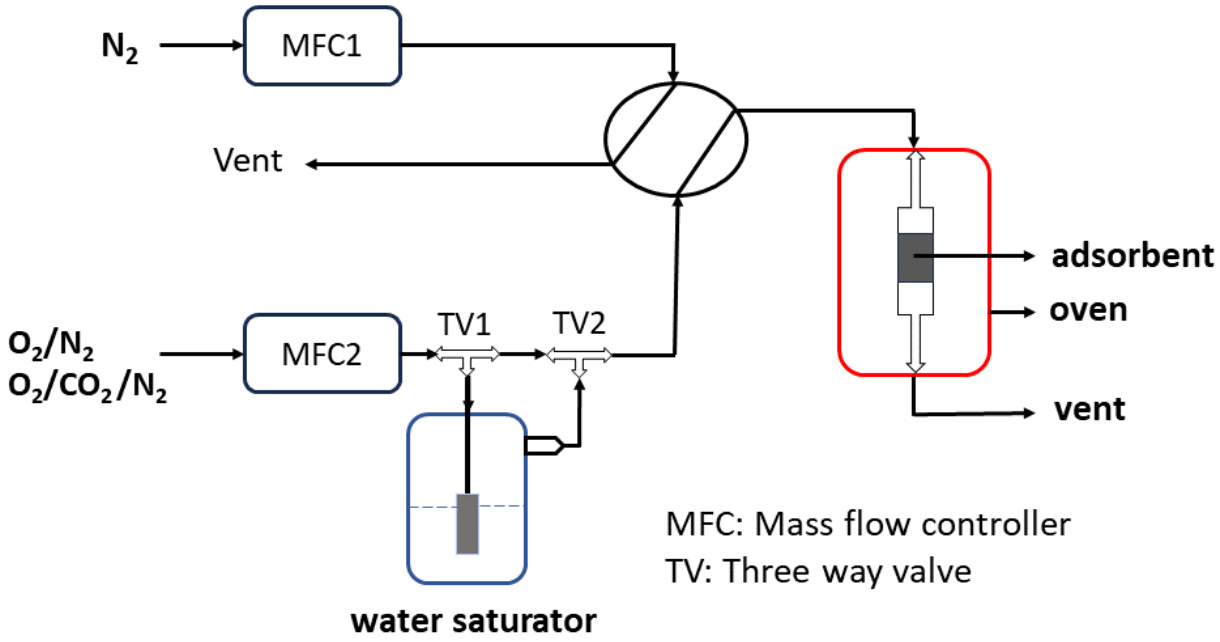

Figure 3.1. Schematic of oxidation experiments in column breakthrough.

3.4. Results and Discussion

3.4.1. Characterization of Adsorbents

The HES-PEI material showed all the ^{1}H NMR signals, corresponding to HES as well as PEI (Figure 3.2a), confirming the co-impregnation of both polymers. The corresponding IR spectra shown in Figure 3.2b also exhibited a combination of bands attributable to PEI and HES. ^{13}C NMR data for unsupported PEI and EB-PEI (Figure A3.2), confirmed the successful epoxide

functionalization of PEI. The percentage of primary, secondary and tertiary amines calculated as reported by Choi's group,[18] was 36:36:28 for pristine PEI and 11:58:31 for EB-PEI. This is consistent with Min *et al.*'s findings[17,18] who reported a composition of 36:37:27 and 10:56:34 for PEI and 0.37EB-PEI (equivalent to our EB-PEI), respectively.

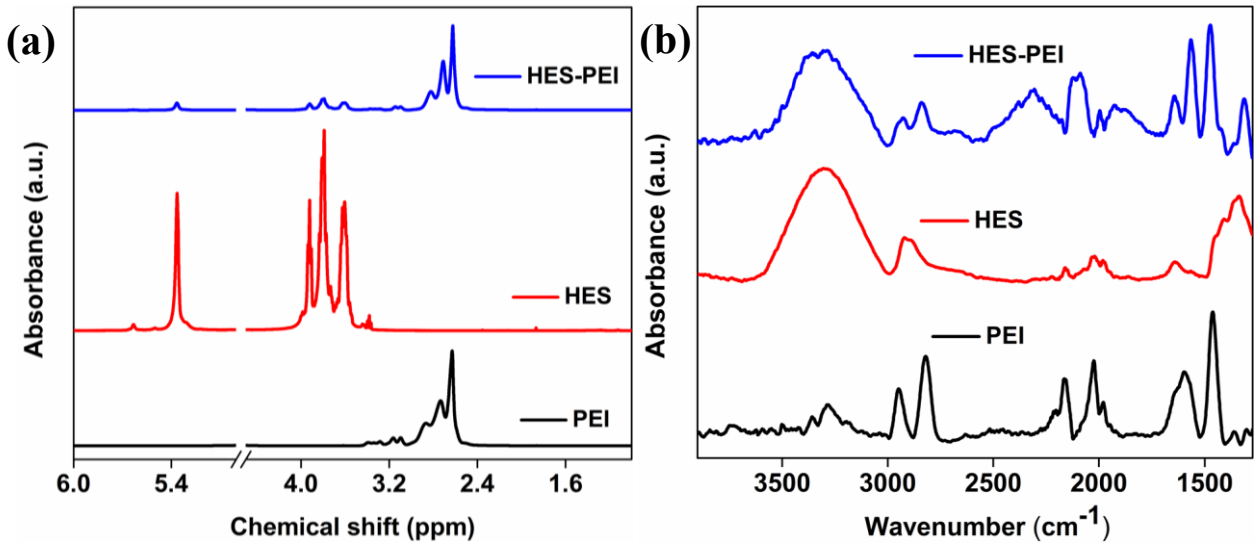

Figure 3.2. (a) ^{1}H NMR data for PEI, HES and HES-PEI; (b) corresponding IR spectra.

3.4.2. Effect of HES on the Oxidation Stability of PEI

PEI/S and HES-PEI/S were exposed to flowing air at two different temperatures, 100 °C and 108 °C, and their oxidative degradation was monitored over time by CO_2 uptake measurements at 75 °C as shown in Figure 3.3. The oxidative degradation of PEI versus time showed a sigmoidal curve with an induction period, followed by fast-deactivation, then a final stage with much slower degradation as the material approached complete deactivation. These oxidation stages are consistent with the proposed radical reaction mechanism for supported[15,28] and dissolved[43] amines. Briefly, the induction period corresponds to the radical initiation stage in which abstraction of alpha hydrogen with respect to amine groups takes place, leading to the generation of carbon-centred radicals. Another probable radical initiation reported by Rochelle and co-workers for aqueous amine groups, corresponds to the abstraction of electrons from amine groups, which rearrange to provide carbon-centred radicals as shown in Scheme 3.1.[33,34] This event may be triggered by traces

of transition metals that could occur in commercial PEI,[17,21,40] the alumina support[15] or from the reactor material.[28] In this stage, the extent of deactivation remained limited; however, in the following radical propagation step, the adsorbent undergoes rapid oxidation.[15,28] Amines are converted to imine/amide as demonstrated by Sayari and co-workers,[16,30,31] and Jones' group,[15] while the polymer chain undergoes partial decomposition, giving rise to low molecular weight species, such as water, ammonia and others.[15,30,32]

After co-impregnation of HES and PEI, the CO_2 uptake with respect to PEI decreased from 3.9 to 3.7 mmol/g PEI (1.7 mmol/g adsorbent to 1.2 mmol/g adsorbent), whereas the oxidation stability of PEI was greatly enhanced (Figure 3.3). For example, after exposure to air at 100 °C for 48 h, the decrease in CO_2 uptake for PEI/S was 53%, whereas the HES-PEI/S deactivation under the same condition was only 7%. The higher oxidation stability of HES-PEI/S compared to PEI/S was further supported by FTIR measurements as shown in Figure 3.4. The intensity of the imine/amide band at 1650 cm^{-1} was higher for PEI/S than HES-PEI/S at different oxidation durations (24 and 48 h). This improvement may be attributed to the formation of hydrogen bonds between amine and the HES hydroxyl groups (Scheme 3.2), which may decrease the availability of the lone pair of nitrogen. In addition, HES-PEI showed increased viscosity compared to pristine PEI, which decreases the polymer chain mobility. This may in turn, decrease the rate of oxygen diffusion, and retard the initiation of radicals, thus enhancing the oxidation stability of the adsorbent. This is in agreement with earlier statements reported in the literature.[24,26,38,39] Other researchers reported that hydrogen bonds increase the oxidation stability of adsorbents, by acting as a barrier for radical propagation.[30] Furthermore, numerous studies showed that the overall degradation of amines is largely dependent on the oxidation rate during the induction period.[33,34,44,45] Therefore, slowing down the radical initiation can play a crucial role in determining the overall stability of adsorbent.

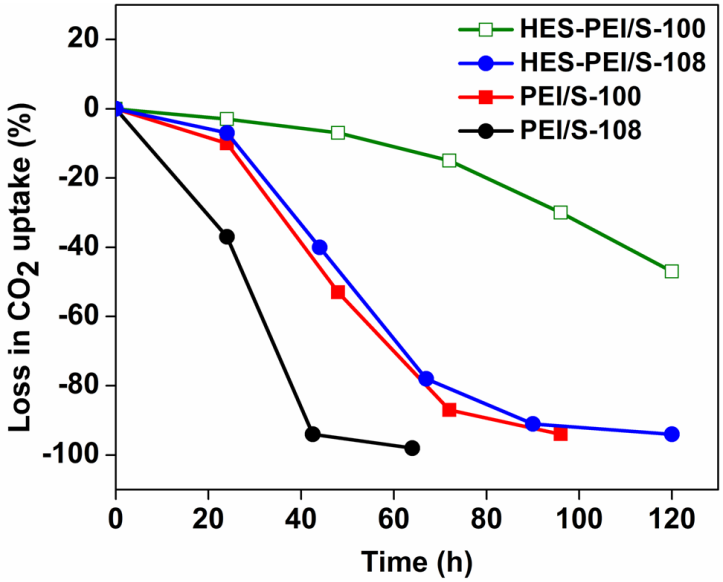

Figure 3.3. Percentage loss of CO_2 uptake for PEI/S and HES-PEI/S after exposure to air at 100 (open symbols) and 108 °C (closed symbols) for different periods of time.

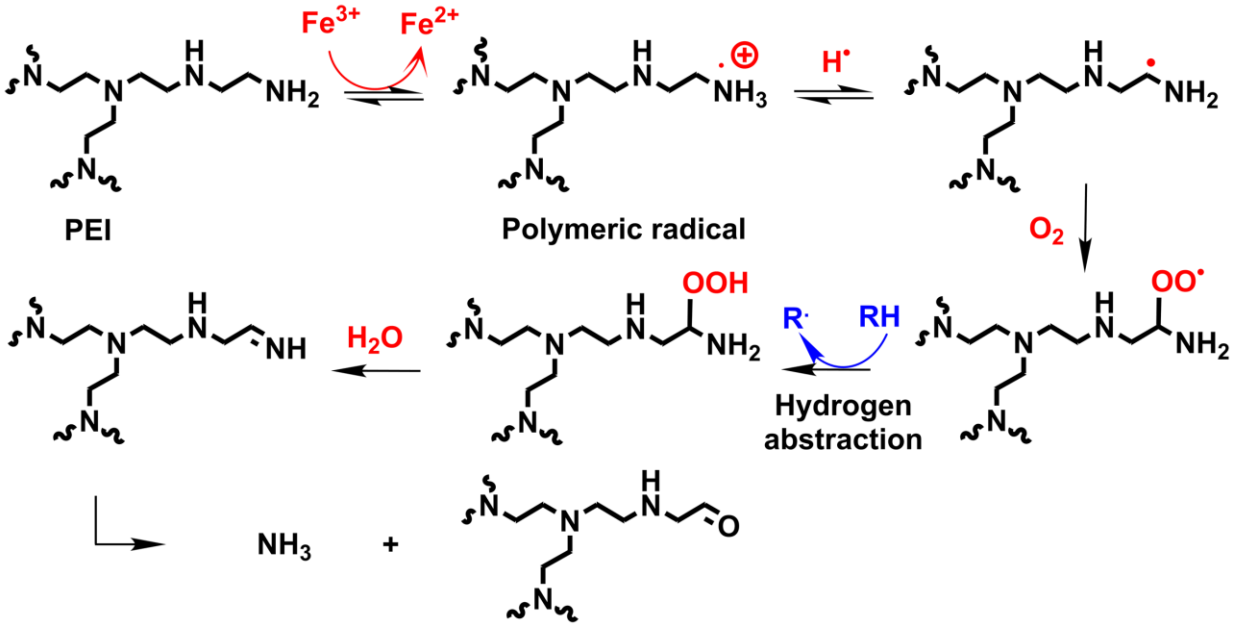

Scheme 3.1 Schematic mechanism for oxidative degradation of PEI.[15,30,33,34]

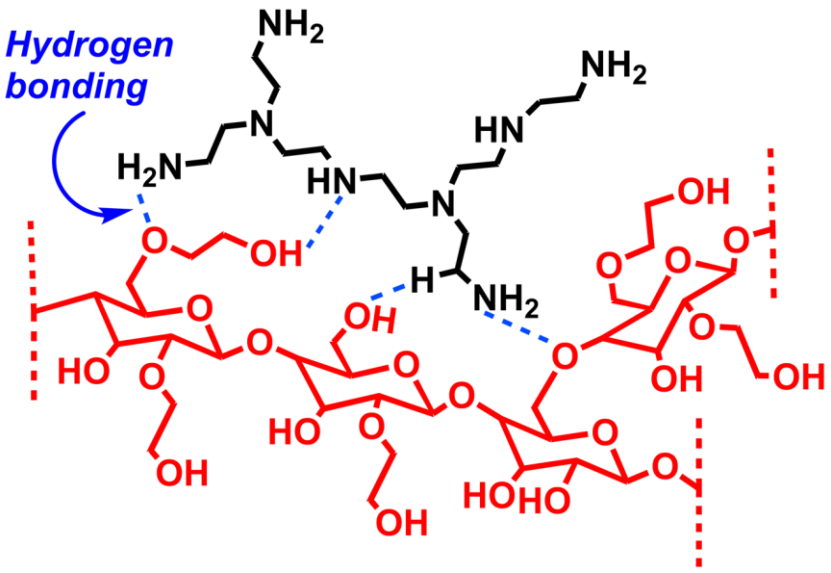

Scheme 3.2. Hydrogen bonding between HES and PEI.

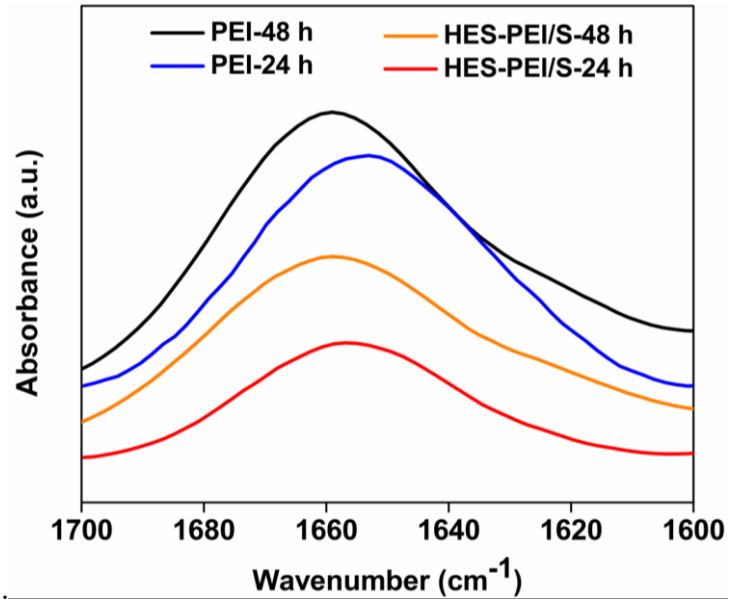

Figure 3.4. IR spectra of PEI/S and HES-PEI/S when oxidized to air at 108 °C for 24 and 48 h.

3.4.3. Loss of Organic Content During Oxidation

During the oxidation of PEI, the formation of species containing C=O and/or C=N unsaturation is accompanied by the release of volatile compounds such as H_2O, NH_3 and CO_2.[30,32] As a result, both the CO_2 uptake and organic content of the adsorbent decreases; however, the decrease in CO_2 uptake is far greater than the decrease in organic content[15,32] (Figure 3.3 and Figure 3.5a). To investigate the reason, oxidized PEI/S, HES-PEI/S were examined using ^{1}HNMR and volatile

compounds formed during oxidation were analyzed by mass spectrometry. In agreement with Pang *et al.*[22], ^{1}HNMR of oxidized samples showed peaks between 8.0-8.5 ppm (Figure 3.5b), indicative of the formation of (-C*H*=N-) and/or (C*H*(=O)NH-). This reflects the insertion of oxygen (increase in the weight of polymer) and the formation of less basic groups. Furthermore, the intensity and area of MS peaks of the main fragments increased as follows $H_2O^+ > NH_3^+ > CO_2^+ > 53 \sim 80$ (m/z) (Figure 3.6a and b). The decrease in intensity of fragments with m/z < 50, like H_2O^+, NH_3^+ and CO_2^+ was consistent with that reported by Racicot *et al.*,[32] whereas among the fragments with m/z > 50 reported by Yan and Sayari[30], only fragments with m/z = 53 and 80 were detected. This indicates that the loss of organic content was mostly due to the production of H_2O and ammonia as opposed to species generated by the backbone cleavage of PEI. Consequently, during oxidation, PEI has fewer amines, therefore reduced CO_2 uptake. Notice that the observed organic loss is a combination of the actual organic loss and the oxygen addition. Nevertheless, the decrease in CO_2 uptake of PEI/S is significantly higher than the decrease of organic content.

Similar to PEI/S, HES-PEI/S lost more CO_2 uptake during oxidation than its organic content. Also, the intensity of MS fragments produced during oxidation of HES-PEI/S followed the same trend as PEI/S. However, the partial pressure of fragments produced by HES-PEI/S was much lower than PEI/S, which strongly supports the improved oxidation stability upon addition of HES.

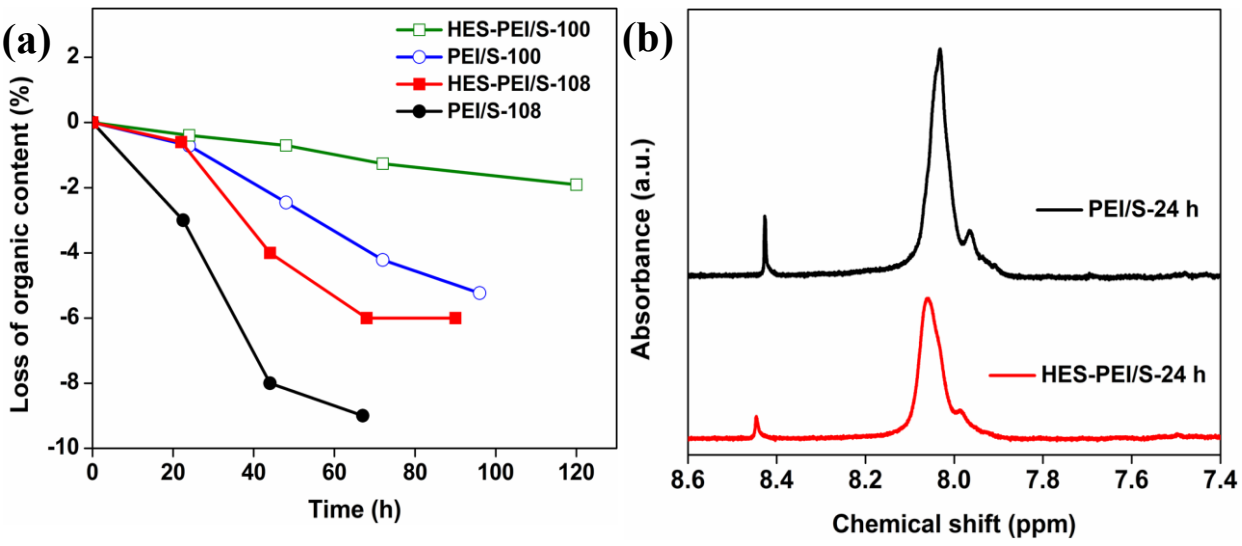

Figure 3.5. (a) Loss of organic content (%) for PEI/S and HES-PEI/S upon exposure to air at 100

and 108 °C; (b) 1H NMR spectra of PEI/S and HES-PEI/S after 24 h oxidation.

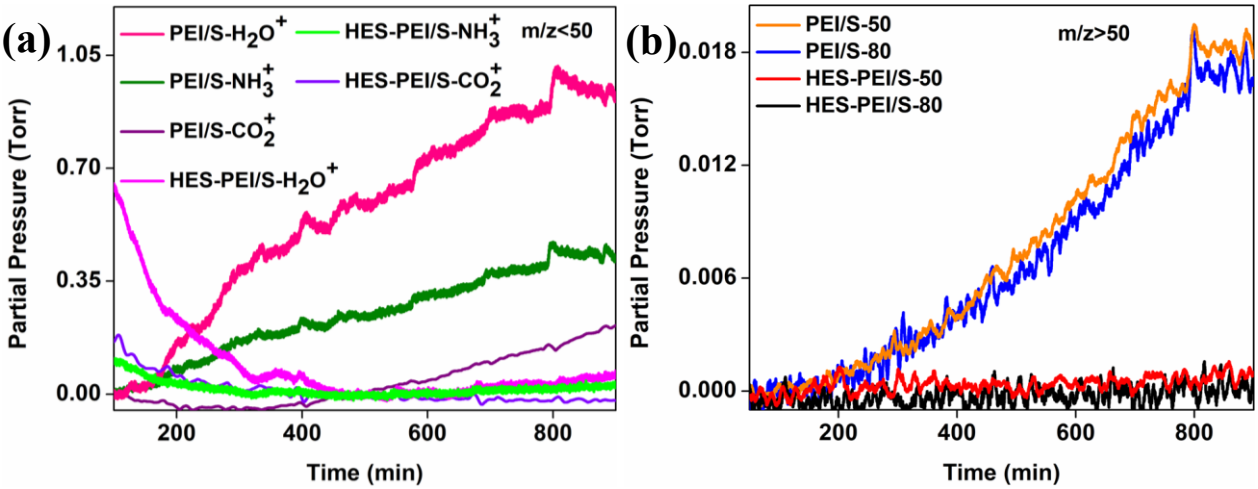

Figure 3.6. Partial pressure of different degradation fragments of PEI/S and HES-PEI/S with (a) m/z < 50 and (b) m/z > 50 during exposure to air at 108 °C.

3.4.4. Importance of Hydroxyl Species

Oxidative deactivation of PEI and PEI co-impregnated with non-modified, and hydroxyethyl-modified starch upon exposure to air at 110 °C for 24 h, as measured by CO_2 uptake at 75 °C is shown in Figure 3.7. It is clearly seen that starch co-impregnated PEI oxidized more rapidly than HES-containing counterpart. Moreover, during air exposure at 110 °C for 24 h, the HES-containing material showed a weight loss of 0.6%, compared to 3.2% for the starch-containing material, indicative of higher degradation of Starch-PEI/S. Starch contains only hydroxyl and hydroxymethylene groups attached directly to the glucose ring, with limited mobility. The associated steric hindrance may lead to inefficient interaction with PEI. Thus, it has hardly any effect compared to pristine PEI. In contrast, HES contains longer chains terminated with higher mobility hydroxyl groups. It is believed that the latter form hydrogen bonds with amine groups more readily and more efficiently. In agreement with other reports,[37–39] it is inferred that the higher resistance to oxidative degradation upon HES addition, is associated with the efficient formation of hydrogen bonding with amine groups. Short of direct evidence, the current comparison between the effect of starch and HES on the oxidation resistance of PEI provides the strongest support to the contention that hydrogen bonding plays a key role in enhancing the oxidation resistance of PEI.

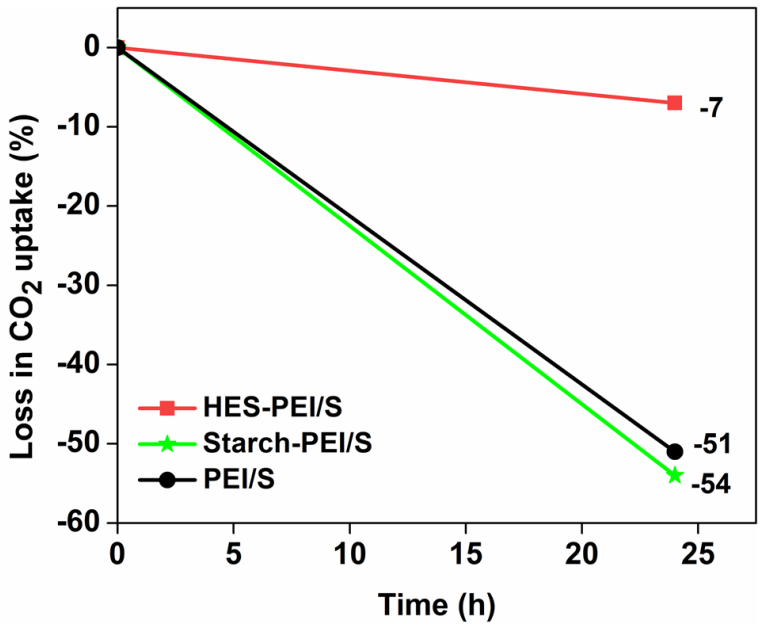

Figure 3.7. Percentage loss of CO_2 uptake at 75 °C for PEI/S, Starch-PEI/S and HES-PEI/S exposed to air at 110 °C for 24 h.

3.4.5. Effect of HES versus Epoxy Functionalization and Stability Analysis of HES

The oxidation stability of PEI/S, EB-PEI/S and HES-PEI/S was compared by exposing the adsorbents at 108 °C under air for 67 h. Figure 3.8 shows that the oxidation stability of HES-PEI/S was comparable to EB-PEI/S. However, the CO_2 uptake of EB-PEI/S (1.8 mmol/g PEI; 0.6 mmol/g adsorbent) was 51% lower than HES-PEI/S (3.7 mmol/g PEI; 1.2 mmol/g adsorbent). This significant difference can be attributed to the conversion of primary amines to secondary and tertiary amines upon functionalization of PEI with EB. In contrast, the integrity of PEI in HES-PEI/S is preserved, and hence the CO_2 uptake of HES-PEI/S is comparable to PEI/S.

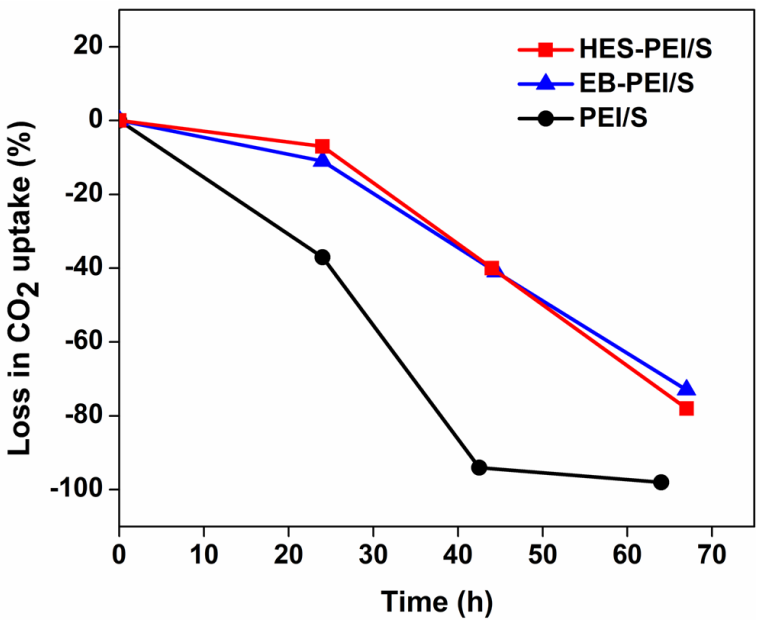

Figure 3.8. Percentage loss in CO_2 uptake of PEI, HES-PEI/S and EB-PEI/S after exposure to air at 108 °C for different time intervals. CO_2 adsorption was carried at 75 °C.

CO_2 adsorption-desorption measurements were performed on HES-PEI/S to evaluate its stability and regenerability. As shown in Figure 3.9, CO_2 uptake of HES-PEI/S was stable over 25 cycles, indicating that the stability of supported PEI was not affected by HES addition. Although cycling experiments were carried out under dry conditions, there was no loss in CO_2 uptake, indicating that the material was resistant to urea formation.

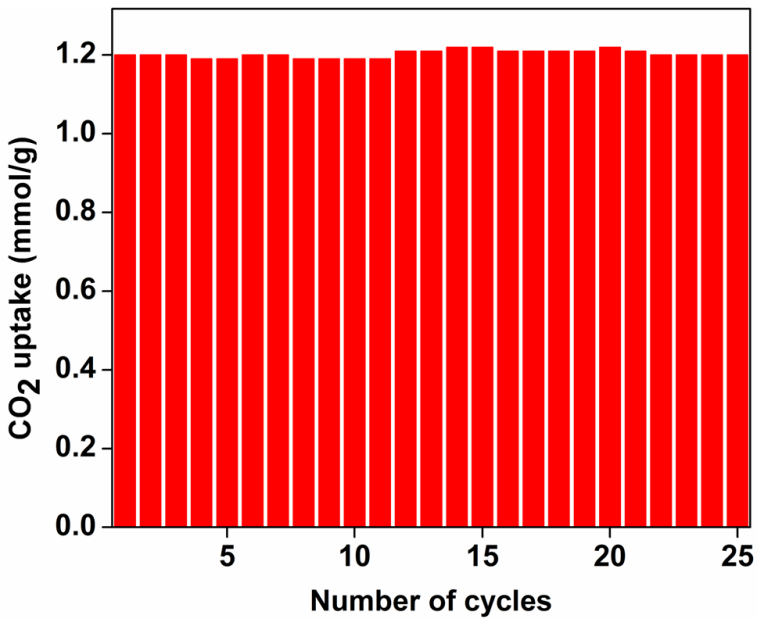

Figure 3.9. Cyclic CO_2 adsorption-desorption on HES-PEI/S.

3.4.6. Effect of HES Versus Other Hydroxyl-containing Polymers

The effect of HES on the oxidation stability of PEI was also compared to two hydroxyl-containing polymers, namely PVA and PEG. As shown in Figure 3.10, the trend of oxidation stability was as follows HES-PEI/S > PVA-PEI/S > PEI/S > PEG-PEI/S. The higher oxidation stability of PVA-PEI/S in comparison to PEI/S is in agreement with other studies.[30,38] However, oxidation stability of PVA-PEI/S is less compared to HES-PEI/S, likely due to its higher hydrophilicity and less favorable geometry. As shown in Figure A3.3, PVA-PEI/S exhibits greater H_2O uptake at various relative humidities compared to HES-PEI/S, which can enhance the propagation of radicals like $OH^{\bullet}$ and $O_2^{\bullet-}$, thereby reducing its oxidation stability. These findings are consistent with the study by Jones and colleagues[15]. Moreover, HES features longer chains ending in hydroxyl groups, which may serve as effective barriers against the diffusion of reactive oxygen species. On contrary, the vinyl hydroxyl groups directly attached to PVA may not provide the same level of protection. This is consistent with the findings of Yan and Sayari[30], who found that the additives primarily enhance the oxidation stability of PEI by acting as tough barriers.

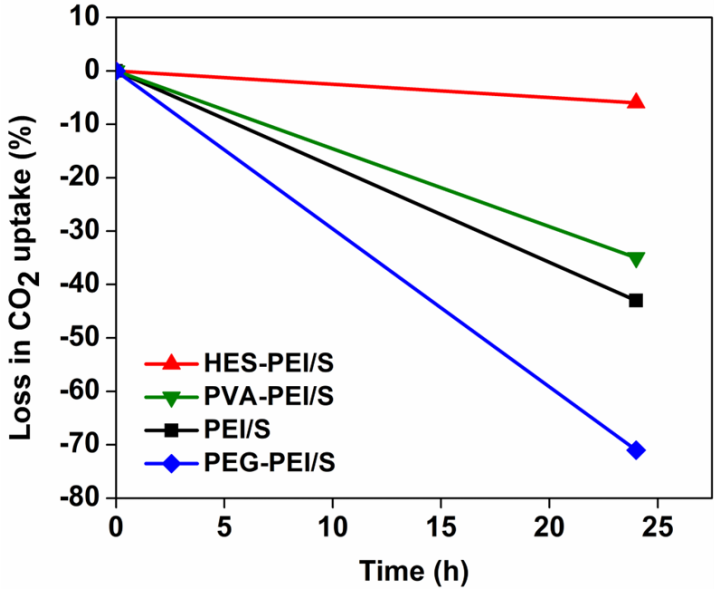

Figure 3.10. Oxidation stability of adsorbents containing hydroxyl additive. CO_2 adsorption was carried at 75 °C.

However, PEG-PEI/S was found to be less stable than PEI/S (Figure A3.4a). Srikanth and

Chuang[37] investigated the effect of PEG (Mw = 200) on supported tetraethylenepentamine in flowing air at 100 °C. The fresh PEG-containing materials exhibited significantly higher CO_2 uptake, consistent with the surfactant effect reported in the literature.[46] However, over time, the CO_2 uptake decreased much faster than PEG-free material. Interpretation of this behavior is tedious since it is difficult to discriminate between the contribution of oxidative degradation and the effect of PEG evaporation. Notice that when treated under N_2 and air at 110 °C for 24 h, the weight loss of PEG was 72% and 98% respectively, whereas PEI remains almost stable (Figure A3.4b and Table A3.1). Furthermore, in agreement with Payne *et al.*,[47] ^{13}C NMR spectrum of PEG treated in air at 110 °C for 3.5 h showed two new peaks at 68.8 and 161.4 ppm, indicative of oxidation products (Figure 3.11), consistent with the fact that PEG generate radicals under such conditions.[48] Overall, our results demonstrate that regarding its effect on PEI's oxidation stability, HES outperform other hydroxyl-containing additives.

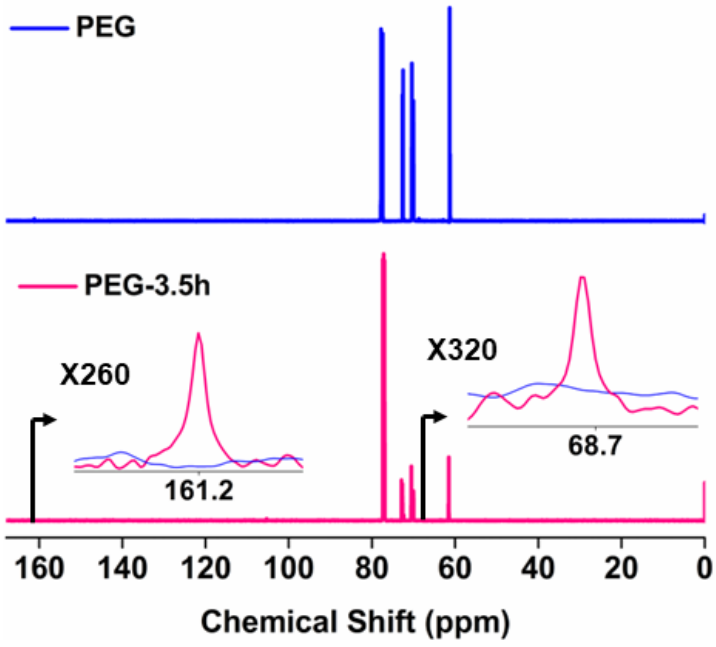

Figure 3.11. ^{13}C NMR of fresh PEG and PEG oxidized under air at 110 °C for 3.5 h.

3.4. Conclusions

Simple co-impregnation of PEI with hydroxyethyl starch was found to impart oxidation resistance comparable to that of PEI functionalized to the same level with 1,2-epoxybutane. The HES-modified PEI was also found to be significantly more stable against oxidation than PEI co-impregnated with other hydroxyl-containing polymers, such as PEG and PVA. The ability of the additive to form hydrogen bonding with PEI was often mentioned as the reason behind their stabilizing effect. Accordingly, it is surmised that HES forms hydrogen bonds with amine groups in PEI, slowing down the formation of imine/amide species and the radical initiation step.

Additional benefits of HES addition compared to EB-functionalization include their much easier preparation procedure, and the preservation of the adsorptive properties of PEI.

3.5. References

(1) Ritchie, H.; Roser, M.; Rosado, P. *CO_2 and Greenhouse Gas Emissions*. Our World in Data. https://ourworldindata.org/co2-and-greenhouse-gas-emissions (accessed 2023-10-23).

(2) *Trends in Atmospheric Carbon Dioxide*. https://gml.noaa.gov/ccgg/trends/weekly.html (accessed 2023-10-23).

(3) *Overview of Greenhouse Gases*. https://www.epa.gov/ghgemissions/overview-greenhouse-gases (accessed 2023-10-23).

(4) *Intergovernmental Panel on Climate Change (IPCC), Climate change 2023: Synthesis report*. https://www.ipcc.ch/report/ar6/syr/downloads/report/IPCC_AR6_SYR_LongerReport.pdf (accessed 2024-03-11).

(5) Buckingham, J.; Reina, T. R.; Duyar, M. S. Recent Advances in Carbon Dioxide Capture for Process Intensification. *Carbon Capture Sci. Technol.* **2022**, *2*, 100031.

(6) Choi, S.; Drese, J. H.; Jones, C. W. Adsorbent Materials for Carbon Dioxide Capture from Large Anthropogenic Point Sources. *ChemSusChem* **2009**, *2*, 796–854.

(7) Kolle, J. M.; Fayaz, M.; Sayari, A. Understanding the Effect of Water on CO_2 Adsorption. *Chem. Rev.* **2021**, *121*, 7280–7345.

(8) Jaffar, M. M.; Rolfe, A.; Brandoni, C.; Martinez, J.; Snape, C.; Kaldis, S.; Santos, A.; Lysiak, B.; Lappas, A.; Hewitt, N.; Huang, Y. A Technical and Environmental Comparison of Novel Silica PEI Adsorbent-Based and Conventional MEA-Based CO_2 Capture Technologies in the Selected Cement Plant. *Carbon Capture Sci. Technol.* **2024**, *10*, 100179.

(9) Abdullatif, Y.; Sodiq, A.; Mir, N.; Bicer, Y.; Al-Ansari, T.; El-Naas, M. H.; Amhamed, A. I. Emerging Trends in Direct Air Capture of CO_2: A Review of Technology Options Targeting Net-Zero Emissions. *RSC Adv.* **2023**, *13*, 5687–5722.

(10) Sayari, A.; Belmabkhout, Y.; Serna-Guerrero, R. Flue Gas Treatment via CO_2 Adsorption. *Chem. Eng. J.* **2011**, *171*, 760–774.

(11) Bollini, P.; Choi, S.; Drese, J. H.; Jones, C. W. Oxidative Degradation of Aminosilica Adsorbents Relevant to Postcombustion CO_2 Capture. *Energy Fuels* **2011**, *25*, 2416–2425.

(12) Heydari-Gorji, A.; Belmabkhout, Y.; Sayari, A. Degradation of Amine-Supported CO_2 Adsorbents in the Presence of Oxygen-Containing Gases. *Microporous Mesoporous Mater.* **2011**, *145*, 146–149.

(13) Heydari-Gorji, A.; Sayari, A. Thermal, Oxidative, and CO_2-Induced Degradation of Supported Polyethylenimine Adsorbents. *Ind. Eng. Chem. Res.* **2012**, *51*, 6887–6894.

(14) Lashaki M.J.; Khiavi, S.; Sayari, A. Stability of Amine-Functionalized CO_2 Adsorbents: A Multifaceted Puzzle. *Chem. Soc. Rev.* **2019**, *48*, 3320–3405.

(15) Carneiro, J. S. A.; Innocenti, G.; Moon, H. J.; Guta, Y.; Proaño, L.; Sievers, C.; Sakwa-Novak, M. A.; Ping, E. W.; Jones, C. W. Insights into the Oxidative Degradation

Mechanism of Solid Amine Sorbents for CO_2 Capture from Air: Roles of Atmospheric Water. *Angew. Chem., Int. Ed.* **2023**, *62*, e202302887.

(16) Ahmadalinezhad, A.; Sayari, A. Oxidative Degradation of Silica-Supported Polyethylenimine for CO_2 Adsorption: Insights into the Nature of Deactivated Species. *Phys. Chem. Chem. Phys.* **2014**, *16*, 1529–1535.

(17) Min, K.; Choi, W.; Kim, C.; Choi, M. Oxidation-Stable Amine-Containing Adsorbents for Carbon Dioxide Capture. *Nat. Commun.* **2018**, *9*, 726.

(18) Choi, W.; Min, K.; Kim, C.; Ko, Y. S.; Jeon, J. W.; Seo, H.; Park, Y. K.; Choi, M. Epoxide-Functionalization of Polyethyleneimine for Synthesis of Stable Carbon Dioxide Adsorbent in Temperature Swing Adsorption. *Nat. Commun.* **2016**, *7*, 12640.

(19) Bali, S.; Chen, T. T.; Chaikittisilp, W.; Jones, C. W. Oxidative Stability of Amino Polymer-Alumina Hybrid Adsorbents for Carbon Dioxide Capture. *Energy Fuels* **2013**, *27*, 1547–1554.

(20) Buijs, W. CO_2 Capture with PEI: A Molecular Modeling Study of the Ultimate Oxidation Stability of LPEI and BPEI. *ACS Eng. Au* **2023**, *3*, 28–36.

(21) Choi, W.; Park, J.; Kim, C.; Choi, M. Structural Effects of Amine Polymers on Stability and Energy Efficiency of Adsorbents in Post-Combustion CO_2 Capture. *Chem. Eng. J.* **2021**, *408*, 127289.

(22) Pang, S. H.; Lee, L. C.; Sakwa-Novak, M. A.; Lively, R. P.; Jones, C. W. Design of Aminopolymer Structure to Enhance Performance and Stability of CO_2 Sorbents: Poly(propylenimine) vs Poly(ethylenimine). *J. Am. Chem. Soc.* **2017**, *139*, 3627–3630.

(23) Li, S.; Cerón, M. R.; Eshelman, H. V.; Varni, A. J.; Maiti, A.; Akhade, S.; Pang, S. H. Probing the Kinetic Origin of Varying Oxidative Stability of Ethyl- vs. Propyl-Spaced Amines for Direct Air Capture. *ChemSusChem* **2023**, *16*, e202201908.

(24) Pang, S. H.; Lively, R. P.; Jones, C. W. Oxidatively-Stable Linear Poly(Propylenimine)-Containing Adsorbents for CO_2 Capture from Ultradilute Streams. *ChemSusChem* **2018**, *11*, 2628–2637.

(25) Sarazen, M. L.; Sakwa-Novak, M. A.; Ping, E. W.; Jones, C. W. Effect of Different Acid Initiators on Branched Poly(propylenimine) Synthesis and CO_2 Sorption Performance. *ACS Sustainable Chem. Eng.* **2019**, *7*, 7338–7345.

(26) Vu, Q. T.; Yamada, H.; Yogo, K. Effects of Amine Structures on Oxidative Degradation of Amine-Functionalized Adsorbents for CO_2 Capture. *Ind. Eng. Chem. Res.* **2021**, *60*, 4942–4950.

(27) Lee, J. J.; Yoo, C. J.; Chen, C. H.; Hayes, S. E.; Sievers, C.; Jones, C. W. Silica-Supported Sterically Hindered Amines for CO_2 Capture. *Langmuir* **2018**, *34*, 12279–12292.

(28) Guta, Y. A.; Carneiro, J.; Li, S.; Innocenti, G.; Pang, S. H.; Sakwa-Novak, M. A.; Sievers, C.; Jones, C. W. Contributions of CO_2, O_2, and H_2O to the Oxidative Stability of Solid Amine Direct Air Capture Sorbents at Intermediate Temperature. *ACS Appl. Mater. Interfaces* **2023**, *15*, 46790–46802.

(29) Vu, Q. T.; Yamada, H.; Yogo, K. Stability of Polyamine Based Adsorbents to Gas Impurities for CO_2 Capture. *ISIJ Int.* **2022**, *62*, 2442–2445.

(30) Yan, C.; Sayari, A. Spectroscopic Investigation into the Oxidation of Polyethylenimine for CO_2 Capture: Mitigation Strategies and Mechanism. *Chem. Eng. J.* **2024**, *479*, 147498.

(31) Ahmadalinezhad, A.; Tailor, R.; Sayari, A. Molecular-Level Insights into the Oxidative Degradation of Grafted Amines. *Chem. – Eur. J.* **2013**, *19*, 10543–10550.

(32) Racicot, J.; Li, S.; Clabaugh, A.; Hertz, C.; Akhade, S. A.; Ping, E. W.; Pang, S. H.; Sakwa-Novak, M. A. Volatile Products of the Autoxidation of Poly(ethylenimine) in CO_2 Sorbents. *J. Phys. Chem. C* **2022**, *126*, 8807–8816.

(33) Goff, G. S.; Rochelle, G. T. Monoethanolamine Degradation: O_2 Mass Transfer Effects under CO_2 Capture Conditions. *Ind. Eng. Chem. Res.* **2004**, *43*, 6400–6408.

(34) Chi, S.; Rochelle, G. T. Oxidative Degradation of Monoethanolamine. *Ind. Eng. Chem. Res.* **2002**, *41*, 4178–4186.

(35) Yoo, C. J.; Park, S. J.; Jones, C. W. CO_2 Adsorption and Oxidative Degradation of Silica-Supported Branched and Linear Aminosilanes. *Ind. Eng. Chem. Res.* **2020**, *59*, 7061–7071.

(36) Vu, Q. T.; Yamada, H.; Yogo, K. Inhibitors of Oxidative Degradation of Polyamine-Modified Silica Sorbents for CO_2 Capture. *Ind. Eng. Chem. Res.* **2019**, *58*, 15598–15605.

(37) Srikanth, C. S.; Chuang, S. S. C. Spectroscopic Investigation into Oxidative Degradation of Silica-Supported Amine Sorbents for CO_2 Capture. *ChemSusChem* **2012**, *5*, 1435–1442.

(38) Zhai, Y.; Chuang, S. S. C. Enhancing Degradation Resistance of Polyethylenimine for CO_2 Capture with Cross-Linked Poly(vinyl alcohol). *Ind. Eng. Chem. Res.* **2017**, *56*, 13766–13775.

(39) Li, S.; Andrade, M. F.; Varni, A. J.; Russell-Parks, G. A.; Braunecker, W. A.; Hunter-Sellars, E.; Marple, M. A.; Pang, S. H. Enhanced Hydrogen Bonding via Epoxide-Functionalization Restricts Mobility in Poly(ethylenimine) for CO_2 Capture. *Chem. Commun.* **2023**, *59*, 10737–10740.

(40) Choi, W.; Park, J.; Choi, M. Cation Effects of Phosphate Additives for Enhancing the Oxidative Stability of Amine-Containing CO_2 Adsorbents. *Ind. Eng. Chem. Res.* **2021**, *60*, 6147–6152.

(41) Goeppert, A.; Zhang, H.; Sen, R.; Dang, H.; Prakash, G. K. S. Oxidation-Resistant, Cost-Effective Epoxide-Modified Polyamine Adsorbents for CO_2 Capture from Various Sources Including Air. *ChemSusChem* **2019**, *12*, 1712–1723.

(42) Ziaei-Azad, H.; Kolle, J. M.; Al-Yasser, N.; Sayari, A. One-Pot Synthesis of Large-Pore AlMCM-41 Aluminosilicates with High Stability and Adjustable Acidity. *Microporous Mesoporous Mater.* **2018**, *262*, 166–174.

(43) Fredriksen, S. B.; Jens, K.-J. Oxidative Degradation of Aqueous Amine Solutions of MEA, AMP, MDEA, Pz: A Review. *Energy Procedia* **2013**, *37*, 1770–1777.

(44) Goff, G. S.; Rochelle, G. T. Oxidation Inhibitors for Copper and Iron Catalyzed Degradation of Monoethanolamine in CO_2 Capture Processes. *Ind. Eng. Chem. Res.* **2006**, *45*, 2513–2521.

(45) Lepaumier, H.; Picq, D.; Carrette, P. L. New Amines for CO_2 Capture. II. Oxidative Degradation Mechanisms. *Ind. Eng. Chem. Res.* **2009**, *48*, 9068–9075.

(46) Sayari, A.; Liu, Q.; Mishra, P. Enhanced Adsorption Efficiency through Materials Design for Direct Air Capture over Supported Polyethylenimine. *ChemSusChem* **2016**, *9*, 2796–2803.

(47) Payne, M. E.; Kareem, O. O.; Williams-Pavlantos, K.; Wesdemiotis, C.; Grayson, S. M. Mass Spectrometry Investigation into the Oxidative Degradation of Poly(ethylene glycol). *Polym. Degrad. Stab.* **2021**, *183*.

(48) Wang, J. Q.; He, L. N.; Miao, C. X.; Gao, J. The Free-Radical Chemistry of Polyethylene Glycol: Organic Reactions in Compressed Carbon Dioxide. *ChemSusChem* **2009**, *2*, 755–760.

Appendix A3 Supplementary Information for Chapter 3

Preparation and Characterization of PE-$AlSiO_2$ Support

PE-$AlSiO_2$ was synthesized using following method: In solution A, 40 grams of fumed silica and 820 g of TMAOH was added in 800 g of water. In another beaker (solution B), 488 g of CTAB and 157 g of NH_3 solution was added in 4000 g of water. After 30 minutes of stirring, solution B was added in solution A under vigorous stirring. After a duration of 30 minutes, 37 grams of $NaAlO_2$ (sodium aluminate) was introduced, and the stirring process was sustained for an additional 30 minutes. Thereafter fumed silica, specifically, Cab-O-Sil, was slowly added to the mixture. After stirring the solution for an hour, 460 mL of DMHA (dimethylhexadecylamine) was added to the mixture and stirring continued for an additional 30 minutes. Next, the mixture was loaded in an autoclave and placed in a preheated oven at 70 °C for 3 days. Afterward, the autoclave was allowed to cool down to room temperature. The resulting material was separated through filtration, thoroughly washed with distilled water, and left to dry under ambient conditions. Finally, the material was calcination in a furnace, where it was heated under a flowing nitrogen at a rate of 1°C per minute upto 550 °C. It was then subjected to air treatment at 550 °C for 5 h to eliminate any remaining carbonaceous substances. The resultant support was then named as PE-$AlSiO_2$.

The pore structure of PE-$AlSiO_2$ was investigated by N_2 adsorption measurements at −196 °C using a 3Flex instrument (Micromeritics). The sample was pretreated in flowing N_2 at 120 °C for 4 h. The specific surface area of all samples was determined using the Brunauer-Emmett-Teller (BET) method at relative pressures ranging from 0.06 to 0.2. The total pore volume was measured at $P/P_0 = 0.99$. PE-$AlSiO_2$ support has 818 m^2/g surface area, 1.66 cm^3/g pore volume and 8.13 nm pore size.

The state of aluminum sites in PE-$AlSiO_2$ was determined by ^{27}Al MAS NMR of PE-$AlSiO_2$ support using a AVIII 400 spectrometer with a MAS probe of 4 mm triple resonance. Echo pulse sequence was used, and the sample was rotated at 10 kHz. Other parameters include a 1-second delay, 90-degree pulse at 3.6 db for 3 μs. Spectra (shown in Figure A3.1) was referenced to 0 ppm

NMR signal of 1M $Al(NO_3)_3$.

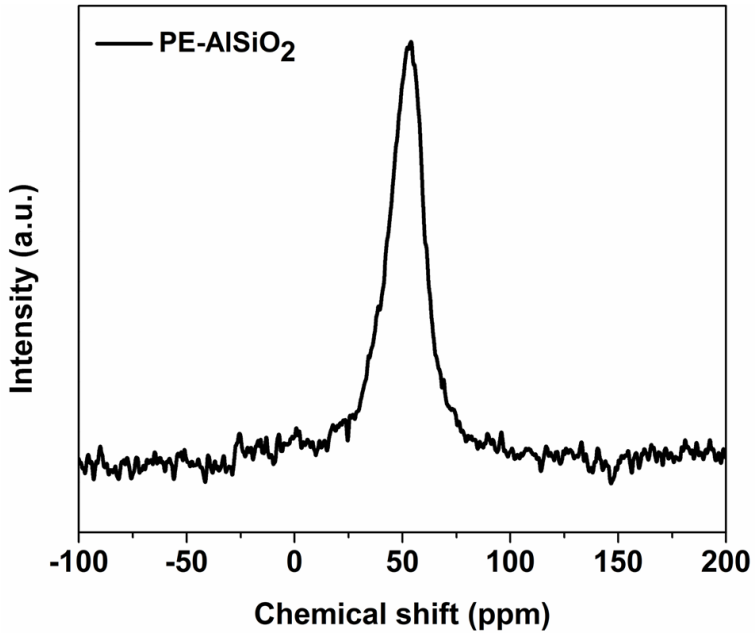

Figure A3.1. ^{27}Al MAS NMR spectra of $PE\text{-}AlSiO_2$.

Functionalization of PEI with EB

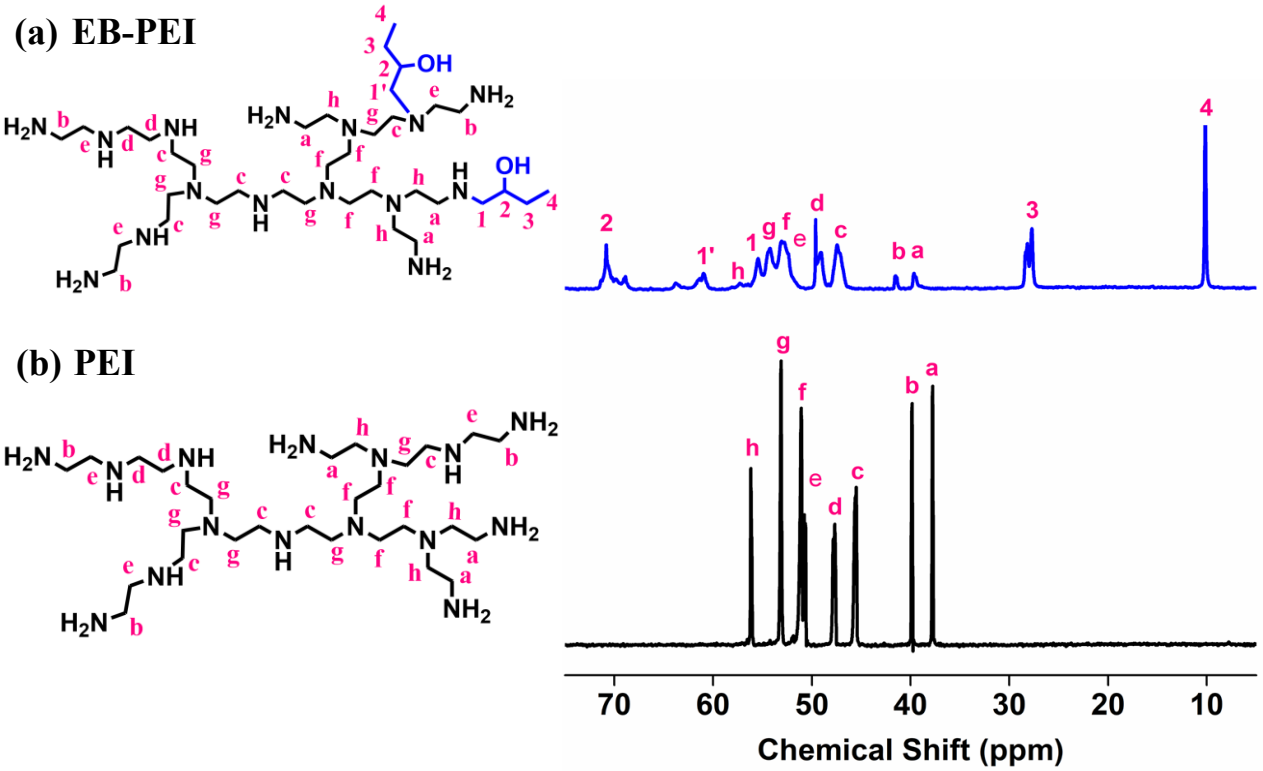

Figure A3.2. ^{13}C NMR spectra for (a) PEI (b) EB-PEI.

H_2O uptake of PVA-PEI/S and HES-PEI/S

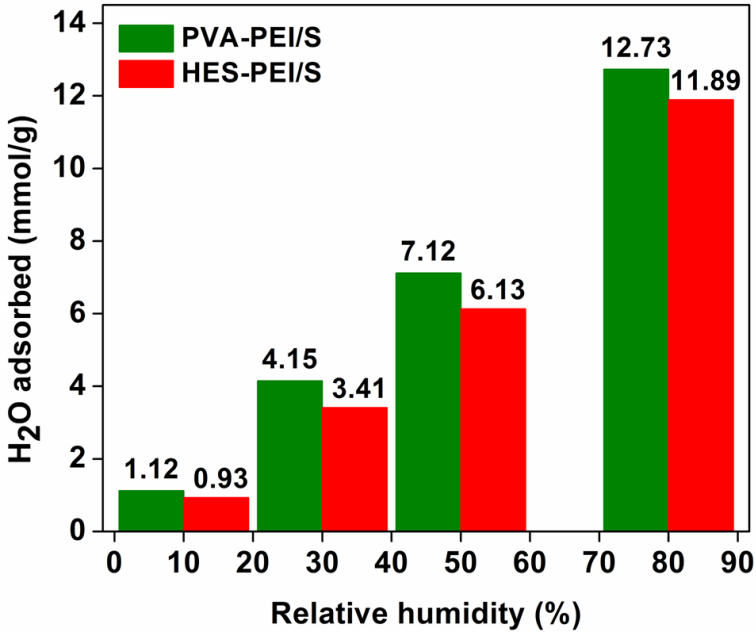

Figure A3.3. H_2O adsorption capacity of PVA-PEI/S and HES-PEI/S under different relative humidities.

Thermal and Oxidative Stability of PEG

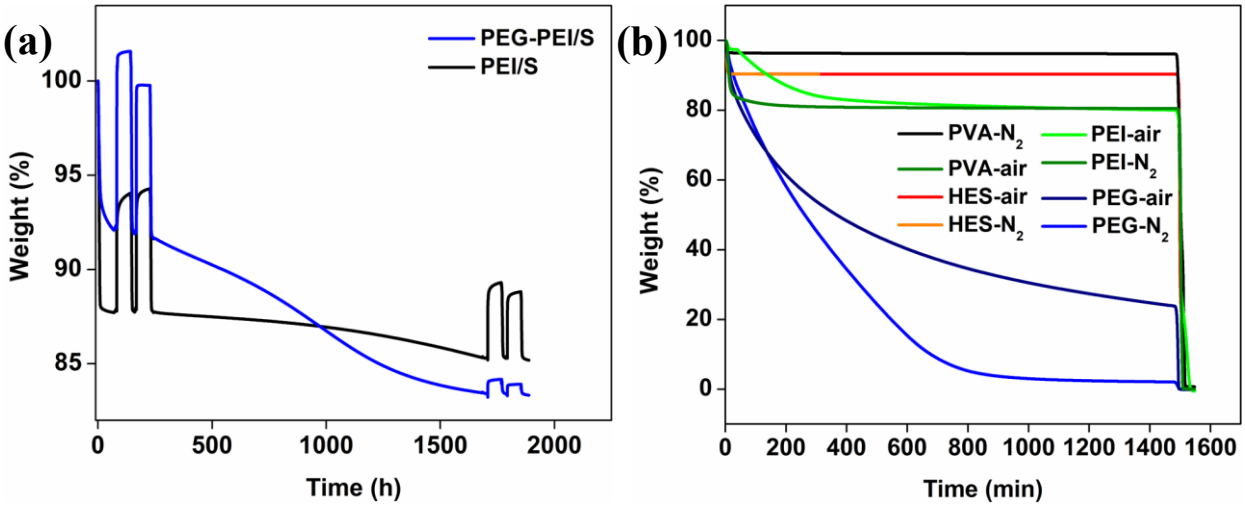

Figure A3.4. (a) TGA curve of CO_2 adsorption and oxidation for PEG-PEI/S and PEI/S (b) Thermal and oxidation stability of different additives; Additives were pretreated under nitrogen for 30 min. Thereafter, for investigating thermal/oxidation stability, treated under N_2/air at 110 °C for 24 h and then temperature was increased to 700 °C.

Table A3.1. Weight loss (%) of different hydroxyl-containing additives under N_2 and air at 110 °C for 24 h.

Sample	HES	PVA	PEI	PEG
Weight loss (%) under air in 24 h	0	0	18	98
Weight loss (%) under N_2 in 24 h	0	0	3	72

CHAPTER 4 CO_2 UPTAKE - RELATIVE HUMIDITY - PORE SIZE RELATIONSHIP: A NEW TOOL FOR THE DESIGN OF AMINE-CONTAINING ADSORBENTS

4.1. Abstract

Optimization of amine-containing CO_2 adsorbents, including CO_2 uptake, adsorption and desorption kinetics, energy requirements, and material stability, is a recurrent theme since the inception of this field. The objective of this work is (1) to establish a relationship between CO_2 uptake in amine-containing adsorbents as a function of relative humidity (RH) of feed gas and material pore size, and (2) to use this relationship to design adsorbents that maximize CO_2 uptake depending on RH. To this end, periodic mesoporous silicas with similar morphology and different pore sizes, ranging from 3 to 9.2 nm, are synthesized and grafted with comparable amounts of triaminosilane. All materials exhibit S-shaped water adsorption isotherms, with a steep rise as the water vapor reaches the capillary condensation pressure. All humid CO_2 adsorption isotherms versus RH, show prominent maxima at vapor pressures corresponding to the water capillary condensation. The enhanced CO_2 uptake at specific RHs is attributed to the occurrence of liquid-like water at capillary condensation pressure, which facilitates the formation of ammonium bicarbonate. Hence, maximum CO_2 uptake may be achieved using an adsorbent whose average pore size corresponds to the water capillary condensation at the feed gas RH.

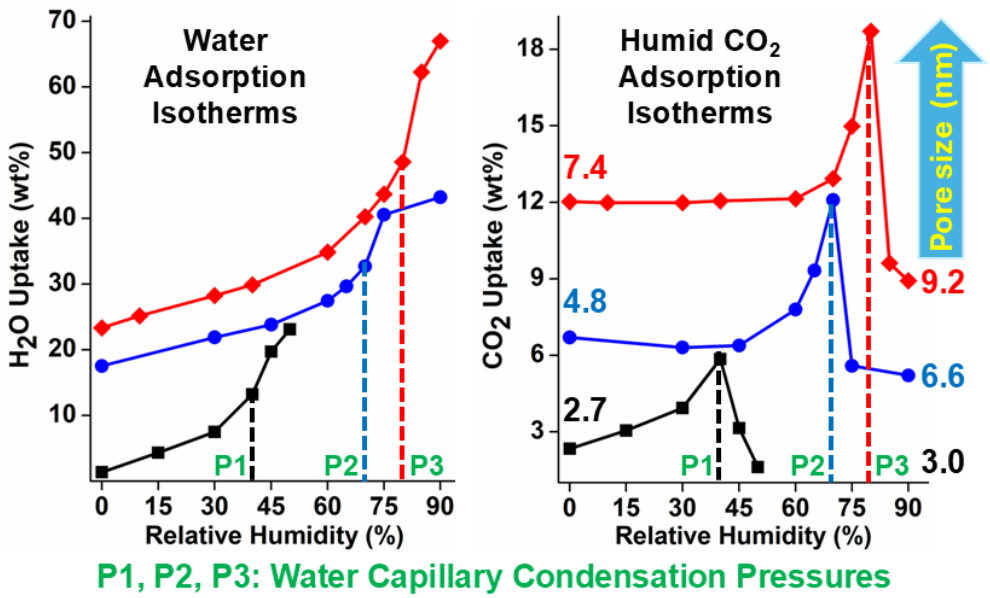

4.2. Introduction

Although it is not the most potent greenhouse gas (GHG), carbon dioxide stemming mostly from fossil fuel combustion, is the main contributor to the overall GHG effect and associated global warming.[1,2] With worldwide CO_2 emissions exceeding 40 gigatons a year, the CO_2 concentration in the atmosphere reached the alarming level of 425 ppm in 2024.[3] While the world is transitioning to more environment friendly sources of energy, carbon capture and sequestration has been recognized as the only single technology capable of alleviating the effect of GHGs to a significant extent. Therefore, extensive effort has been deployed over the last two to three decades to develop viable carbon capture technologies. Recent progress in this field has been reported in many authoritative reviews.[4–6] Of particular interest, adsorption processes using a wide variety of materials, including zeolites, carbons, metal-organic frameworks (MOFs), covalent organic frameworks (COFs) and amine-containing materials[7,8] are playing a leading role. Currently, many of these materials are being used at pilot and demonstration scale, toward commercial implementation.[9,10]

Material optimization is possibly the most recurrent topic in the CO_2 adsorption literature. Key metrics include selectivity, adsorption and desorption kinetics, physical, chemical and mechanical stability, cost, energy requirements and process engineering.[11–14] In particular, there has been considerable interest in investigating the effect of the most ubiquitous species, namely water vapor, on CO_2 adsorption in the presence of a variety of materials. As discussed in a recent review[15], water plays many different roles, depending on the nature of the adsorbents and the relative humidity. Among its desirable effects on amine-containing adsorbents, water often promotes CO_2 uptake by facilitating the formation of ammonium bicarbonate (CO_2/N = 1) instead of carbamate (CO_2/N = 0.5)[16,17] or by enhancing CO_2 diffusion through supported polyamines.[18,19] It also plays a key role in stabilizing the adsorbent over time by preventing the formation of stable urea linkages at the expense of amine groups.[20,21] In other instances, particularly at high RH, water may not only inhibit CO_2 adsorption, but affects the integrity of the material, as observed for some MOFs.[15,22,23]

There is often an optimum water concentration corresponding to maximum CO_2 uptake. The rising section is the result of cooperative mechanisms between both adsorbates, such as the occurrence of a more favorable surface chemistry,[16,17,24,25] facilitated CO_2 transport as water may lubricate polyamine chains,[26,27] creation of additional CO_2-binding sites by adsorbed water[28] or other mechanisms.[29] The declining CO_2 uptake at higher RH is often associated with the available adsorption volume being occupied by water, with less and less room for CO_2 adsorption.[26,29,30] The optimum RH varied widely, depending on the nature of the adsorbent. It was found to be 10% for a polyimide COF,[29] 25% for a PEI impregnated single-walled zeolite.[26] 30% for a diamine appended MOF,[30] and more than 74% for a propylamine grafted pore-expanded silica.[17] Interestingly, in the latter instance, as the RH increased from 0 to 27 and 61%, there was a modest increase in CO_2 uptake by 16 and 22%, respectively compared to dry condition. However, further increase of RH to 74% was accompanied by as much as 60% increase in CO_2 uptake. It was surmised that this sharp increase is related to the occurrence of water capillary condensation. Hence, it is hypothesized that for a feed gas with a particular water vapor content, the CO_2 uptake of an amine-containing adsorbent could be maximized using a material with a specific pore size. It is further hypothesized that the optimum pore size should correspond to the capillary condensation of water at its partial pressure in the feed gas. Hence, the objective of this contribution is to establish empirical CO_2 uptake – pore size – relative humidity relationships, so that for any feed gas with a given water content, amine-containing materials with maximum CO_2 uptake may be designed systematically by adjusting the pore size accordingly.

To reach this goal, we designed a series of adsorbents with, as much as possible, the same physical characteristics, but different pore sizes ranging from 3.0 to 9.2 nm. All materials were then grafted with 2-[2-(3-trimethoxysilylpropylamino)ethylamino]ethylamine (denoted TRI for triamine) to comparable loadings using 1 g triamine per gram silica. We also measured their water adsorption isotherms and their CO_2 uptake in the presence of the full range of relative humidity.

The support materials consisted mostly of SBA-15 ordered mesoporous silicas with rodlike morphology, and different pore sizes, prepared using a highly reproducible method reported earlier.[31] The only variable to obtain materials with different pore sizes, was the synthesis temperature. Increasing the temperature from 40 to 115 °C led to materials with 5.2 to 9.2 nm pores. These are denoted SBA-15/t, where t indicates the synthesis temperature in °C. An additional material MCM-41/70 with an average pore size of 3.0 nm consisted of MCM-41 silica, synthesized at 70 °C. Admittedly, SBA-15 and MCM-41 silicas, even when partially protected by grafted amines, are not ideal materials in terms of long-term stability in the presence of high humidity feed gases.[32,33] Nonetheless, we used such materials because of their highly periodical pore structure and the easy control of their pore size/volume and morphology.

4.3. Experimental Section

4.3.1. Materials

Triblock copolymer Pluronic P123, tetramethylammonium hydroxide (TMAOH, 25 wt% solution), tetraethyl orthosilicate (TEOS, 98%), fumed silica (Cab-O-Sil, M5), cetyltrimethylammonium bromide (CTAB, 98%) and 2-[2-(3-trimethoxysilylpropylamino)ethylamino]ethylamine (TRI, 97%) were purchased from Sigma-Aldrich. Ammonia solution (NH_4OH, 30 wt%), pentane (99.6%), hydrochloric acid (HCl) and toluene (99.9%) were obtained from Fischer. All chemicals were used as obtained. Ultra-high purity (99.999%) N_2 and CO_2 gas cylinders were supplied by Messer.

4.3.2. Material Synthesis

SBA-15 silicas with different pore sizes were prepared at 40, 60, 80, and 115 °C using the method proposed by Sayari *et al.*[31] Briefly, 4 g of Pluronic P123 was added in an aqueous solution of 120 mL of HCl (2M) and 30 mL distilled H_2O in a Teflon-lined container and stirred at 40 °C until complete dissolution. Then, 8.5 g of TEOS was added, and the solution was vigorously stirred for 5 min. The solution was then maintained at 40°C for 20 h under static condition, and subsequently

heated in an autoclave for 40 h at the aforementioned temperatures. The final product was filtered, washed with distilled H_2O and dried at room temperature, followed by calcination at 550 °C for 6 h under air. Supports were designated as SBA-15/X, where X indicates the synthesis temperature.

MCM-41 silica was prepared as reported elsewhere[34] using 1 SiO_2:0.17 NH_4OH:0.17 CTAB:17 H_2O:0.33 TMAOH composition. Typically, 1.8 g of Cab-O-Sil was added into 3 g of water in a Teflon-lined container followed by addition of 3.08 g of TMAOH under vigorous stirring. In another beaker, 1.83 g of CTAB was stirred with 3.28 g of distilled H_2O until completely dissolved, and then 0.59 g of NH_4OH was added into the solution. This solution was then added to the mixture containing Cab-O-Sil, and stirred for another 30 min. Subsequently, the mixture was heated at 70 °C for 72 h in an autoclave. Thereafter, the product was separated and calcined using the same procedure as mentioned above for the SBA-15 silicas. The obtained material was designated as MCM-41/70.

4.3.3. Triamine (TRI) Grafting Procedure

TRI was grafted on different silicas using the method proposed by Harlick and Sayari.[35] Supports were dried at 130 °C for 3 h and then 1 g of support was dispersed in 30 mL of toluene followed by stirring for 1 h. The temperature of the solution was then increased to 110 °C, and 1 mL of TRI was added. The mixture was refluxed for 16 h and the product was separated by filtration, washed with toluene followed by pentane and dried at room temperature for 24 h. Grafted supports were designated as TRI/SBA-15/X or TRI/MCM-41/X depending on support used. Here, x refers to synthesis temperature. Due to small pore sizes of MCM-41/70 and SBA-15/40, these supports were also grafted with 0.4 mL of TRI per gram of support and referred as TRI/MCM-41/70-0.4 and TRI/SBA-15/40-0.4 respectively.

4.3.4. Material Characterizations

The pore structure of supports was determined by N_2 adsorption measurements at −196 °C using a Surface Area and Pore Size Analyzer (Quantachrome NOVA 1200e). The samples were degassed

in flowing N_2 at 120 °C for 5 h. The specific surface area was measured using the Brunauer-Emmett-Teller (BET) method at relative pressures from 0.05 to 0.3. The total pore volume was recorded at $P/P_0 = 0.95$, and the pore size distribution was determined using the Barrett, Joyner & Halenda (BJH) model. A JEOL JSM-7500F field emission scanning electron microscopy (SEM) operating at an accelerating voltage of 2 kV was used to obtain images of supports.

4.3.5. Adsorption Measurements

Water and CO_2 uptake measurements of grafted materials under dry and humid conditions were performed using a gravimetric sorption analyzer (DVS Carbon, Surface Measurement Systems). Around 15 mg of sample was loaded in the pan, and the material was pretreated under flowing N_2 (100 mL/min) at 120 °C for 90 min to remove any adsorbed moisture and impurities. For water adsorption measurements, the temperature was maintained at 25 °C, and the sample was exposed to stepwise increases in relative humidity. At each RH level, the mass change was recorded once the sample mass stabilized. To measure CO_2 uptake under dry conditions, the temperature was decreased to 25 °C, and gas was then switched to a mixture of 5% CO_2 in N_2 at a flow rate of 100 mL/min till the adsorbent reached a steady state. Under humid conditions, the sample was pre-humidified by bubbling N_2 (100 mL/min) through a water saturator. After the material reached a steady state, the gas mixture was switched to humid 5% CO_2 in N_2 to measure the CO_2 uptake. A constant RH was monitored throughout the pre-hydration and CO_2 adsorption stages. Steady state was defined as a rate of mass change (dm/dt) less than 0.001% per min for 10 min under isothermal conditions.

Temperature programmed desorption and dynamic breakthrough measurements were performed using a breakthrough curve analyzer (mixSorb S series, 3P Instruments) connected to a mass spectrometer (MKS Cirrus 3 instrument). Approximately 0.5 g of sample was loaded into a stainless-steel column with an inner diameter of 0.5 cm and a length of 6 cm. CO_2 adsorption measurements were carried out under both dry and humid conditions as described previously.

During CO_2 desorption, the temperature was ramped up to 140 ºC at a rate of 10 ºC min^{-1}, held at that temperature for 30 min and then gradually decreased to 25 ºC.

The organic content (%) of the materials was determined using thermogravimetric analyzer (Q550 TGA, TA Instruments). Samples were pretreated under flowing N_2 at 120 °C for 30 min, then the temperature was increased to 700 °C at a rate of 10 °C min^{-1}. The samples were exposed to flowing air for 15 min to remove any remaining carbonaceous material. The organic content was determined by measuring the weight loss (%) beyond 200 °C.

4.4. Results and Discussion

4.4.1. Morphology of Silica Supports

Scanning electron microscopy (SEM) images for calcined SBA-15/t silicas are shown in Figure 4.1a to 1d. Lower and higher magnification SEM Images for SBA-15/115 are depicted in Figure 4.1e and 1f. Additional low-magnification images for SBA-15/t with t = 40, 60 and 80 °C in Figure A4.1. It is seen that all SBA-15/t silicas consisted of monodispersed and hexagonally facetted rodlike particles with a diameter of 0.40-0.45 μm and 1.1-1.5 μm in length (Figure 4.1a, b, c, d).[31]

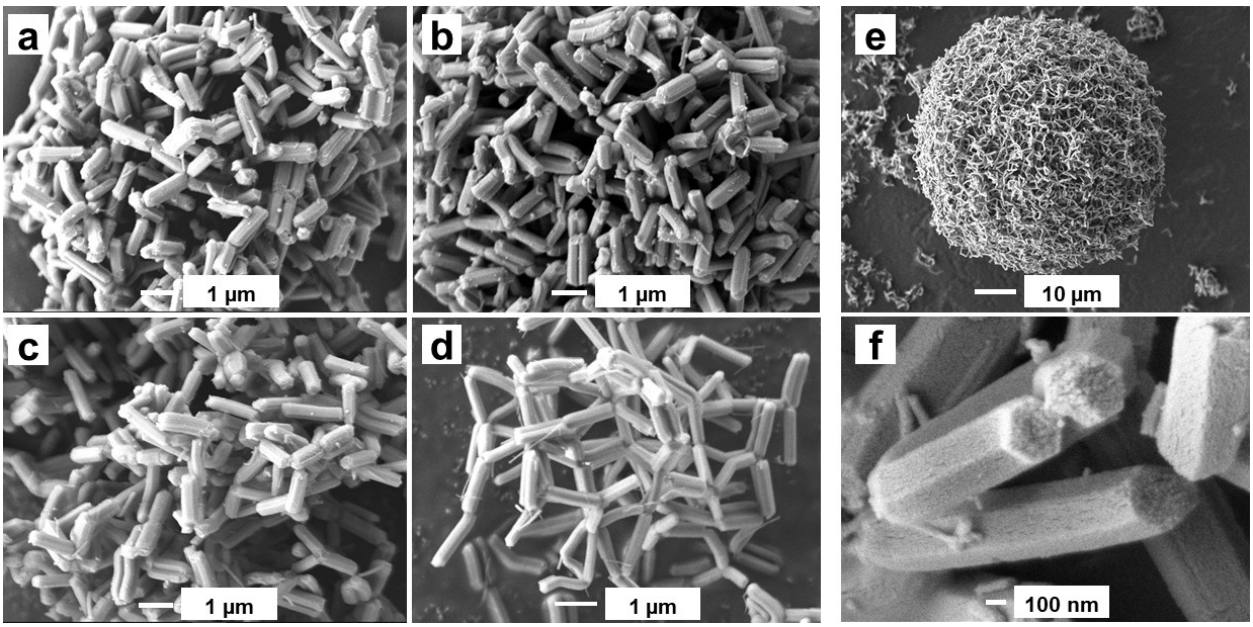

Figure 4.1. (a, b, c, d) High-magnification SEM images of SBA-15/40, SBA-15/60, SBA-15/80

and SBA-15/115 respectively. (e, f) Low- and high-magnification images of SBA-15/115 respectively.

4.4.2. Textural Properties of SBA-15 Silicas

Nitrogen adsorption-desorption isotherms shown in Figure 4.2, were of Type IV according to the IUPAC classification,[36] with H1 hysteresis loops and sharp capillary condensation, indicating the occurrence of mesopores with narrow size distributions. The nitrogen capillary condensation moved to higher pressures as the synthesis temperature increased, indicative of increasing average pore size. The corresponding textural properties and pore size distributions (PSDs) of supports are shown in Table 4.1 and Figure 4.3, respectively, which indicate the upward shift of the average pore sizes with increasing synthesis temperature. Furthermore, the narrow PSDs observed for all silica supports revealed the excellent uniformity and periodicity of the pore structure.

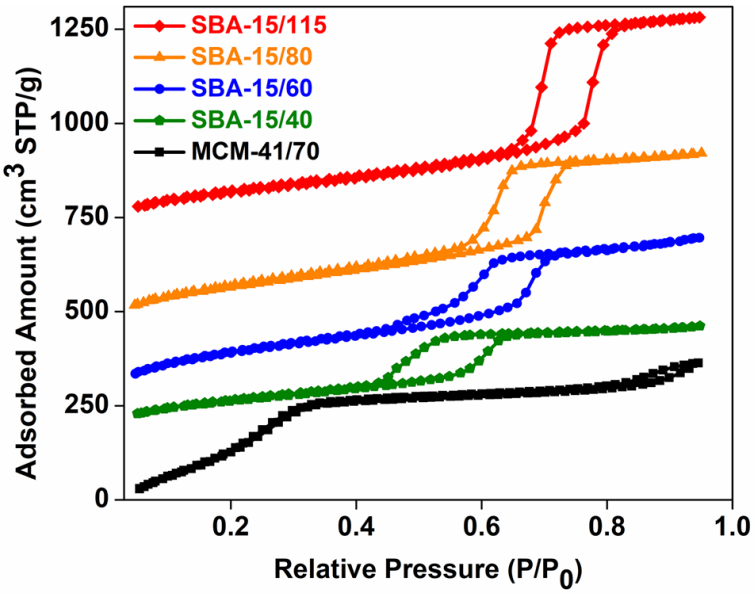

Figure 4.2. (a) N_2 adsorption-desorption isotherms for SBA-15/t and MCM-41/70 silicas.

Table 4.1. Structural properties of silica supports.

Material Support	T (°C)[a]	S_{BET} (m^2/g) [b]	w (nm)[c]	V_{total} (cc/g)[d]
MCM-41/70	70	1112	3.0	0.75
SBA-15/40	40	949	5.2	0.57
SBA-15/60	60	829	6.6	0.84
SBA-15/80	80	718	7.0	0.87
SBA-15/115	115	546	9.2	0.95

[a] Synthesis temperature of silica supports. [b] BET (Brunauer, Emmett, and Teller) specific surface area. [c] Pore size. [d] Total pore volume calculated at P/P_0 ca. 0.95.

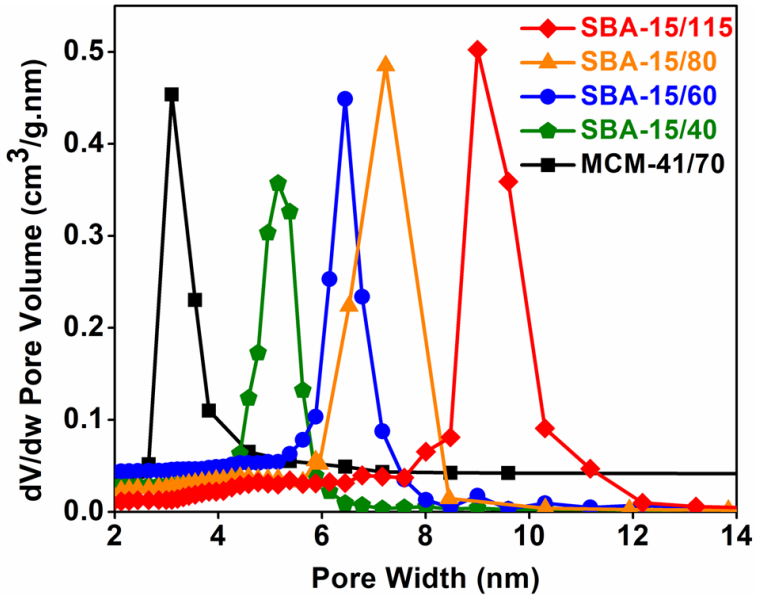

Figure 4.3. (a) N_2 adsorption-desorption isotherms. (b) Pore size distributions for SBA-15/t and MCM-41/70 silicas.

4.4.3. Carbon dioxide Uptake and Amine Efficiency

All silica supports were grafted with the same relative amount of triamine (1 g per g), and the corresponding CO_2 uptakes were measured at 25, 50 and 75 °C for 120 min using a 5% CO_2/N_2 mixture flowing at 100 mL/min. It was established that the CO_2 concentration of 5% corresponds to the onset of physisorption, while the chemisorption is almost complete.[37] The data (Figure 4.4) showed that CO_2 adsorption in the presence of TRI/SBA-15/t with t = 60, 80 and 115 °C was thermodynamically controlled, as the CO_2 uptake and amine efficiency decreased at increasing

adsorption temperature, indicating the absence of diffusion resistance. In contrast, as shown in Figure A4.2, materials with smaller pore sizes, namely TRI/MCM-41/70 and TRI/SBA-15/40, showed higher CO_2 uptake at 50 °C compared to 25 °C, indicating the occurrence of kinetically controlled adsorption. Hence, we decreased the amount of triamine in the grafting mixture of these two silicas to 0.4 g per g, to obtain the diffusion-free adsorption data shown in Figure 4.4 for TRI/MCM-41/70-0.4 and TRI/SBA-15/40-0.4. These materials were used for subsequent adsorption measurements. As shown in Table A4.1, the amine content of the adsorbents ranged from 4.06 to 5.51 mmol/g, with TRI/SBA-15/80 and TRI/SBA-15/115 showing similar organic contents. Furthermore, both CO_2 uptake and amine efficiency showed positive correlations with the pore size. As mentioned by Lashaki and Sayari,[38] this may be because amines are more accessible in adsorbents with larger pore size.

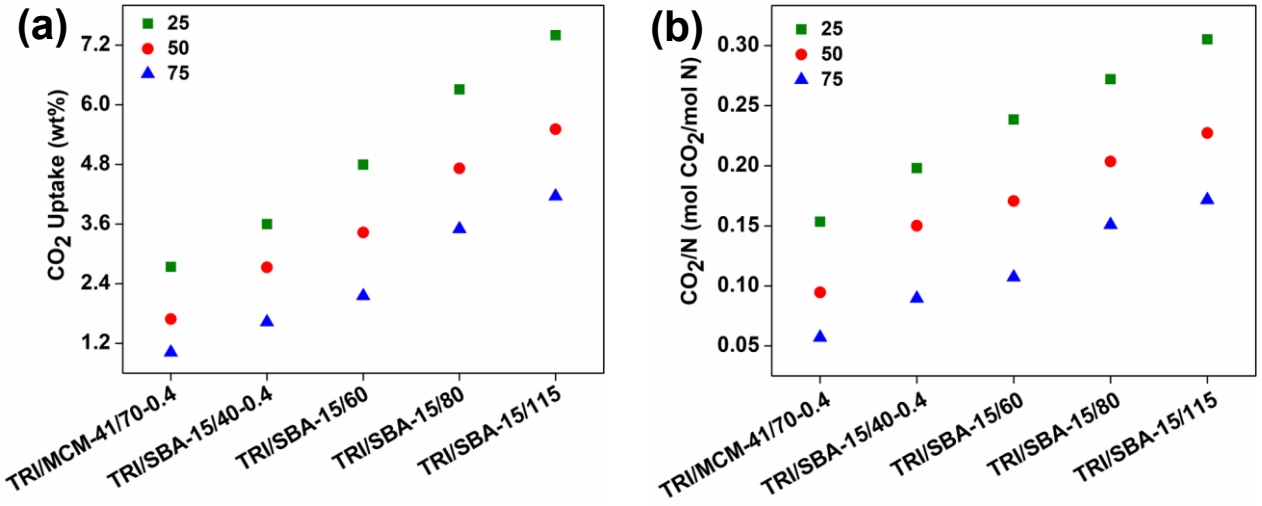

Figure 4.4. (a) CO_2 uptake and (b) amine efficiency of TRI grafted adsorbents at 25, 50 and 75 °C.

4.4.4. Water and Carbon dioxide Adsorption Isotherms

Water adsorption isotherms at 25 °C and relative humidities up to 90%, are shown in Figure 4.5. All materials exhibited S-shaped isotherms with capillary condensation occurring at higher RH as the pore size increased. The overall CO_2 and water uptakes were measured for all adsorbents using 5% CO_2/N_2 with different RHs from 0 to 90%. The humid CO_2 uptake data shown in Figure 4.6, were calculated based on the weight gain of the adsorbent upon exposure to humid CO_2 after pre-

humidifying the material under the same water partial pressure, assuming that water uptake remains the same regardless of the presence of CO_2. Figure A4.3 provides direct evidence of this contention as the column downstream water content was not affected by the presence of CO_2, while maintaining the water partial pressure constant. This behavior was also confirmed by literature data.[39–41] All samples showed striking dependence of CO_2 uptake versus RH, with prominent maxima at the humidity level corresponding to the water capillary condensation. TRI/MCM-41/70-0.4, TRI/SBA-15/40-0.4, TRI/SBA-15/60, TRI/SBA-15/80 and TRI/SBA-15/115 showed their highest CO_2 uptake at 40, 65, 70, 75 and 80% RH, respectively. Figure A4.4 compares CO_2 uptake under dry and humid conditions at these RH values, underscoring the enhancement associated with water capillary condensation within the pores. Moreover, the graph shows that the RH at which water capillary condensation occurs and consequently adsorbent achieves maximum CO_2 uptake increases systematically with pore size. The corresponding amine efficiency of the adsorbents at these water capillary condensation pressures are given in Table A4.1. Figure 4.7 showing both isotherms for the same adsorbent (TRI/SBA-15/115), indicates clearly that the maximum CO_2 uptake achieved at RH of 80%, corresponding to the water capillary condensation pressure was about twice as high as the uptake at RHs below 60%. Likewise, the amine efficiency increased from 0.31 under dry conditions to 0.58 at RH of 80%. Numerous studies reported the formation of ammonium bicarbonate, with increased amine efficiency, upon adsorption of CO_2 over amine-containing adsorbents under humid conditions[17,42–45]. It is surmised that the enhancement in CO_2 uptake and amine efficiency observed in the current investigation is attributed to the formation of ammonium bicarbonate in the presence of moisture. This is further supported by the higher maximum CO_2 desorption temperature observed under humid conditions compared to dry condition (Figure 5b), due to the greater stability of ammonium bicarbonate relative to carbamate, as reported in the literature.[17,45,46] Additional data regarding water and CO_2 uptakes vs RH over the other adsorbents are shown in Figure A4.5. The sharp increase of CO_2 uptake at RHs corresponding to water capillary condensation seems to indicate that adsorbed

liquid-like water at such a pressure, has a stronger promotion effect on CO_2 uptake than gas-like water, occurring at lower RH. However, as soon as the RH increases further, the pores are filled with water, and the CO_2 uptake decreases sharply.

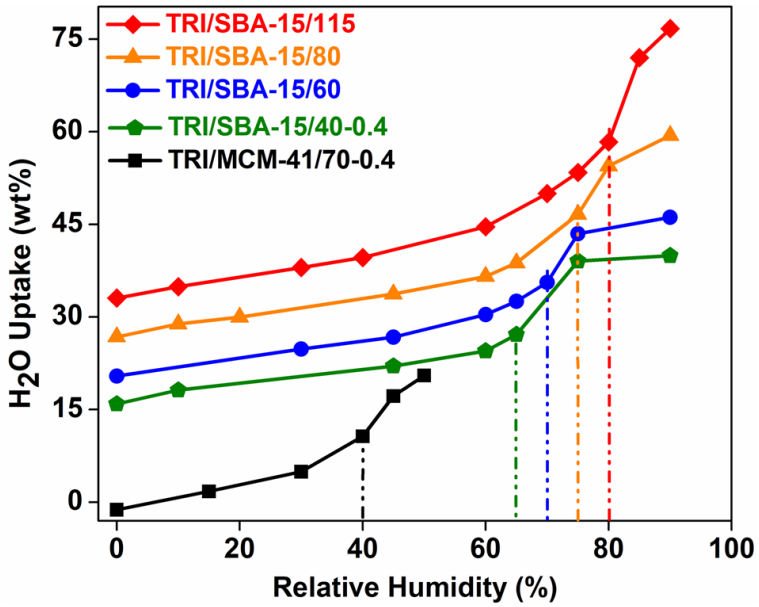

Figure 4.5. H_2O adsorption isotherms of TRI grafted adsorbents versus RH. Isotherms were shifted upward for clarity.

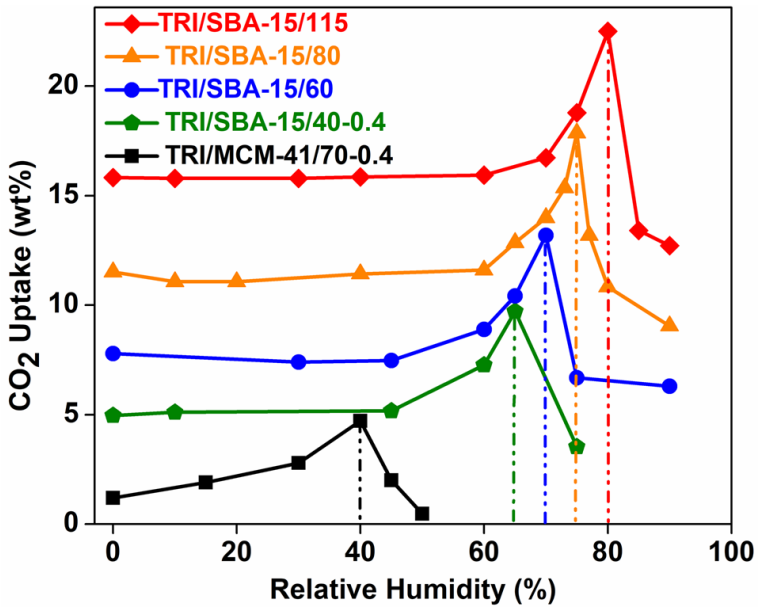

Figure 4.6. CO_2 adsorption isotherms of TRI grafted adsorbents versus RH. Isotherms were shifted upward for clarity. CO_2 uptake (wt%) under dry condition (RH = 0) from bottom up was 2.7, 3.6, 4.8, 6.3 and 7.4.

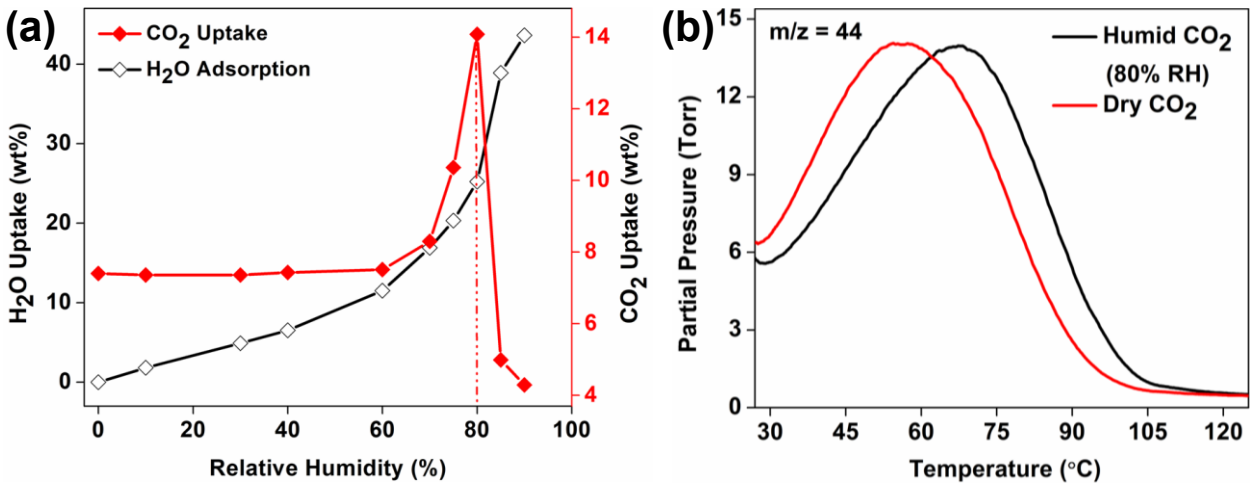

Figure 4.7. (a) H_2O and humid CO_2 adsorption isotherms versus RH. (b) Temperature-programmed desorption of CO_2 over TRI/SBA-15/115.

4.5. Conclusions

A series of amine-functionalized CO_2 adsorbents with comparable organic contents, were prepared using periodic mesoporous silicas with similar rodlike morphology and different pore sizes, ranging from 3 to 9.2 nm. Systematic measurements of water and humid CO_2 adsorption isotherms were carried out for all adsorbents over a range of relative humidities from 0 to 90%. All water adsorption isotherms were S-shaped with significant increase at relative humidity corresponding to the water capillary condensation, which increases with the pore size. The CO_2 uptake also increased by up to 100% at the same pressure corresponding to the water capillary condition. Beyond such a water pressure, the CO_2 uptake decreases precipitously. It was surmised that the dramatic increase in CO_2 uptake is due to improved promoting effect of liquid-like water at the capillary condensation pressure, favorable for the formation of ammonium bicarbonate, compared to gaseous water at lower pressures. The sharp decrease in CO_2 uptake at higher water pressures is believed to be due to the shrinking space associated with the water filling the pores of the adsorbent. The CO_2 uptake – RH – pore size relationship demonstrated here, may be used to design amine-containing materials with maximum uptake, by adjusting the pore size to correspond to the capillary condensation of water at the feed gas relative humidity.

4.6. References

(1) Crippa, M., Guizzardi, D., Pagani, F., Banja, M., Muntean, M., Schaaf E., Becker, W., Monforti-Ferrario, F., Quadrelli, R., Risquez Martin, A., Taghavi-Moharamli, P., Köykkä, J., Grassi, G., Rossi, S., Brandao De Melo, J., Oom, D., Branco, A., San-Miguel, E. *GHG Emissions of All World Countries*; 2023.

(2) International Energy Agency. *CO_2 Emissions in 2023*; 2024. https://www.iea.org/reports/co2-emissions-in-2023 (accessed 2024-12-19).

(3) *Trends in Atmospheric Carbon Dioxide*. Global Monitoring Laboratory. https://gml.noaa.gov/ccgg/trends/weekly.html (accessed 2024-08-19).

(4) Wu, C.; Huang, Q.; Xu, Z.; Sipra, A. T.; Gao, N.; Vandenberghe, L. P. de S.; Vieira, S.; Soccol, C. R.; Zhao, R.; Deng, S.; Boetcher, S. K. S.; Lu, S.; Shi, H.; Zhao, D.; Xing, Y.; Chen, Y.; Zhu, J.; Feng, D.; Zhang, Y.; Deng, L.; Hu, G.; Webley, P. A.; Liang, D.; Ba, Z.; Mlonka-Mędrala, A.; Magdziarz, A.; Miskolczi, N.; Tomasek, S.; Lam, S. S.; Foong, S. Y.; Ng, H. S.; Jiang, L.; Yan, X.; Liu, Y.; Ji, Y.; Sun, H.; Zhang, Y.; Yang, H.; Zhang, X.; Sun, M.; Tsang, D. C. W.; Shang, J.; Muller, C.; Rekhtina, M.; Krödel, M.; Bork, A. H.; Donat, F.; Liu, L.; Jin, X.; Liu, W.; Saqline, S.; Wu, X.; Xu, Y.; Khan, A. L.; Ali, Z.; Lin, H.; Hu, L.; Huang, J.; Singh, R.; Wang, K.; He, X.; Dai, Z.; Yi, S.; Konist, A.; Baqain, M. H. S.; Zhao, Y.; Sun, S.; Chen, G.; Tu, X.; Weidenkaff, A.; Kawi, S.; Lim, K. H.; Song, C.; Yang, Q.; Zhao, Z.; Gao, X.; Jiang, X.; Ji, H.; Akinola, T. E.; Lawal, A.; Otitoju, O. S.; Wang, M.; Zhang, G.; Ma, L.; Sempuga, B. C.; Liu, X.; Oko, E.; Daramola, M.; Yu, Z.; Chen, S.; Kang, G.; Li, Q.; Gao, L.; Liu, L.; Zhou, H. A Comprehensive Review of Carbon Capture Science and Technologies. *Carbon Capture. Sci. Technol.* **2024**, *11*, 100178.

(5) Zhu, X.; Xie, W.; Wu, J.; Miao, Y.; Xiang, C.; Chen, C.; Ge, B.; Gan, Z.; Yang, F.; Zhang, M.; O'Hare, D.; Li, J.; Ge, T.; Wang, R. Recent Advances in Direct Air Capture by Adsorption. *Chem. Soc. Rev.* **2022**, *51*, 6574–6651.

(6) Dziejarski, B.; Krzyżyńska, R.; Andersson, K. Current Status of Carbon Capture, Utilization, and Storage Technologies in the Global Economy: A Survey of Technical Assessment. *Fuel* **2023**, *342*, 127776.

(7) Siegelman, R. L.; Kim, E. J.; Long, J. R. Porous Materials for Carbon Dioxide Separations. *Nat. Mater.* **2021**, *20*, 1060–1072.

(8) Halliday, C.; Hatton, T. A. Sorbents for the Capture of CO_2 and Other Acid Gases: A Review. *Ind. Eng. Chem. Res.* **2021**, *60*, 9313–9346.

(9) Abdullatif, Y.; Sodiq, A.; Namra Mir; Bicer, Y.; Al-Ansari, T.; El-Naas, M. H.; Amhamed, A. I. Emerging Trends in Direct Air Capture of CO_2: A Review of Technology Options Targeting Net-Zero Emissions. *RSC Adv.* **2023**, *13*, 5687–5722.

(10) Lin, J. Bin; Nguyen, T. T. T.; Vaidhyanathan, R.; Burner, J.; Taylor, J. M.; Durekova, H.; Akhtar, F.; Mah, R. K.; Ghaffari-Nik, O.; Marx, S.; Fylstra, N.; Iremonger, S. S.; Dawson, K. W.; Sarkar, P.; Hovington, P.; Rajendran, A.; Woo, T. K.; Shimizu, G. K. H. A Scalable Metal-Organic Framework as a Durable Physisorbent for Carbon Dioxide Capture. *Science (1979)* **2021**, *374*, 1464–1469.

(11) Sayari, A.; Belmabkhout, Y.; Serna-Guerrero, R. Flue Gas Treatment via CO_2 Adsorption. *Chem. Eng. J.* **2011**, *171*, 760–774.

(12) Lin, L.; Meng, Y.; Ju, T.; Han, S.; Meng, F.; Li, J.; Du, Y.; Song, M.; Lan, T.; Jiang, J. Characteristics, Application and Modeling of Solid Amine Adsorbents for CO_2 Capture: A Review. *J. Environ. Manage.* **2023**, *325*, 116438–116438.

(13) Hack, J.; Maeda, N.; Meier, D. M. Review on CO_2 Capture Using Amine-Functionalized Materials. *ACS Omega* **2022**, *7*, 39520–39530.

(14) Lashaki M.J.; Khiavi, S.; Sayari, A. Stability of Amine-Functionalized CO_2 Adsorbents: A Multifaceted Puzzle. *Chem. Soc. Rev.* **2019**, *48*, 3320–3405.

(15) Kolle, J. M.; Fayaz, M.; Sayari, A. Understanding the Effect of Water on CO_2 Adsorption. *Chem. Rev.* **2021**, *121*, 7280–7345.

(16) Harlick, P. J. E.; Sayari, A. Applications of Pore-Expanded Mesoporous Silica. 5. Triamine Grafted Material with Exceptional CO_2 Dynamic and Equilibrium Adsorption Performance. *Ind. Eng. Chem. Res.* **2007**, *46*, 446–458.

(17) Serna-Guerrero, R.; Da'na, E.; Sayari, A. New Insights into the Interactions of CO_2 with Amine-Functionalized Silica. *Ind. Eng. Chem. Res.* **2008**, *47*, 9406–9412.

(18) Koutsianos, A.; Barron, A. R.; Andreoli, E. CO_2 Capture Partner Molecules in Highly Loaded PEI Sorbents. *J. Phys. Chem. C* **2017**, *121*, 21772–21781.

(19) Russell-Parks, G. A.; Leick, N.; Marple, M. A. T.; Strange, N. A.; Trewyn, B. G.; Pang, S. H.; Braunecker, W. A. Fundamental Insight into Humid CO_2 Uptake in Direct Air Capture Nanocomposites Using Fluorescence and Portable NMR Relaxometry. *J. Phys. Chem. C* **2023**, *127*, 15363–15374.

(20) Sayari, A.; Belmabkhout, Y. Stabilization of Amine-Containing CO_2 Adsorbents: Dramatic Effect of Water Vapor. *J. Am. Chem. Soc.* **2010**, *132*, 6312–6314.

(21) Sayari, A.; Belmabkhout, Y.; Da'na, E. CO_2 Deactivation of Supported Amines: Does the Nature of Amine Matter? *Langmuir* **2012**, *28*, 4241–4247.

(22) Burtch, N. C.; Jasuja, H.; Walton, K. S. Water Stability and Adsorption in Metal–Organic Frameworks. *Chem. Rev.* **2014**, *114*, 10575–10612.

(23) Tan, K.; Nijem, N.; Gao, Y.; Zuluaga, S.; Li, J.; Thonhauser, T.; Chabal, Y. J. Water Interactions in Metal Organic Frameworks. *CrystEngComm* **2015**, *17*, 247–26.

(24) Yu, J.; Chuang, S. S. C. The Role of Water in CO_2 Capture by Amine. *Ind. Eng. Chem. Res.* **2017**, *56*, 6337–6347.

(25) Szego, A. E.; Jaworski, A.; Hedin, N. Chemisorption of CO_2 on Diaminated Silica as Bicarbonates and Different Types of Carbamate Ammonium Ion Pairs. *Mater. Adv.* **2021**, *2*, 448.

(26) Short, G. N.; Burentugs, E.; Proaño, L.; Moon, H. J.; Rim, G.; Nezam, I.; Korde, A.; Nair, S.; Jones, C. W. Single-Walled Zeolitic Nanotubes: Advantaged Supports for Poly(ethylenimine) in CO_2 Separation from Simulated Air and Flue Gas. *JACS Au* **2023**, *3*, 62–69.

(27) Zerze, H.; Tipirneni, A.; McHugh, A. J. Reusable Poly(allylamine)-Based Solid Materials for Carbon Dioxide Capture under Continuous Flow of Ambient Air. *Sep. Sci. Technol.* **2017**, *52*, 2513–2522.

(28) Yu, J.; Xie, L. H.; Li, J. R.; Ma, Y.; Seminario, J. M.; Balbuena, P. B. CO_2 Capture and Separations Using MOFs: Computational and Experimental Studies. *Chem. Rev.* **2017**, *117*, 9674–9754.

(29) Veldhuizen, H.; Butt, S. A.; van Leuken, A.; van der Linden, B.; Rook, W.; van der Zwaag, S.; van der Veen, M. A. Competitive and Cooperative CO_2–H_2O Adsorption through Humidity Control in a Polyimide Covalent Organic Framework. *ACS Appl. Mater. Interfaces* **2023**, *15*, 29186–29194.

(30) Holmes, H. E.; Ghosh, S.; Li, C.; Kalyanaraman, J.; Realff, M. J.; Weston, S. C.; Lively, R. P. Optimum Relative Humidity Enhances CO_2 Uptake in Diamine-Appended M_2(Dobpdc). *Chem. Eng. J.* **2023**, *477*, 147119.

(31) Sayari, A.; Han, B.-H. H.; Yang, Y. Simple Synthesis Route to Monodispersed SBA-15 Silica Rods. *J. Am. Chem. Soc.* **2004**, *126*, 14348–14349.

(32) Jahandar Lashaki, M.; Ziaei-Azad, H.; Sayari, A. Insights into the Hydrothermal Stability of Triamine-Functionalized SBA-15 Silica for CO2 Adsorption. *ChemSusChem* **2017**, *10*, 4037–4045.

(33) Fayaz, M.; Sayari, A. Long-Term Effect of Steam Exposure on CO_2 Capture Performance of Amine-Grafted Silica. *ACS Appl. Mater. Interfaces* **2017**, *9*, 43747–43754.

(34) Sayari, A.; Liu, P.; Kruk, M.; Jaroniec, M. Characterization of Large-Pore MCM-41 Molecular Sieves Obtained via Hydrothermal Restructuring. *Chem. Mater.* **1997**, *9*, 2499–2506.

(35) Harlick, P. J. E.; Sayari, A. Applications of Pore-Expanded Mesoporous Silicas. 3. Triamine Silane Grafting for Enhanced CO_2 Adsorption. *Ind. Eng. Chem. Res.* **2006**, *45*, 3248–3255.

(36) Thommes, M.; Kaneko, K.; Neimark, A. V.; Olivier, J. P.; Rodriguez-Reinoso, F.; Rouquerol, J.; Sing, K. S. W. Physisorption of Gases, with Special Reference to the Evaluation of Surface Area and Pore Size Distribution (IUPAC Technical Report). *Pure Appl. Chem.* **2015**, *87*, 1051–1069.

(37) Serna-Guerrero, R.; Belmabkhout, Y.; Sayari, A. Modeling CO_2 Adsorption on Amine-Functionalized Mesoporous Silica: 1. A Semi-Empirical Equilibrium Model. *Chem. Eng. J.* **2010**, *161*, 173–181.

(38) Jahandar Lashaki, M.; Sayari, A. CO_2 Capture Using Triamine-Grafted SBA-15: The Impact of the Support Pore Structure. *Chem. Eng. J.* **2018**, *334*, 1260–1269.

(39) Gebald, C.; Wurzbacher, J. A.; Borgschulte, A.; Zimmermann, T.; Steinfeld, A. Single-Component and Binary CO_2 and H_2O Adsorption of Amine-Functionalized Cellulose. *Environ. Sci. Technol.* **2014**, *48*, 2497–2504.

(40) Veneman, R.; Frigka, N.; Zhao, W.; Li, Z.; Kersten, S.; Brilman, W. Adsorption of H_2O and CO_2 on Supported Amine Sorbents. *Int. J. Greenhouse Gas Control* **2015**, *41*, 268–275.

(41) Elfving, J.; Sainio, T. Kinetic Approach to Modelling CO_2 Adsorption from Humid Air Using Amine-Functionalized Resin: Equilibrium Isotherms and Column Dynamics. *Chem. Eng. Sci.* **2021**, *246*, 116885.

(42) Chen, C.-H.; Shimon, D.; Lee, J. J.; Mentink-Vigier, F.; Hung, I.; Sievers, C.; Jones, C. W.; Hayes, S. E. The "Missing" Bicarbonate in CO_2 Chemisorption Reactions on Solid Amine Sorbents. *J. Am. Chem. Soc.* **2018**, *140*, 8648–8651.

(43) Chen, C.-H.; Sesti, E. L.; Lee, J. J.; Mentink-Vigier, F.; Sievers, C.; Jones, C. W.; Hayes, S. E. NMR Reveals Two Bicarbonate Environments in SBA 15-Solid-Amine CO_2 Sorbents. *J. Phys. Chem. C* **2021**, *125*, 16759–16765.

(44) Sardo, M.; Afonso, R.; Juźków, J.; Pacheco, M.; Bordonhos, M.; Pinto, M. L.; Gomes, J. R. B.; Mafra, L. Unravelling Moisture-Induced CO_2 Chemisorption Mechanisms in Amine-Modified Sorbents at the Molecular Scale. *J. Mater. Chem. A* **2021**, *9*, 5542–5555.

(45) Chen, O. I. F.; Liu, C. H.; Wang, K.; Borrego-Marin, E.; Li, H.; Alawadhi, A. H.; Navarro, J. A. R.; Yaghi, O. M. Water-Enhanced Direct Air Capture of Carbon Dioxide in Metal-Organic Frameworks. *J. Am. Chem. Soc.* **2024**, *146*, 2835–2844.

(46) Knowles, G. P.; Graham, J. V; Delaney, S. W.; Chafee, A. L. Aminopropyl-Functionalized Mesoporous Silicas as CO_2 Adsorbents. *Fuel Process. Technol.* **2005**, *86*, 1435–1448.

Appendix A4 Supplementary Information for Chapter 4

SEM Images of Silica Supports

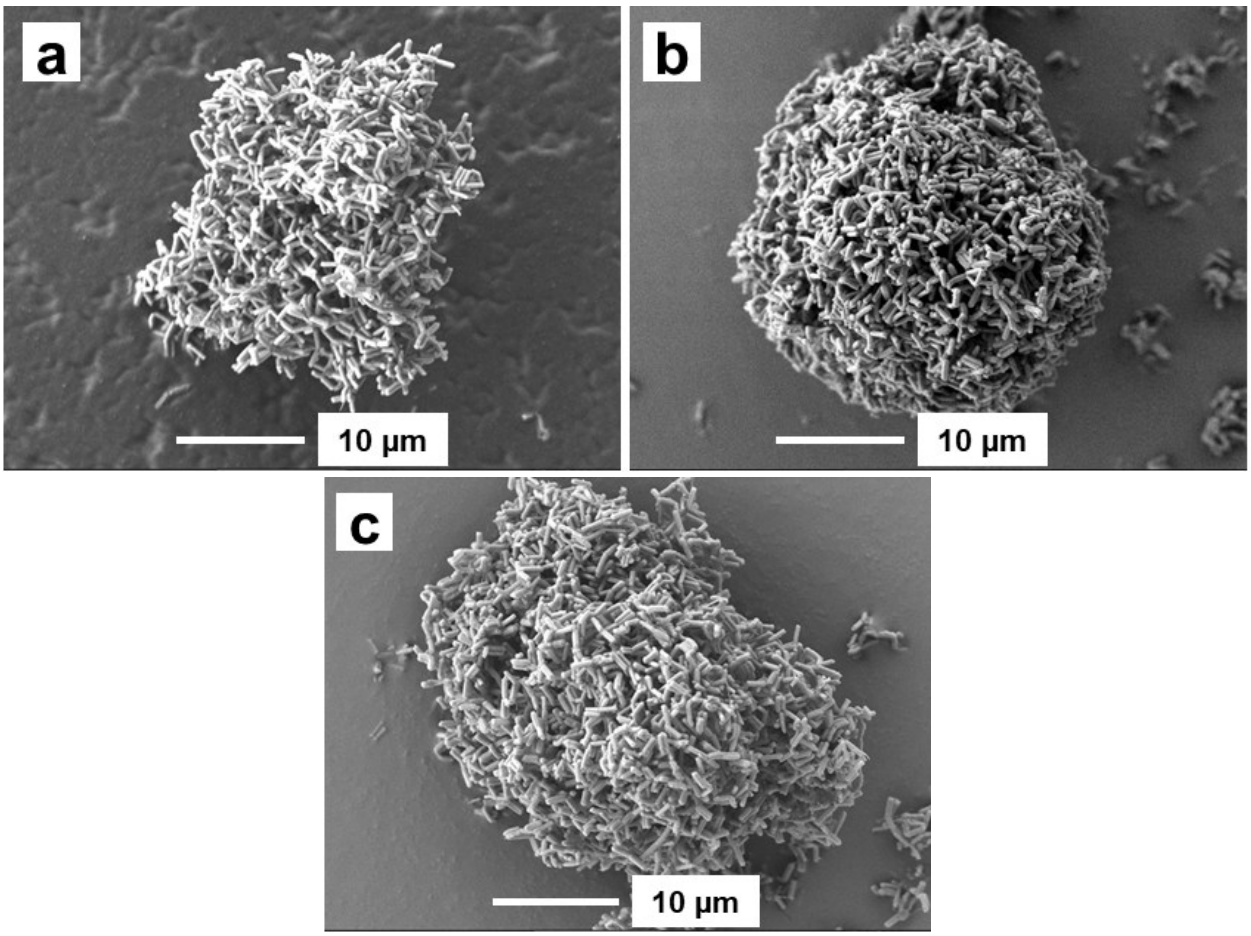

Figure A4.1. Low-magnification SEM images of (a) SBA-15/40, (b) SBA-15/60, and (c) SBA-15/80.

Adsorption of H_2O and CO_2

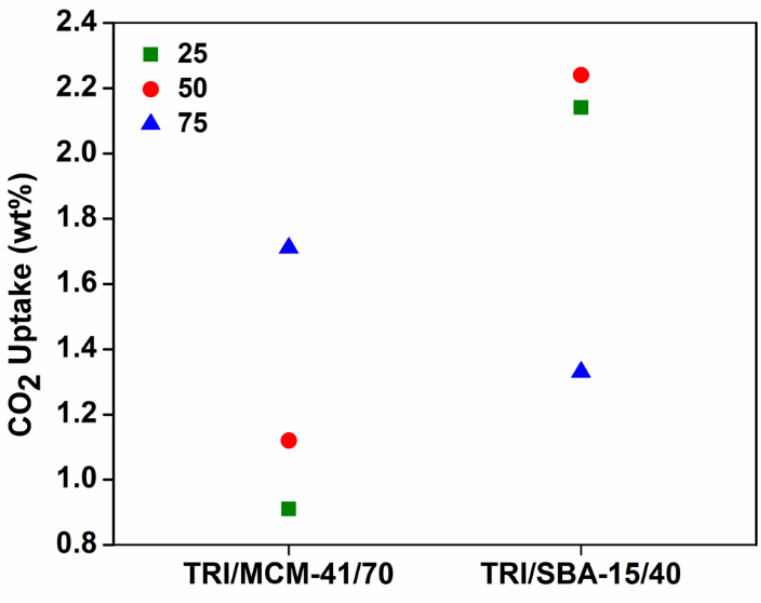

Figure A4.2. CO_2 uptake of TRI/MCM-41/70 and TRI/SBA-15/40 at 25, 50 and 75 °C.

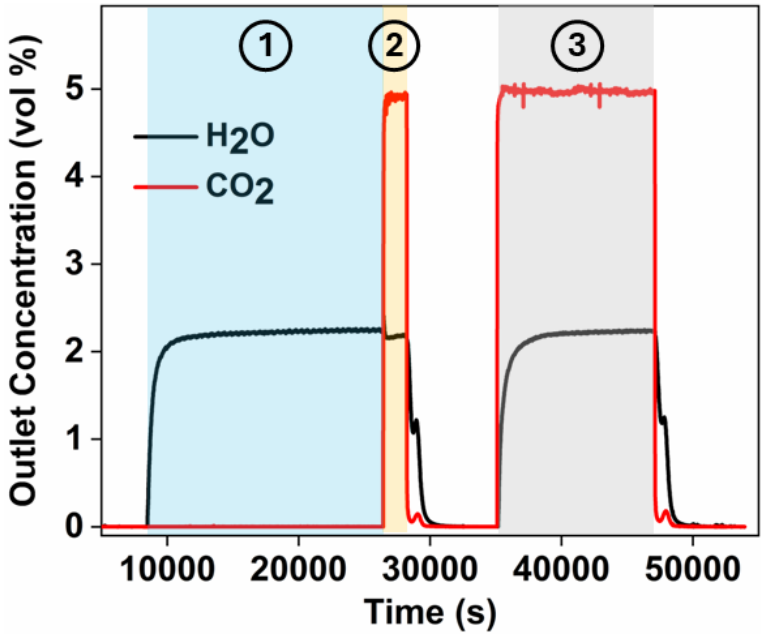

Figure A4.3. Dynamic breakthrough measurements for H_2O and humid (80% RH) 5% CO_2/N_2 mixture at 25 °C on TRI-SBA-15-115. In stage 1, adsorbent is pre-humid before it is exposed to humid CO_2 in stage 2. In stage 3, activated material is directly exposed to humid CO_2 gas stream. No roll-up effect for H_2O was observed when CO_2 was introduced (stage 2) to the pre-humidified adsorbent (stage 1), suggesting that CO_2 does not displace the H_2O. Moreover, H_2O adsorption in stage 1 (10.4 mmol/g) and stage 3 (9.1 mmol/g) remains almost the same indicating that CO_2 does not have a pronounced effect on the adsorption of H_2O.

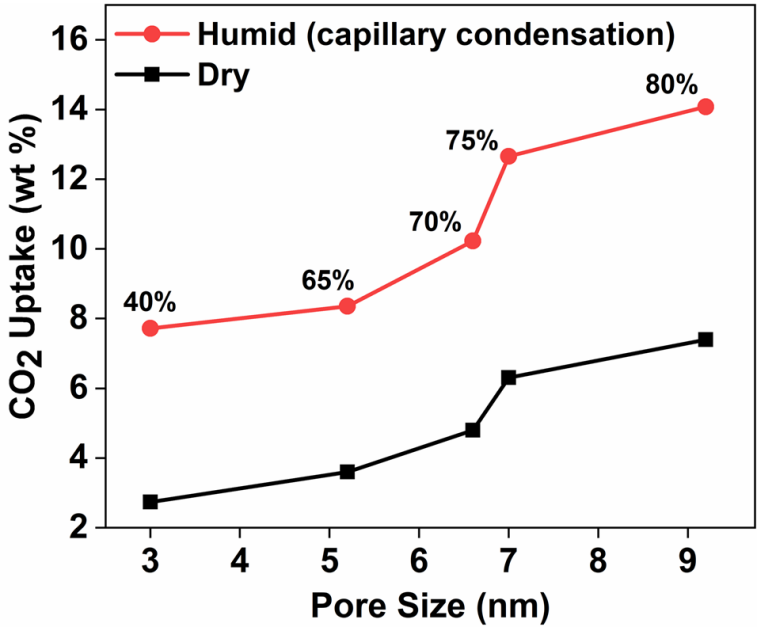

Figure A4.4. CO_2 uptake for triamine-functionalized mesoporous adsorbents, under dry conditions (black) and under humid conditions at the RH corresponding to capillary condensation as indicated (red).

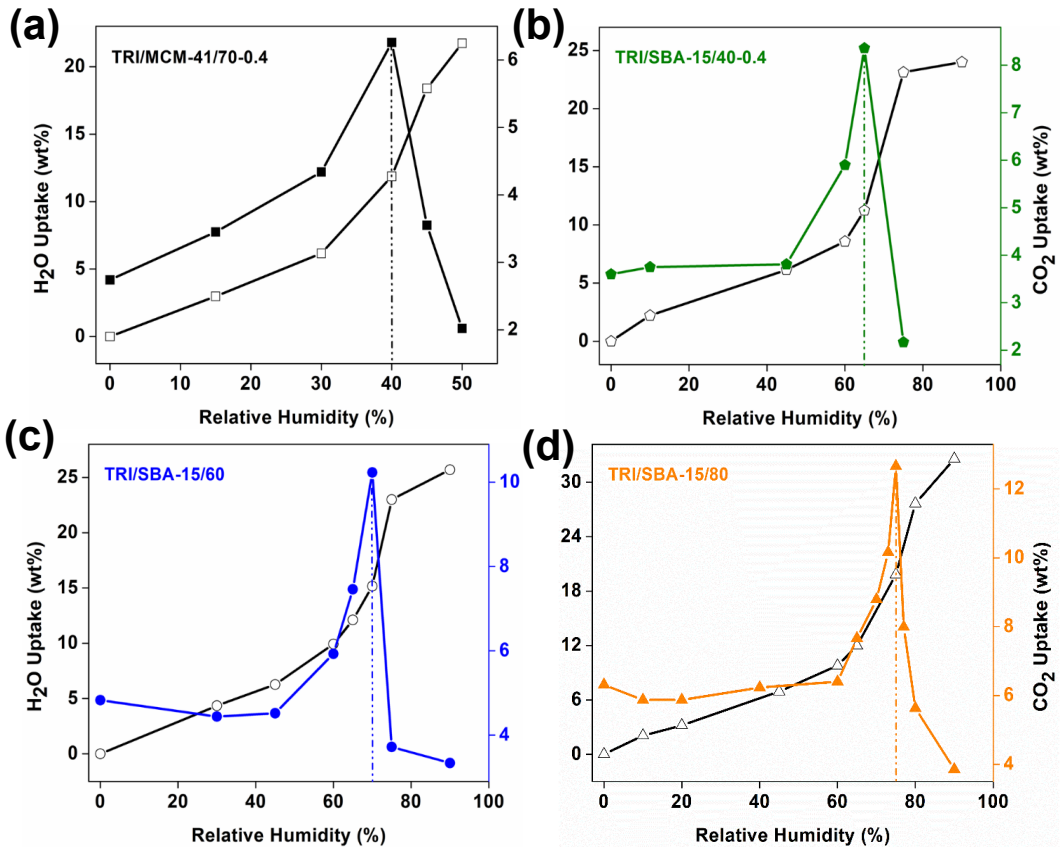

Figure A4.5. H_2O (open symbols) and CO_2 (closed symbols) adsorption isotherms of (a) TRI/MCM-41/70-0.4, (b) TRI/SBA-15/40-0.4, (c) TRI/SBA-15/60, (d) TRI/SBA-15/80 versus relative humidity at 25 °C.

Organic Content and Amine Efficiency

Table A4.1. Organic content, nitrogen content and amine efficiency of adsorbents at 25 °C.

Adsorbent	Organic content (wt%)	Nitrogen content (mmol/g)	CO_2/N	
			Dry condition	At capillary condensation
TRI/MCM-41/70-0.4	19.49	4.06	0.15	0.43
TRI/SBA-15/40-0.4	19.81	4.13	0.19	0.50
TRI/SBA-15/60	21.93	4.57	0.24	0.51
TRI/SBA-15/80	25.27	5.27	0.27	0.55
TRI/SBA-15/115	26.44	5.51	0.31	0.58

CO_2/N: Moles of CO_2 captured per mol of nitrogen.

CHAPTER 5 CONCLUSIONS

5.1. Summary of Contributions

The rising level of atmospheric CO_2 poses an environmental problem, necessitating the development of efficient and durable carbon capture technologies. Amine-based adsorbents have emerged as promising materials, but their large-scale deployment is hindered by challenges such as SO_2 poisoning, oxidative degradation, and low CO_2 uptake. This thesis systematically addresses these challenges by developing strategies to enhance or maintain CO_2 adsorption capacity, while ensuring improved stability and performance of amine-functionalized adsorbents.

The first study of this thesis is focused on the mitigation of SO_2 poisoning, a key issue that leads to irreversible deactivation of amine-based adsorbents, responsible for a sharp decrease in CO_2 uptake. To address this, a tertiary amine-based adsorbent was synthesized using a straightforward methodology. IR and NMR analyses confirmed the complete functionalization of PEI with glycidol, ensuring the conversion of all amine groups to tertiary amines. Breakthrough experiments with a gas mixture containing 5 ppm SO_2 and a CO_2 concentration exceeding 20,000 times that of SO_2 demonstrated that GD-PEI/S is 100% selective for SO_2. This selectivity was further supported by TGA analysis, which revealed negligible CO_2 uptake under a 15% CO_2/N_2 gas stream. Moreover, the material was stable after both dry and humid regeneration cycles. These findings highlight its potential as a protective pretreatment filter for effectively removing SO_2 before CO_2 adsorption. By selectively removing SO_2, GD-PEI/S helps maintain the adsorption capacity of the primary CO_2 adsorbents, thereby enhancing the overall efficiency and longevity of CO_2 capture systems. This research offers a promising step forward for developing efficient gas separation technologies for industrial applications.

The second key challenge tackled in this thesis was the oxidative degradation of amine adsorbents, a critical limitation hindering their long-term industrial deployment by reducing CO_2

uptake capacity and compromising operational longevity. To overcome this, HES-PEI/S was developed by co-impregnating HES and PEI on support. HES-PEI/S demonstrated oxidative stability comparable to supported epoxide-functionalized PEI (EB-PEI/S) while maintaining twice the CO_2 uptake per unit PEI content. Comparative analysis with the state-of-the-art additives (PVA and PEG) confirmed that HES offers the best balance between CO_2 capacity and oxidation resistance, making it a promising stabilizing additive for amine adsorbents.

The final study aimed at optimizing CO_2 uptake of amine-adsorbents by investigating the relationship between relative humidity, pore size, and adsorption capacity. H_2O and CO_2 adsorption isotherms revealed a pore-size dependent enhancement in CO_2 uptake at vapor pressures corresponding to the water capillary condensation, with CO_2 capacity approximately twice as high as those observed under dry conditions. These findings provide critical insights for performance-driven design of the adsorbent. For example, for a feed gas with a given RH, pore size of the adsorbent can be adjusted such that the RH of feed gas is same as the RH of water capillary condensation, thereby maximizing the CO_2 uptake of the adsorbent.

Together, this thesis contributes to the advancement of amine-based CO_2 adsorbents by addressing key limitations that decrease their adsorption efficiency. By preventing SO_2 poisoning, improving oxidation resistance, and optimizing pore structure for enhanced CO_2 uptake, this work provides valuable insights for the development of robust and high-performing adsorbents. The findings of this research contribute to overcoming major barriers in CO_2 capture technology, bringing the field closer to achieving practical solutions for mitigating carbon emissions.

5.2. Limitations and Future Directions

While this study provides valuable insights into the optimization of amine-functionalized adsorbents for CO_2 capture, certain limitations persist and require further investigation. Overcoming these limitations will contribute to the development of more efficient and durable adsorbents for practical applications.

- The SO_2 adsorption capacity of GD-PEI/S was lower compared to other adsorbents reported in the literature. This can be attributed to steric hindrance due to presence of bulky functional groups, which could limit accessibility of SO_2 to amine groups. Future studies should explore less sterically hindered amines or functional groups, which may enhance SO_2 uptake while maintaining high selectivity.
- Another aspect that requires further investigation is the adsorption kinetic of CO_2 in amine adsorbents where hydroxyl-containing additives are incorporated. Although hydroxyl groups have demonstrated beneficial effects in improving oxidation stability, their impact on CO_2 adsorption kinetics remain inconsistent, with some cases exhibiting slower adsorption rates. A systematic study on different types of hydroxyl-functionalized additives and their impact on adsorption kinetics is necessary to better understand this effect. Furthermore, since different hydroxyl groups may interact differently with PEI, their role in influencing oxidation stability of amines should be explored in greater depth.
- Additionally, an important but often overlooked factor is the stability of additives used to enhance oxidative resistance of the amines. The long-term stability of these additives is crucial, as their degradation over multiple adsorption-desorption cycles could limit their effectiveness. Future research should focus on evaluating the stability of potential additives prior to their incorporation into amine-functionalized adsorbents to improve oxidation stability.
- Adjusting parameters such as water content and triamine concentration during amine grafting on the support can influence the resulting pore size of the adsorbent, potentially establishing a

correlation between the pore size of the grafted material—rather than the bare support—CO_2 uptake, and the relative humidity (RH) of the feed gas. However, accurately determining the true pore size of grafted adsorbents remains challenging, as conventional models primarily measure the empty pore spaces and do not account for the spatial distribution of grafted amines. Future research should focus on developing advanced characterization techniques and exploring the impact of pore structure on adsorption performance under different synthesis conditions.